HYDROCALUMITE-BASED CATALYSTS FOR GLYCEROL REVALORIZATION.

Judith Cecilia Granados Reyes

Dipòsit Legal: T 1362-2015

Judith Cecilia Granados Reyes

Hydrocalumite-based catalysts for glycerol revalorization

DOCTORAL THESIS

Supervised by

Prof. Yolanda Cesteros and Dr. Pilar Salagre

Departament de Química Física i Inorgànica

Facultat de Química

UNIVERSITAT ROVIRA I VIRGILI

Tarragona

2015

UNIVERSITAT ROVIRA I VIRGILI
HYDROCALUMITE-BASED CATALYSTS FOR GLYCEROL REVALORIZATION.
Judith Cecilia Granados Reyes
Dipòsit Legal: T 1362-2015

UNIVERSITAT ROVIRA I VIRGILI

We STATE that the present study, entitled “Hydrocalumite-based catalysts for glycerol revalorization”, presented by Judith Cecilia Granados Reyes for the award of the degree of Doctor, has been carried out under our supervision at the Departament de Química Física i Inorgànica of this university. And that it fulfils all the requirements to be eligible for the European Doctorate Mention.

Tarragona, June 2015

Doctoral Thesis Supervisor/s

Prof. Yolanda Cesteros

Dr. Pilar Salagre

UNIVERSITAT ROVIRA I VIRGILI
HYDROCALUMITE-BASED CATALYSTS FOR GLYCEROL REVALORIZATION.
Judith Cecilia Granados Reyes
Dipòsit Legal: T 1362-2015

UNIVERSITAT ROVIRA I VIRGILI
HYDROCALUMITE-BASED CATALYSTS FOR GLYCEROL REVALORIZATION.
Judith Cecilia Granados Reyes
Dipòsit Legal: T 1362-2015

The work performed in the present doctoral thesis has been possible thanks to the funding of Ministerio de Economía y Competitividad of Spain and Feder Funds (CTQ2011-24610), Catalan Government for FI grant (2012FI_B00564) and to a mobility grant (2013AEE-34) from the Universitat Rovira i Virgili.

UNIVERSITAT ROVIRA I VIRGILI

UNIVERSITAT ROVIRA I VIRGILI
HYDROCALUMITE-BASED CATALYSTS FOR GLYCEROL REVALORIZATION.
Judith Cecilia Granados Reyes
Dipòsit Legal: T 1362-2015

UNIVERSITAT ROVIRA I VIRGILI
HYDROCALUMITE-BASED CATALYSTS FOR GLYCEROL REVALORIZATION.
Judith Cecilia Granados Reyes
Dipòsit Legal: T 1362-2015

To Daniel and my mom

UNIVERSITAT ROVIRA I VIRGILI
HYDROCALUMITE-BASED CATALYSTS FOR GLYCEROL REVALORIZATION.
Judith Cecilia Granados Reyes
Dipòsit Legal: T 1362-2015

Table of Contents

Glossary of Terms and Abbreviations

AN	Acetonitrile
FID	Flame ionization detector
FT-IR	Fourier transformed infrared spectroscopy
FWHM	Full width at half maximum
GC	Glycerol carbonate
HC	Hydrocalumite-type compounds
ICP-OES	Inductively coupled plasma- optical emission spectroscopy
IUPAC	International union of pure and applied chemistry
LDH	Layered double hydroxides
MTG	Methanol to gasoline
MTO	Methanol to oleofins
MTP	Methanol to propilene
PN	Pivalonitrile
SEM	Scanning electron microscopy
TEM	Transmission electron microscopy
TGA	Thermogravimetric analysis
XRD	X-ray diffraction

UNIVERSITAT ROVIRA I VIRGILI
HYDROCALUMITE-BASED CATALYSTS FOR GLYCEROL REVALORIZATION.
Judith Cecilia Granados Reyes
Dipòsit Legal: T 1362-2015

UNIVERSITAT ROVIRA I VIRGILI
HYDROCALUMITE-BASED CATALYSTS FOR GLYCEROL REVALORIZATION.
Judith Cecilia Granados Reyes
Dipòsit Legal: T 1362-2015

"No hacen falta alas
para hacer un sueño
basta con las manos
basta con el pecho
basta con las piernas
y con el empeño"

Silvio Rodríguez

UNIVERSITAT ROVIRA I VIRGILI
HYDROCALUMITE-BASED CATALYSTS FOR GLYCEROL REVALORIZATION.
Judith Cecilia Granados Reyes
Dipòsit Legal: T 1362-2015

CAPÍTULO 1

Introducción General

UNIVERSITAT ROVIRA I VIRGILI
HYDROCALUMITE-BASED CATALYSTS FOR GLYCEROL REVALORIZATION.
Judith Cecilia Granados Reyes
Dipòsit Legal: T 1362-2015

En los últimos años ha aumentado considerablemente la preocupación por el agotamiento del petróleo y el impacto ambiental asociado al uso de combustibles fósiles. Para superar este problema, los biocombustibles han surgido como una alternativa, ya que al obtenerse a partir de materias primas renovables y producir una combustión con un bajo contenido de azufre y compuestos aromáticos,[1] contribuyen a reducir las emisiones de dióxido de carbono procedentes de los combustibles fósiles y a mitigar la contaminación atmosférica y el calentamiento global.[2]

Uno de los biocombustibles más populares es el biodiesel. Este biocombustible se produce a partir de aceites vegetales y metanol en presencia de un catalizador básico, mediante una reacción de transesterificación (Figura 1). En esta reacción se genera como subproducto glicerol (conocido comercialmente como glicerina) en grandes cantidades (1 kg /10 kg de biodiesel).[2–6]

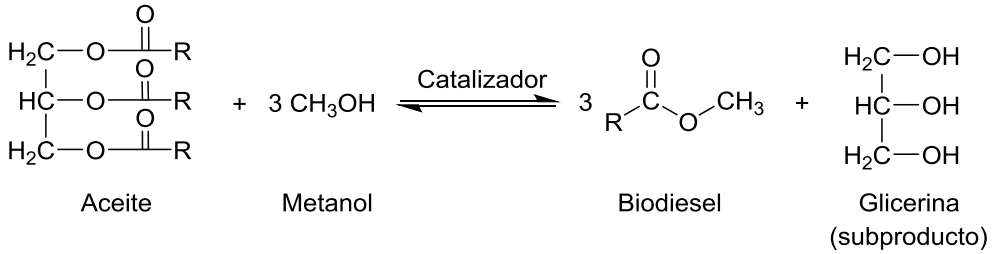

Figura 1. Transesterificación de triglicéridos para la obtención de biodiesel.

El glicerol (1,2,3-propanotriol) es un componente de los triglicéridos que se encuentran en la grasa animal, el aceite vegetal o el crudo de petróleo. Se caracteriza por tener una alta viscosidad y por ser inodoro, incoloro y de un sabor dulce. La molécula de glicerol es muy reactiva debido a que contiene tres grupos hidroxilo hidrófilos (Figura 2) que pueden intercambiarse por otros grupos químicos mediante reacciones biológicas o químicas. Además, estos grupos son responsables de que el glicerol sea higroscópico y soluble en agua.[2,3,5,7]

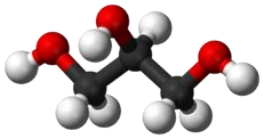

Figura 2. Estructura molecular del glicerol.

El glicerol es una de las sustancias químicas más versátiles y valiosas conocidas, con más de mil usos y aplicaciones.[8] Por sus propiedades físico-químicas, como la alta estabilidad, baja toxicidad, baja tasa de evaporación y baja inflamabilidad, se le considera un nuevo "solvente verde".

Aunque el glicerol tiene numerosas aplicaciones en la industria farmacéutica, alimentaria, cosmética, entre otras (en la Figura 3 se muestra con mayor detalle sus aplicaciones), la actual sobreproducción de glicerol ha provocado que los usos tradicionales sean insuficientes para dar salida a la cantidad producida, generando un excedente y como consecuencia una disminución de su precio[4,7] (Figura 4).

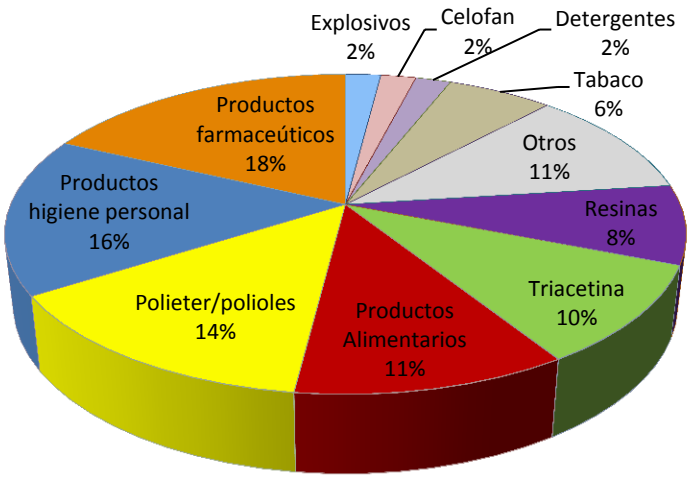

Figura 3. Mercado del glicerol.[9]

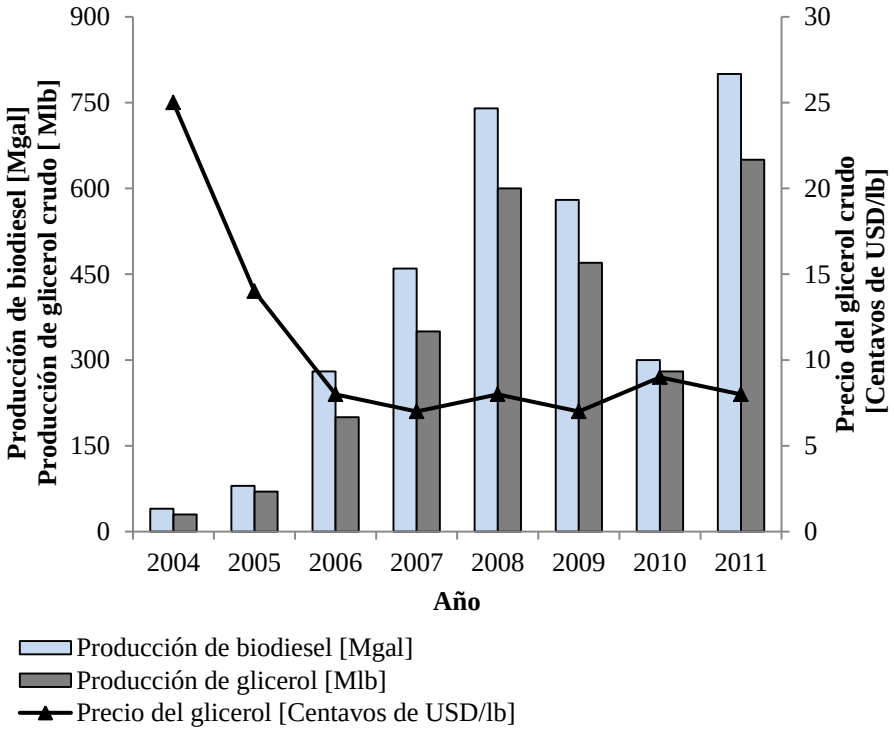

Figura 4. Relación entre la producción de biodiesel y el precio del glicerol.[4]

Una alternativa para dar uso a este gran excedente de glicerol consiste en revalorizarlo mediante su utilización como materia prima para obtener productos de mayor valor comercial. La Figura 5 muestra algunos de los derivados del glicerol más relevantes como el propilenglicol (1,2-propanodiol) y el 1,3-propanodiol, utilizados en la producción de polímeros, que se obtienen mediante la hidrogenólisis del glicerol utilizando catalizadores metálicos soportados; la acroleína (2-propenal), que se emplea en la industria química para la producción de súper absorbentes, polímeros, detergentes y ésteres de ácido acrílico, puede obtenerse a partir de la deshidratación de glicerol en presencia de catalizadores ácidos; el ácido glicérico, utilizado para el tratamiento de trastornos de la piel y en la elaboración de polímeros o emulsionantes biodegradables, se produce mediante oxidación catalítica de glicerol, o la epiclorhidrina, que se emplea en la producción de resinas epoxi, y se sintetiza a partir de glicerol mediante reacción con HCl seguida de deshidrodecloración con NaOH.[5,8,10,11]

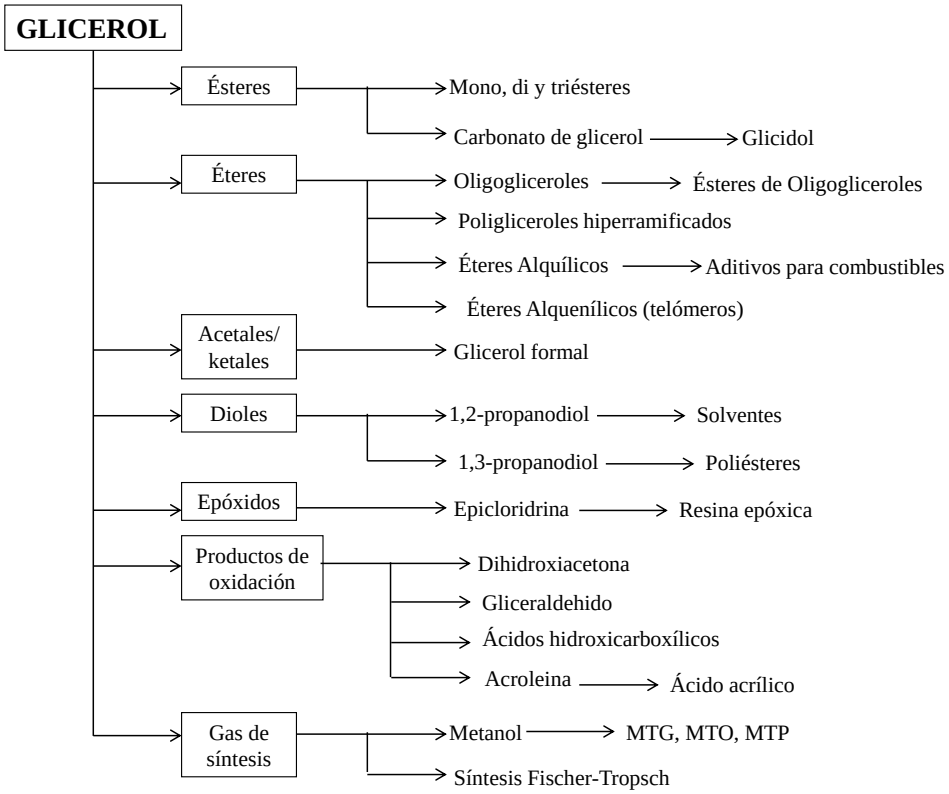

Figura 5. Transformaciones catalíticas del glicerol.[5]

Otro de los productos derivados del glicerol de gran relevancia es el carbonato de glicerol (4-hidroximetil-1,3-dioxolan-2-ona). Este compuesto relativamente nuevo en la industria química tiene un gran potencial como componente de membranas de separación de gases; como disolvente para diversos tipos de materiales; y como biolubricante (debido a su adhesión a superficies metálicas y resistencia a la oxidación, la hidrólisis, y la presión). El carbonato de glicerol es además una fuente de nuevos materiales poliméricos como el glicidol, un componente de alto valor en la producción de polímeros.[12]

UNIVERSITAT ROVIRA I VIRGILI
HYDROCALUMITE-BASED CATALYSTS FOR GLYCEROL REVALORIZATION.
Judith Cecilia Granados Reyes
Dipòsit Legal: T 1362-2015

UNIVERSITAT ROVIRA I VIRGILI
HYDROCALUMITE-BASED CATALYSTS FOR GLYCEROL REVALORIZATION.
Judith Cecilia Granados Reyes
Dipòsit Legal: T 1362-2015

CAPÍTULO 2

Objetivos

UNIVERSITAT ROVIRA I VIRGILI
HYDROCALUMITE-BASED CATALYSTS FOR GLYCEROL REVALORIZATION.
Judith Cecilia Granados Reyes
Dipòsit Legal: T 1362-2015

El objetivo principal de esta tesis es sintetizar y caracterizar hidróxidos dobles laminares tipo hidrocalumita mediante la utilización de radiación microondas y ultrasonidos, para ser utilizados como catalizadores en reacciones de gran interés industrial, como la reacción de transesterificación del glicerol para la obtención de carbonato de glicerol, además de realizar un estudio preliminar de la síntesis de glicidol a partir de carbonato de glicerol empleando diversos catalizadores.

Los objetivos parciales que se proponen en esta tesis son:

1. Preparar hidróxidos dobles laminares tipo hidrocalumita (CaAl-LDH) mediante el método de coprecipitación de las correspondientes sales (cloruros o nitratos), variando el tiempo, la temperatura y utilizando reflujo o autoclave durante su envejecimiento.

2. Estudiar el efecto del uso de ultrasonidos durante la etapa de coprecipitación y la influencia de la radiación microondas durante el envejecimiento de los materiales tipo hidrocalumita.

3. Calcinar los hidróxidos dobles laminares de CaAl a diferentes temperaturas, atmósferas (nitrógeno, aire) y en sistema estático o dinámico.

4. Modificar algunos CaAl-LDH mediante impregnación con soluciones de KOH, KNO_3 y H_3PO_4 o variando el pH de coprecipitación. Sintetizar dos hidrotalcitas de Mg/Al y Ni/Al y preparar diversos hidróxidos de aluminio utilizando microondas.

5. Caracterizar los catalizadores obtenidos mediante las técnicas clásicas de caracterización de sólidos: difracción de rayos X, fisisorción de N_2, análisis elemental, análisis termogravimétrico, microscopía electrónica de barrido y transmisión, espectroscopía infrarroja, espectroscopía raman.

6. Estudiar la fuerza básica de los hidróxidos dobles laminares tipo hidrocalumita y sus formas calcinadas utilizando indicadores de Hammett. Estudiar los centros ácidos y básicos de algunas hidrocalumitas mediante adsorción de nitrilos seguido de espectrocopía infrarroja.

7. Evaluar la actividad catalítica de los CaAl-LDH preparados, antes y después de su calcinación, en la reacción de transesterificación de glicerol con carbonato de dimetilo para obtener carbonato de glicerol, en reactor batch mediante calentamiento convencional.

8. Estudiar el efecto de la radiación microondas en la actividad catalítica de varios materiales tipo hidrocalumita y algunas de sus formas calcinadas, para la obtención de carbonato de glicerol a partir de la reacción de transesterificación de glicerol con carbonato de dimetilo.

9. Estudiar la actividad catalítica de algunos materiales tipo hidrocalumita, así como hidrotalcitas e hidróxidos de aluminio, en la producción de glicidol a partir de carbonato de glicerol

UNIVERSITAT ROVIRA I VIRGILI
HYDROCALUMITE-BASED CATALYSTS FOR GLYCEROL REVALORIZATION.
Judith Cecilia Granados Reyes
Dipòsit Legal: T 1362-2015

UNIVERSITAT ROVIRA I VIRGILI
HYDROCALUMITE-BASED CATALYSTS FOR GLYCEROL REVALORIZATION.
Judith Cecilia Granados Reyes
Dipòsit Legal: T 1362-2015

CAPÍTULO 3

Parte experimental

UNIVERSITAT ROVIRA I VIRGILI
HYDROCALUMITE-BASED CATALYSTS FOR GLYCEROL REVALORIZATION.
Judith Cecilia Granados Reyes
Dipòsit Legal: T 1362-2015

3.1. Descripción de los hidróxidos dobles laminares tipo hidrocalumita (CaAl-LDH).

Los compuestos tipo hidrocalumita (HC) pertenecen a la familia de los hidróxidos dobles laminares (LDH). Los LDHs son arcillas aniónicas, con fórmula general $[M^{II}_{1-x}M^{III}_{x}(OH)_2][X^{q-}_{x/q}]\cdot nH_2O$, constituidas por láminas $[M^{II}_{1-x}M^{III}_{x}(OH)_2]$ cargadas positivamente que quedan compensadas por la presencia de aniones $[X^{q-}_{x/q}]$ en el espacio interlaminar (ver Figura 6) donde también se encuentran moléculas de agua. En el caso particular de los compuestos tipo hidrocalumita, las láminas están formadas por $[Ca_2Al(OH)_6]^+$ con una relación molar Ca^{2+} y Al^{3+} igual a 2, mientras que los aniones interlaminares habituales son OH^-, NO_3^-, SO_4^{2-}, CO_3^{2-}, o Cl^-.[13–15] Específicamente, estos compuestos reciben el nombre de hidrocalumitas, cuando los aniones son cloruros.

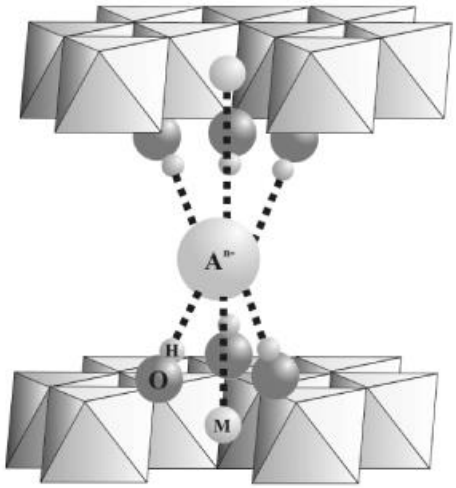

Figura 6. Estructura de un compuesto LDH. M= catión divalente o trivalente, O= oxígeno del grupo OH, H= hidrógeno del grupo OH, A= anión interlaminar que compensa la carga de las láminas.

La estructura de las CaAl-LDH colapsa a temperaturas entre 400 y 600 ºC debido a la deshidroxilación de sus capas octaédricas, dando lugar a la formación de óxidos mixtos amorfos, $Ca(Al)O_x$, observándose a temperaturas de calcinación

superiores la formación de fases cristalinas de CaO y mayenita ($Ca_{12}Al_{14}O_{33}$). Las CaAl-LDH calcinadas presentan, en general, propiedades básicas, pequeños tamaños de cristalitos y efecto memoria; lo que las hace atractivas en aplicaciones de catálisis heterogénea o como adsorbentes de iones para la purificación de aguas.[16]

3.2. Preparación de hidróxidos dobles laminares (LDH) tipo hidrocalumita

En esta tesis, se han sintetizado dos series de materiales tipo hidrocalumita empleando el método de coprecipitación a partir de diferentes sales de partida: cloruros (HC1) y nitratos (HC2), utilizando agua descarbonatada/desionizada. Las muestras se prepararon a pH constante (11.5), temperatura constante (60 ºC) bajo una atmósfera de nitrógeno. Además, como método alternativo a la agitación magnética, se utilizó un equipo de ultrasonidos para favorecer la homogeneidad en la coprecipitación de las sales. Por último, las sales coprecipitadas se envejecieron mediante calentamiento convencional o microondas, en autoclave o en condiciones de reflujo.

3.2.1. Método convencional de coprecipitación de sales

Dos soluciones acuosas de $CaCl_2 \cdot 2H_2O$ (Sigma Aldrich) y $AlCl_3 \cdot 6H_2O$ (Riedel de Haën) o $Ca(NO_3)_2 \cdot 4H_2O$ (Sigma Aldrich) y $Al(NO_3)_3 \cdot 9H_2O$ (Sigma Aldrich) se prepararon con una relación molar 2:1 de Ca^{2+}/Al^{3+}. Las soluciones se añadieron gota a gota a un balón de 500 ml de fondo redondo de cuatro bocas, el cual contenía 250 ml de una mezcla de agua/etanol en una proporción volumétrica de 2:3. El pH se mantuvo constante a 11,5 ± 0,1, mediante la adición simultánea de una solución acuosa de NaOH 2 M (Panreac) bajo agitación magnética vigorosa. Se utilizó como medio de calentamiento un baño de aceite a 60 ºC con temperatura controlada mediante una sonda de temperatura.

Después de completar la precipitación de las sales metálicas, se aplicaron diferentes tratamientos hidrotérmicos a los dos precipitados obtenidos. Las muestras envejecidas a reflujo se calentaron a 60 ºC durante 24 h y las muestras envejecidas en autoclave a 180 ºC durante 1 h.

3.2.2. Utilización de ultrasonidos en la preparación de materiales

El uso de ultrasonidos en la preparación de materiales ayuda a obtener una mayor homogeneidad en las muestras, así como a disminuir los tiempos de reacción. Los ultrasonidos son ondas sonoras con frecuencias superiores al rango normal de audición humana, aproximadamente 20 KHz. Los efectos benéficos de los ultrasonidos son debidos al fenómeno de cavitación, el cual genera agitación y calentamiento a través de la producción y destrucción de pequeñas burbujas que aparecen cuando se impacta un líquido con ondas de ultrasonido.[17]

Figura 7. Ultrasonido utilizado en la preparación de materiales

En esta tesis se utilizó un equipo ultrasonidos ULTRASONS-H 3000838 (de marca Selecta, ver Figura 7) como fuente de agitación y calentamiento para la síntesis de los materiales tipo hidrocalumita, manteniendo la temperatura del baño sonicador a 60 ºC durante el tiempo de la coprecipitación de las sales.

3.2.3. Utilización de microondas en la preparación y modificación de materiales

La utilización de microondas se ha convertido recientemente en una herramienta clave para la preparación y modificación de materiales. Este proceso se considera económico y limpio, ya que reduce el tiempo de obtención de materiales cristalinos, lo que conduce a un ahorro de energía considerable.[18]

Las microondas son ondas electromagnéticas que se encuentran en el rango de frecuencia entre 300 MHz y 300 GHz. El proceso de calentamiento con

microondas tiene lugar mediante dos principios: a) el mecanismo de conducción iónica, que se debe a la resistencia parcial de las cargas a seguir los cambios de un campo eléctrico; b) el mecanismo de rotación de dipolos, en el cual las moléculas polares rotan para orientarse con el campo electromagnético de las microondas, generando colisiones entre las moléculas y produciendo un incremento en la temperatura de la muestra.

En la etapa de envejecimiento de los materiales tipo hidrocalumita se utilizó un horno microondas de laboratorio marca MILESTONE ETHOS TOUCH CONTROL equipado con una sonda térmica, en condiciones de reflujo o autoclave (ver figura 8):

- Para las muestras envejecidas en microondas a reflujo, se colocó la solución precipitada en un matraz de fondo redondo conectado a un reflujo. El matraz se depositó sobre un soporte y se introdujo una sonda térmica para controlar la temperatura. Este procedimiento se realizó mediante agitación magnética a 60 ºC durante 6 h.

Figura 8. Montaje microondas en autoclave y reflujo utilizado en el tratamiento hidrotérmico de las muestras.

- Para las muestras envejecidas en microondas y autoclave se utilizaron 6 autoclaves de teflón con capacidad de 85 ml, con un volumen de muestra de 55 ml por autoclave. Los reactores se depositaron en un rotor de 6 posiciones. El envejecimiento se llevó a cabo a una temperatura de 180 ºC

controlada por una sonda térmica y bajo agitación magnética. El tratamiento hidrotérmico se realizó durante 1 o 3 h. Para observar el efecto de la temperatura en la preparación de estos materiales, se envejeció parte de la solución precipitada a partir de sales de nitratos en microondas y autoclave a 100 ºC durante 1 h.

3.2.4. Calcinación de hidróxidos dobles laminares (LDH) tipo hidrocalumita

Todas las CaAl-LDH preparadas anteriormente se calcinaron en una mufla marca Carbolite CWF11/5P8, a una temperatura de 450 ºC durante 15 h. Para determinar la influencia del tiempo de calcinación, y el efecto de la utilización de un sistema dinámico con paso de un gas inerte durante la calcinación, se calcinó una muestra a 450 °C durante 24 h en la mufla, y otra a 450 °C durante 10 h en un reactor de cuarzo tubular en flujo de N_2 (1 ml/s), respectivamente. Por último, para estudiar el efecto de la temperatura de calcinación, algunas muestras se calcinaron a 750 °C durante 4 h en la mufla.

3.2.5. Modificación de hidrocalumitas con KOH y KNO_3

Con el fin de aumentar la basicidad en las hidrocalumitas, se ha impregnado una muestra con una solución de KOH (0.02 g de K_2O/ g de muestra). La solución fue adicionada gota a gota a 1 g de hidrocalumita y fue agitada para obtener una mezcla homogénea. Una vez adicionada la solución de KOH se secó a 80 ºC toda la noche.

Para poder realizar una comparación con la hidrocalumitas calcinadas se ha impregnado una hidrocalumita, adicionando gota a gota con una solución de KNO_3. Una vez impregnado, se calcinó a 450 ºC durante 15 h

3.3. Preparación de otros materiales catalíticos

Con el fin de comparar diferentes tipos de catalizadores en la reacción de descarboxilación de carbonato de glicerol, se ha sintetizado un material a pH 8 siguiendo la metodología utilizada en la preparación de materiales tipo

hidrocalumita; además, se sintetizaron dos hidrotalcitas y tres hidróxidos de aluminio.

Se ha preparado una hidrocalumita a pH 8 mediante el método de precipitación de sales, a partir de sales de nitratos bajo ultrasonidos a 60 ºC. Una vez precipitadas las sales, la muestra se envejeció en reflujo y calentamiento convencional a 60 ºC durante 24 h. Además, para añadir mayor acidez a esta muestra, se impregnó con una solución de H_3PO_4 0.7 M. Una vez impregnada, se secó a 80 ºC toda la noche.

Se prepararon 2 hidrotalcitas (Ni/Al=4 y Mg/Al=3) mediante el método de precipitación de sales a pH 8 constante. La hidrotalcita preparada con sales metálicas de Ni y Al se preparó a temperatura ambiente, bajo vigorosa agitación magnética. La hidrotalcita preparada con sales metalicas de Mg y Al se precipitó a 70 ºC bajo vigorosa agitación magnética. Una vez completada la precipitación de las sales metálicas, las soluciones resultantes de las dos hidrotalcitas se envejecieron a la respectiva temperatura de precipitación durante 18 h.

Por último, se prepararon 3 hidróxidos de aluminio a 75 °C, utilizando una solución de nitrato de aluminio nonahidratado. El pH fue llevado a 8 utilizando una solución de amoniaco al 0.25 %. El precipitado resultante se envejeció en microondas bajo reflujo a 75 °C durante 1, 2 y 3 h. Finalmente, las muestras se lavaron hasta pH neutro y se secaron a 80 ºC toda la noche.

3.4. Técnicas de caracterización

3.4.1. Difracción de rayos X (DRX)

La técnica de difracción de rayos X permite determinar las fases cristalinas presentes en las muestras, así como las diferencias de cristalinidad entre ellas. También se utiliza para calcular los parámetros de celda, a partir de las distancias interplanares de los picos característicos de cada fase cristalina. Esto es posible gracias a la difracción de un haz de rayos X que incide sobre una muestra cristalina con un determinado ángulo θ. El fenómeno de difracción sólo ocurre si el sólido analizado cumple las condiciones de la ley de Bragg (1):

$$n\lambda = 2d_{hkl}\sin\theta \qquad (1)$$

la ecuación (1) indica la relación entre el espacio interplanar (d_{hkl}), la longitud de onda de la radiación X (λ) y el ángulo de incidencia del haz de rayos X (θ), siendo *n* un numero entero (Figura 9).

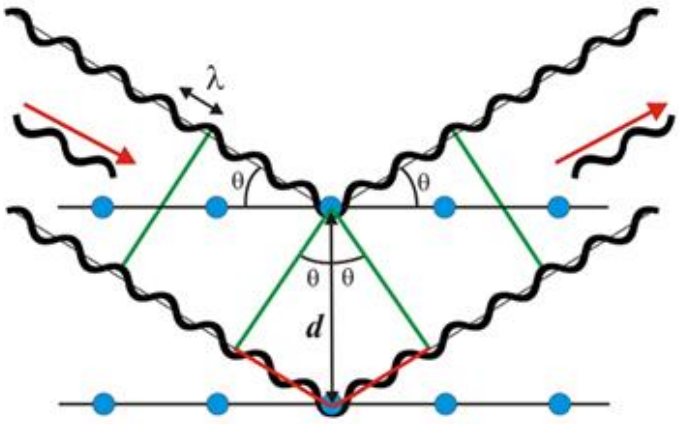

Figura 9. Esquema del cumplimiento de la ley de Bragg.

En el caso de la difracción en polvo, se obtiene el llamado "cono de radiación difractada" ya que los cristales de la muestras en polvo presentan diferentes orientaciones.

En esta tesis se ha utilizado un difractómetro Siemens D5000 (Bragg-Brentano con geometría de para focalización y goniómetro vertical θ-θ), equipado con un cromador de grafito y un haz difractor Soller. La muestra se tritura antes del análisis para obtener un polvo cristalino que se distribuye sobre una superficie completamente plana y se introduce en un portamuestras de Si(510). Se empleó un rango de difracción angular 2θ entre 5º y 70º. Los datos se recogieron con una medida angular de 0.05º por 3 s en rotación simple. La radiación CuKα con filtro de níquel y λ= 1.45 Å, se obtiene a partir de un tubo de rayos X de cobre operando a 40 kV y 30 mA.

Las fases cristalinas se identificaron utilizando las siguientes fichas de la base de datos Joint Committee for Powder Diffraction Sources (JCPDS):

35-0105 Cloruros CaAl-LDH $Ca_2Al(OH)_6Cl{\cdot}2H_2O$

89-6723 Nitratos CaAl-LDH $Ca_2Al(OH)_6NO_3{\cdot}2H_2O$

89-0217 Katoita $Ca_3Al_2(OH)_{12}$

86-2340 Calcita $CaCO_3$

48-1882 Mayenita $Ca_{12}Al_{14}O_{33}$

37-1497 Lima CaO

15-0087 Takovita $Ni_6Al_2(OH)_{16}(CO_3,OH){\cdot}4H_2O$,

89-0460 Hidrotalcita $(Mg_{0.667}Al_{0.333})(OH)_2(CO_3)_{0.167}(H_2O)_{0.5}$

73-6509 Boehmita γ-AlO(OH)

74-1775 Gibbsita γ-$Al(OH)_3$

74-0087 Bayerita α-$Al(OH)_3$.

El difractograma es una representación de los picos de difracción. Cada pico pertenece a una difracción (*hkl*) y se caracteriza por el valor del ángulo 2θ y por su intensidad. Cada fase cristalina tiene un conjunto de picos característicos que son más estrechos cuando las muestras son más cristalinas y el tamaño de partícula es más grande.

El cálculo del tamaño de cristalito se realizó de acuerdo con la ecuación de Scherrer (2) empleando el pico (006) y el pico (002) para los materiales tipo hidrocalumita preparados con cloruros o nitratos, respectivamente.

$$dp = \frac{k\lambda}{B \cdot \cos\theta} \qquad (2)$$

en la ecuación de Scherrer, *dp* es el diámetro de partícula, λ es la longitud de onda de radiación, θ es el ángulo de difracción, *k* es la constante de Scherrer, que tiene un valor medio de 0.9, y *B* es el ancho del pico a media altura (FWHM, full widht at half maximun) expresado en radianes.

Se calcularon los parámetros de celda de las muestras CaAl-LDH a partir de la ecuación que relaciona las distancias interplanares (d_{hkl}) con los parámetros de celda (*a*,*b*,*c*) (que son funciones de la simetría espacial de cada muestra). El parámetro de celda *a*, se calculó a partir del pico (110) con la siguiente ecuación (3):

$$a = 2 \cdot d_{(110)} \qquad (3)$$

mientras que el parámetro de celda c, se calculó a partir del pico (006) y (002) para las CaAl-LDH preparadas con cloruros y nitratos, utilizando la ecuación (4) y (5), respectivamente.

$$c = 6 \cdot d_{(006)} \qquad (4)$$

$$c = 2 \cdot d_{(002)} \qquad (5)$$

El análisis cuantitativo de mezclas de fases cristalinas de los materiales tipo hidrocalumita se realizó mediante el método de Rietveld a partir de los datos obtenidos mediante difracción de Rayos X.[19]

3.4.2. Espectroscopía de emisión por plasma de acoplamiento inductivo (ICP-OES)

La espectroscopía de emisión por plasma acoplado inductivamente, ICP-OES, es una técnica de análisis que utiliza una fuente de plasma para disociar la muestra en los átomos o iones que la constituyen. Estos átomos son excitados a un nivel en el que emiten luz de una longitud de onda característica (la longitud de onda nos permite determinar el metal cualitativamente). Un detector mide la intensidad de la luz emitida, y calcula cuantitativamente la concentración del elemento particular en la muestra.

El análisis elemental de las muestras se obtuvo con un analizador ICP-OES de Spectro Arcos. En la digestión de todas las muestras se utilizaron 2 ml de HNO_3 concentrado en 50 mg de muestra. La disolución resultante se llevó a un volumen de 25 ml, y finalmente 1 ml de esta solución se diluyó en 25 ml de agua destilada. Todos los análisis se realizaron por triplicado.

3.4.3. Fisisorción de nitrógeno

La fisisorción de nitrógeno es una técnica muy reconocida en la caracterización de sólidos que permite determinar el área superficial, la porosidad y la distribución de tamaño de poro en muestras sólidas. La fisisorción de nitrógeno se basa en la adsorción de N_2 a una temperatura de -196 ºC en una monocapa del sólido y posteriormente en multicapas, dependiendo de la presión de N_2.

Las isotermas de adsorción-desorción de nitrógeno representan el volumen de nitrógeno adsorbido-desorbido en la superficie de las muestras en función de la presión relativa de N_2. En este proceso se produce histéresis cuando la isoterma de adsorción no coincide con la isoterma de desorción. En la Figura 10, se pueden observar los 6 tipos de isotermas según la clasificación de Brunauer, Deming y Teller.[20]

- Isoterma tipo I: es característica de sólidos microporosos con una superficie externa muy pequeña. La accesibilidad de los microporos es limitante del volumen de gas adsorbido en el material.
- Isoterma tipo II: corresponde a la adsorción en mono-multicapas, en sólidos no porosos o macroporosos, que representan heterogeneidad superficial. El punto *B* indica el inicio de la adsorción multicapa.
- Isoterma tipo III: aparece cuando la interacción adsorbato-adsorbente es débil, menor que la existente entre las moléculas de adsorbato.
- Isoterma tipo IV: sigue el patrón de la isoterma tipo II en la zona de presiones bajas e intermedias (monocapa-multicapa). Este tipo de isoterma presenta histéresis a presiones relativas altas y es característica de materiales mesoporosos.

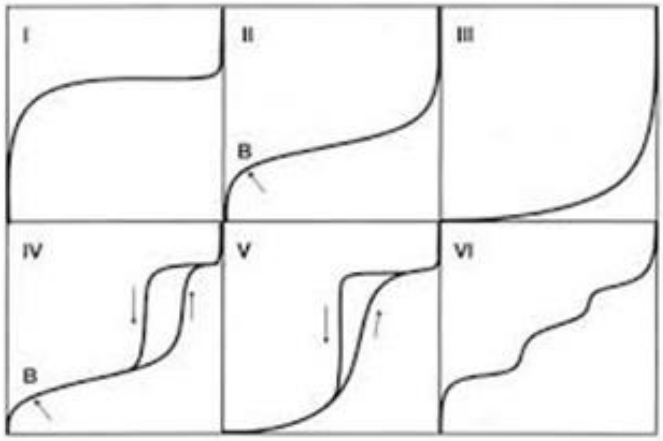

Figura 10: Tipo de isotermas de adsorción-desorción de nitrógeno

- Isoterma tipo V: está relacionada con la isoterma tipo III, donde las interacciones adsorbato-adsorbente son débiles. Este tipo de isoterma presenta una adsorción débil al principio, seguida de condensación capilar. Nos indica la presencia de mesoporos en el sólido.
- Isoterma tipo VI: no es muy común en la naturaleza; aparece cuando la adsorción se realiza en superficies muy homogéneas, donde cada capa comienza a formarse cuando la anterior está ya prácticamente completa.

La presencia de histéresis entre adsorción-desorción se da fundamentalmente en sólidos que presentan características mesoporosas, es decir, en sólidos que presentan isotermas tipo VI y V. Los tipos de histéresis se pueden clasificar según De Boer en 5 grupos dependiendo de la forma del poro (Figura 11).[21]

- Histéresis tipo A: es característica de poros tubulares abiertos en los extremos.
- Histéresis tipo B: está relacionada con poros formados por láminas cristalinas paralelas, separadas por pequeñas partículas y en algunos casos, por defectos cristalinos.

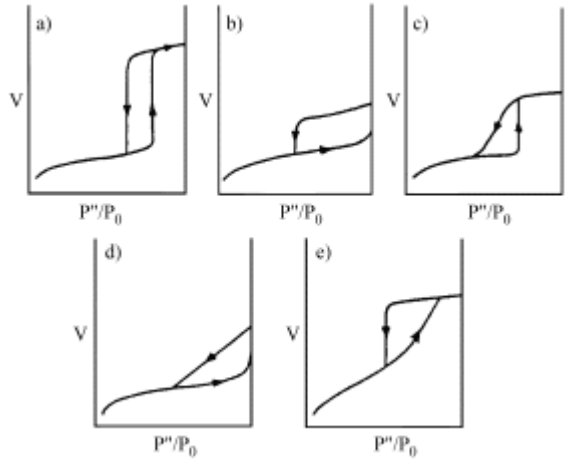

Figura 11: Tipos de histéresis según De Boer.

- Histéresis tipo C y D: derivan del tipo A y B, respectivamente. La histéresis de tipo C corresponde a poros cónicos o piramidales y la tipo D a poros formados entre láminas cristalinas no paralelas.
- Histéresis tipo E: indica la presencia de poros bastante anchos con una boca muy estrecha.

El área superficial de los materiales porosos se determina habitualmente mediante el método BET (Brunauer, Emmett y Teller), utilizando la ecuación (6):

$$\frac{P}{V(P^{\circ}-P)} = \frac{1}{V_m \cdot C} + \frac{(C-1)\cdot P}{V_m \cdot C \cdot P^{\circ}} \qquad (6)$$

donde V es el volumen adsorbido a una determinada presión relativa P/P^o y V_m es el volumen de la monocapa. El parámetro C, está relacionado con el calor de adsorción en la monocapa. El intervalo de linealidad está restringido a una zona limitada de la isoterma que normalmente está entre valores de presión relativa P/P^o de 0.05-0.30.

El valor de área BET se calcula a partir del volumen adsorbido en la monocapa mediante la ecuación (7):

$$A\ (BET) = \frac{V_m \cdot L \cdot A_m}{M} \qquad (7)$$

donde L es el número de Avogadro, A_m es el área ocupada por la molécula de nitrógeno adsorbida (0.162 mn^2 a -196 ºC) y M es la masa del gas adsorbido.

Para las medidas de fisisorción de N_2 se utilizó un equipo Quadrasorb *SI.*Automated surface area & Pore Size Analyzer (de marca Quantachrome). Todas las muestras fueron desgasificadas a 90 ºC durante 24 h. La distribución del tamaño de poro se determinó a partir de las isotermas obtenidas empleando el método BJH (Barret, Joyner y Halenda).

3.4.4. Análisis Termogravimétrico (TGA)

Esta técnica consiste en observar la variación de peso de una muestra cuando se somete a un tratamiento térmico en una atmósfera seleccionada (O_2, N_2, H_2, etc). Un termograma representa la variación de peso de la muestra en función de la temperatura, lo que permite identificar las diferentes etapas que se producen durante el tratamiento térmico. Al representar la derivada de la función se puede observar el máximo punto de inflexión de temperatura en cada etapa.

El análisis termogravimétrico de los materiales tipo hidrocalumita se llevó a cabo en una termobalanza Perkin Elmer TGA 7 con precisión de ± 1 μg. Se pesaron aproximadamente 50 mg de muestra y se calentaron en un flujo de N_2 desde 25 °C a 1000 °C a una velocidad de 5 °C/min.

3.4.5. Espectroscopía electrónica de barrido (SEM)

La microscopía electrónica de barrido es una técnica simple que permite observar el tamaño y la morfología de las partículas en materiales sólidos. Esta técnica se basa en el bombardeo de una muestra mediante un haz de electrones. Este haz de electrones (enfocado por lentes electromagnéticas a través de una columna de alto vacío) se proyecta sobre la superficie de la muestra donde los electrones rebotan o provocan la emisión de electrones secundarios. Estos electrones secundarios son registrados por un detector que proporciona una imagen tridimensional.

Las micrografías se obtuvieron con un microscopio JEOL JSM-35C operando a un voltaje de aceleración en el intervalo de 15-30 kV, la distancia focal de 14 mm y los valores entre 5000 y 30000 aumentos, dependiendo de la muestra.

Para la preparación de las muestras se adicionó un adhesivo de grafito de doble cara a un soporte metálico. A continuación, se fijaron las muestras al adhesivo de grafito y se cubrieron con una capa de oro fina para aumentar su conductividad antes de ser analizadas.

3.4.6. Microscopía electrónica de transmisión (TEM)

En microscopía electrónica de transmisión un haz de electrones dirigido a través de lentes electromagnéticas se proyecta sobre una muestra muy delgada que se encuentra en una columna de alto vacío. El haz de electrones atraviesa la muestra, proyectándose sobre una pantalla fluorescente formando una imagen visible, obteniendo información morfológica de la muestra a partir de los diferentes haces de electrones.

La microscopía electrónica de transmisión de las muestras se realizó en un microscopio electrónico *JEOL* Modelo 1011, con un acelerador de voltaje de 80 kV. Una pequeña cantidad de muestra se dispersó en etanol y una gota de la suspensión resultante se depositó sobre un polímero de carbono soportado en una rejilla de cobre. Se evaporó el disolvente a temperatura ambiente antes de las mediciones. En los análisis realizados se utilizaron valores de ampliación entre 20-100 aumentos.

3.4.7. Espectroscopía infrarroja con transformada de Fourier (FT-IR)

La técnica de espectroscopía infrarroja con transformada de Fourier se utiliza para el estudio cualitativo de los grupos funcionales presentes en una muestra. Cuando los grupos funcionales y las unidades estructurales de los sólidos absorben la radiación infrarroja experimentan una alteración en su momento dipolar, como consecuencia de sus movimientos de vibración y rotación.

El espectro infrarrojo se divide en tres regiones (infrarrojo cercano, medio y lejano), en el rango de longitudes de ondas entre 800 y los 400000 nm (0.8 y 400 μm). Las unidades de medida de la técnica FT-IR son la longitud de onda (nm) o el

número de onda (cm^{-1}). Esta técnica se centra en la región de infrarrojo medio comprendida entre 4000 a 400 cm^{-1} o 2500 a 25000 nm.

Los espectros infrarrojos se registraron en un espectrómetro FT-IR Nicolet 380. Los espectros se adquirieron por la acumulación de 100 scans a una resolución de 4 cm^{-1} en el rango de 400-4000 cm^{-1}. Las muestras se mezclaron con KBr en una relación de masa de 1:100.

Además, se utilizó pivalonitrilo como molécula sonda para estudiar la acides de las muestras. Con este fin, se activó a 400 ºC durante 1 h y bajo vacío, una pastilla de muestra pura dentro de una celda de IR. El pivalonitrilo fue introducido a temperatura ambiente, y evacuado para eliminar las especies fisisorbidas. Luego la adsorción y desorción se continuó a 100 ºC y 400 ºC. Los espectros infrarrojos de adsorción y desorción de pivalonitrilo fueron substraídos y analizados utilizando el programa OMNIC.

Para los análisis de adsorción de acetonitrilo se preparó una pastilla de muestra pura y se activó a 400 ºC durante 1 h en vacío. Una vez a temperatura ambiente se adsorbió el acetonitrilo en la superficie del material durante 10 min. Posteriormente, se tomó un espectro del gas y otro de la muestra a temperatura ambiente. Sin desorber, la muestra se calentó a 100 °C durante 10 min y se volvió a analizar un espectro (tanto de la muestra como del acetonitrilo gas). El proceso se repitió para 200 ºC, 300 ºC y 400 °C, cada 10 min.

Estos análisis se realizaron como resultado de una estancia de 3 meses en el laboratorio de Química de la superficie y Catálisis Industrial de la Universidad de Génova (Italia), bajo la supervisión del Profesor Guido Busca.

3.4.8. Espectroscopía Raman

La espectroscopía raman proporciona información química y estructural, en pocos segundos, mediante el análisis vibracional y rotacional de especies químicas. Es complementaria al infrarrojo, pues vibraciones inactivas en IR pueden ser activas en Raman.

Esta técnica se basa en el análisis de la luz dispersada por un material al incidir un haz monocromático sobre él. Una pequeña porción de la luz es dispersada

inelásticamente experimentando ligeros cambios de frecuencia que son característicos del material analizado (e independiente de la frecuencia de la luz incidente).

El análisis de las muestras se realizó con un Espectrómetro Raman FT-IR de marca RENISHAW, equipado con un Microscopio confocal Leica DM 2500, con un objetivo de 50x. Se utilizó un láser de 514 nm para el rango de 3000-4000 cm^{-1} y el láser 785 nm para el rango de 100-2000 cm^{-1}, con un tiempo de exposición de 60 s. Se realizaron 2 scans con una potencia del láser del 10 %.

3.5. Evaluación catalítica

3.5.1. Reacción catálitica de glicerol con carbonato de dimetilo para obtener carbonato de glicerol utilizando calentamiento convencional o microondas

La actividad catalítica de los catalizadores preparados se estudió en la reacción de transesterificación de glicerol con carbonato de dimetilo (DMC) para obtener carbonato de glicerol (Figura 12).

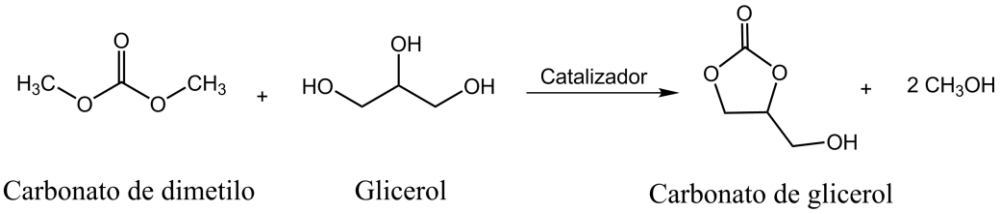

Figura 12. Esquema de la reacción catalítica de transesterificación de glicerol con carbonato de dimetilo (DMC) para obtener carbonato de glicerol.

El DMC y el glicerol se mezclaron en una relación 3.5:1 (21 g y 6.16 g, respectivamente) en un balón de fondo redondo de tres bocas de 50 ml, equipado con un agitador magnético y un condensador de reflujo. La temperatura se reguló por medio de una sonda térmica tanto en calentamiento convencional como en microondas (Figura 13). La mezcla se calentó a 90 ºC con microondas o en un baño de aceite (según el caso de estudio), con agitación constante bajo atmósfera de N_2 a diferentes tiempos de reacción. Se añadieron 0.15 g de catalizador para iniciar la

reacción. La mezcla resultante después de la reacción se filtró para separar los productos de reacción del catalizador y se lavó 3 veces con 10 ml de metanol. La mezcla filtrada se evaporó en un rotavapor para separar el DMC y metanol del producto.

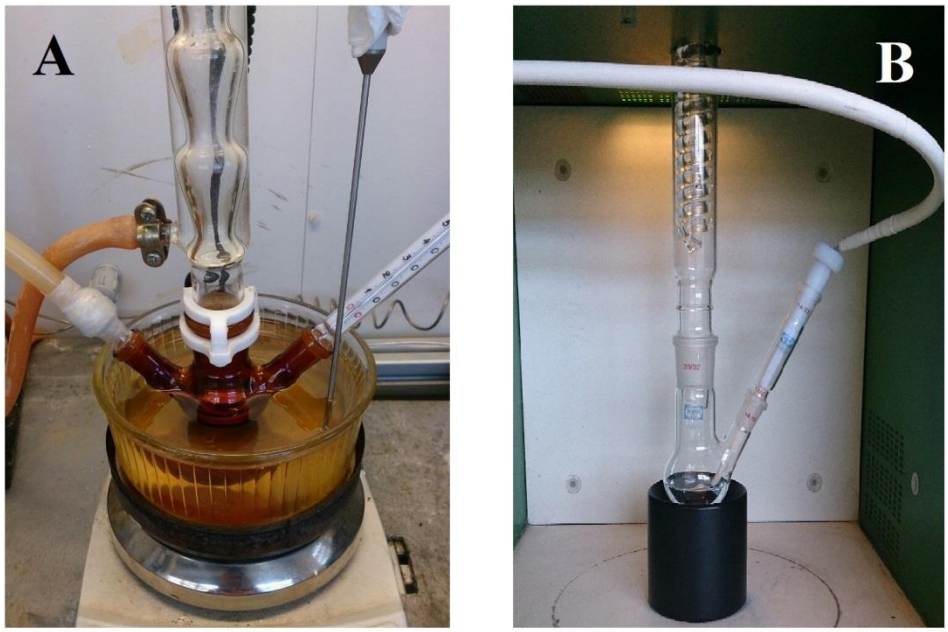

Figura 13. Montaje de la reacción de transesterificación de glicerol con DMC para obtener carbonato de glicerol. A) calentamiento convencional, B) calentamiento con microondas.

Para evaluar la conversión de glicerol y la selectividad a carbonato de glicerol, se preparó una solución (productos de reacción 9:1 de butanol) utilizando butanol como patrón interno. 1 μl de la solución resultante se analizó mediante cromatografía de gases. Los análisis de cromatografía de gases se realizaron en un equipo ZHIMADSU GC-2010, equipado con un autoinyector y un detector de ionización de llama. Se utilizó una columna SUPRAWAX - 280 (60 m x 0,25 mm x 50 μm). Se seleccionó el modo de inyección Split y una relación de separación de 20/1, utilizando Helio como gas portador. Las temperaturas del inyector y del detector se fijaron en 250 ºC, se realizó una rampa de temperatura del horno que se inició a 120 ºC durante 3 min y se incrementó a 15 ºC/min hasta 200 ºC, a

continuación, la temperatura se aumentó a 20 ºC/min hasta 250 ºC y se mantuvo durante 30 min.

Con el fin de cuantificar el carbonato de glicerol producido en la reacción de transesterificación, se realizaron líneas de calibración utilizando reactivos comerciales, glicerol (VWR, CAS 56-81-5), carbonato de glicerol (TCI, CAS 931-40-8) y glicidol (Sigma-Aldrich, CAS 556-52-5). La conversión de glicerol y selectividad a carbonato de glicerol y glicidol se calcularon utilizando las ecuaciones (8), (9) y (10):

$$\%\, C_{Glicerol} = \frac{número\ de\ moles\ de\ glicerol\ convertido}{número\ de\ moles\ de\ glicerol\ iniciales} \times 100 \qquad (8)$$

$$\%\, S_{GC} = \frac{número\ de\ moles\ de\ glicerol\ convertidos\ a\ GC}{número\ de\ moles\ de\ glicerol\ convertidos} \times 100 \qquad (9)$$

$$\%\, S_{Glicidol} = \frac{número\ de\ moles\ de\ glicerol\ convertidos\ a\ glicidol}{número\ de\ moles\ de\ glicerol\ convertidos} \times 100 \qquad (10)$$

Finalmente se realizaron tres ciclos de reutilización de los mejores catalizadores en la reacción de transesterificación del glicerol, tanto en microondas como por calentamiento convencional a 90 ºC durante 3 h de reacción en atmosfera inerte y bajo agitación magnética.

3.5.2. Reacción de descarboxilación del carbonato de glicerol para la obtención de glicidol utilizando calentamiento convencional

La actividad catalítica de los catalizadores preparados se estudió en la reacción de descarboxilación de carbonato de glicerol (GC) para la obtención de glicidol (Figura 14).

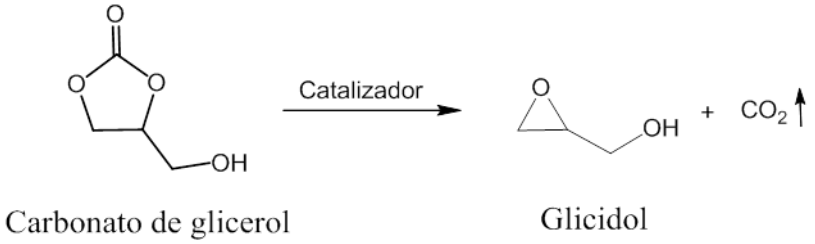

Figura 14. Esquema de la reacción catalítica de descarboxilación de GC para la obtención de glicidol.

Para este propósito se depositaron 1,77 g de carbonato de glicerol en un matraz de fondo redondo de 3 bocas acoplado a un reflujo, el cual fue calentado a 150 °C durante 16 h bajo atmósfera inerte. Una vez completada la reacción, los productos de reacción fueron analizados mediante cromatografía de gases, siguiendo la metodología descrita en la sección 3.5.1. La conversión de carbonato de glicerol y selectividad a glicidol se calcularon utilizando las ecuaciones (11) y (12), respectivamente.

$$\%\, C_{GC} = \frac{número\ de\ moles\ de\ GC\ convertido}{número\ de\ moles\ de\ GC\ iniciales} \times 100 \qquad (11)$$

$$\%\, S_{Glicidol} = \frac{número\ de\ moles\ de\ GC\ convertidos\ a\ glicidol}{número\ de\ moles\ de\ GC\ convertidos} \times 100 \qquad (12)$$

UNIVERSITAT ROVIRA I VIRGILI
HYDROCALUMITE-BASED CATALYSTS FOR GLYCEROL REVALORIZATION.
Judith Cecilia Granados Reyes
Dipòsit Legal: T 1362-2015

CHAPTER 4

Results and discussion

Synthesis and characterization of hydrocalumite-type materials

UNIVERSITAT ROVIRA I VIRGILI
HYDROCALUMITE-BASED CATALYSTS FOR GLYCEROL REVALORIZATION.
Judith Cecilia Granados Reyes
Dipòsit Legal: T 1362-2015

4.1. Background about the synthesis of hydrocalumite-type materials

Hydrocalumite-type materials are part of the family of Layered Double Hydroxides (LDHs). The hydrocalumites are formed by layers of Ca and Al hydroxides, and by Cl^- anions in the interlaminar space to compensate the positive charge of the layers. These materials are known as "Friedel's salt", and present the following formula: $Ca_2Al(OH)_6Cl{\cdot}2H_2O$ (see Figure 6, Chapter 3.1).[22,23] Hydrocalumite-type materials have attracted much interest in research studies due to its multiple applications in catalysis;[24–28] in the pharmaceutical industry (due to its no-toxicity);[29,30] in water treatment plants;[13,31–43] and in the optimization of concrete properties, among other uses.[15,44–47]

There are different methodologies to synthesize hydrocalumite-type materials reported in the literature. Mora *et al*. (2011) introduced the Sol-Gel method, in which calcium propionate was dissolved in ethanol (containing a small amount of HCl) under refluxing with stirring, and the resulting solution was mixed with acetone containing aluminium acetylacetonate. This mixture was adjusted to pH 10 with ammonia until a gel was formed, and finally, the gel was isolated by centrifugation, washed and dried in a stove.[48] The same authors also reported the synthesis of CaAl-LDH by the method of homogeneous precipitation with urea, which consists of adding solid urea to a solution containing calcium and aluminium nitrates in a Ca/Al ratio of 2. The transparent solution obtained was heated at 100 ºC and the resulting solid was washed and dried.[48]

Another methodology for the synthesis of hydrocalumites is that used by Cota *et al*. (2010) which consists of a hydrolysis reaction of the Ca and Al containing alkoxides (calcium methoxide and aluminium triethoxide in a Ca/Al ratio of 2). These compounds were simultaneously dissolved into a beaker with water at room temperature. A gel was immediately formed, which was aged for 18 h at 0, 25 and 60 ºC under stirring in an inert atmosphere and pH of 13.4. The gels obtained were separated by centrifugation and washed with distilled water and ethanol, and finally dried.[24]

Zhang *et al.* (2012) reported the synthesis of CaAl-LDH by hydrating freshly prepared tricalcium aluminate in a $CaCl_2$ solution by the following procedure: a solid phase reaction was used to synthesize tricalcium aluminate by heating $CaCO_3$ and low-alkali Al_2O_3 in a molar ratio of 3:1 at high temperature until the free lime content was reduced to below 0.5 %. The solid phase was mixed with $CaCl_2{\cdot}6H_2O$ solution. The suspension was continuously shaken for more than 18 h under N_2 at 55 ºC, during the hydration process. Finally, the suspension was filtered, washed with water and dried overnight.[33]

Although there are various methods of synthesis of hydrocalumite-type materials, the most used is the coprecipitation of salts, typically chloride and nitrate salts. López-Salinas *et al*. (1996) reported the synthesis of hydrocalumite-type materials by the co-precipitation method.[49] They prepared a Ca–Al solution by dissolving $Al(NO_3)_3{\cdot}9H_2O$ and $Ca(NO_3)_2{\cdot}4H_2O$ in distilled water (with a Ca/Al molar ratio of 2). This solution was added dropwise to a NaOH solution and kept under stirring in an inert atmosphere. The resulting gel was refluxed by using a glycerin bath at 80 °C for 12 h, constant agitation and controlled pH at 11. The mixture was filtered, washed up with abundant distilled water and dried at 100 °C for 18 h.

Other authors follow the methodology reported by Birnin-Yauri *et al*. (1998)[50] to synthesize hydrocalumites by the coprecipitation method. That is, by adding tricalcium aluminate slowly to a $CaCl_2$ solution under vigorous stirring. Then, the mixed suspension was aged between 45 and 55 ºC for 24 h under stirring, with a final pH of 10.5. The precipitate was finally filtered, washed and dried at 100 ºC.[34,39,43]

The most common CaAl-LDH is synthesized from chloride salts. Vieille *et al.* (2003) synthesized hydrocalumites by following the methodology by Miyata, [51] who synthetised hydrotalcite-type materials by the coprecipitation method using chloride and nitrate salts. In the Vieille's synthesis a mixed solution of 0.66 M $CaCl_2{\cdot}2H_2O$ and 0.33 M $AlCl_3{\cdot}6H_2O$ was added dropwise to a reactor previously filled of a mixture of water and ethanol in a 2:3 volumetric ratio at 65 °C under vigorous magnetic stirring and nitrogen atmosphere. The pH was kept constant at

11.5 by the simultaneous addition of 2 M NaOH. The precipitate was aged in the mother solution for 24 h. The precipitate was centrifuged, washed and finally dried under vacuum at room temperature.[23] Segni *et al*. (2006) also used the methodology by Miyata, but the synthesis was carried out at room temperature under vigorous stirring and nitrogen atmosphere and the precipitate obtained was aged in the mother solution at 65 ºC for 24 h.[13]

Mora *et al*. (2011) used the methodology proposed by Lopez-Salinas but with some variations. First, they prepared two solutions containing calcium nitrate and aluminium nitrate. The mixture was slowly dropped over to a Na_2CO_3 solution at pH 10 at 60 ºC under vigorous stirring. The suspension obtained was kept at 80 ºC for 24 h, after which the solid was filtered and washed.[48]

Sankaranarayanan *et al.* (2012) employed the methodology described by Miyata, but precipitating an aqueous solution of calcium and aluminium chloride in a solution of NaCl. The aging was performed at 65 ºC for 18 h under N_2 atmosphere. Finally, the white precipitate was filtered, washed several times with hot water and dried in a vacuum desiccator for 48 h.[52] Guo *et al.* (2013) also used the methodology of Miyata for the synthesis of hydrocalumites. However, the precipitation temperature was kept at 25 ºC and the aging was done at 65 ºC for 24 h. The solid product was dried at 50 ºC for 24 h.[53]

De Sá *et al*. (2013) synthesized CaAl-LDH by coprecipitation at variable pH. The resulting white precipitate was dried at 85 ºC for 18 h under nitrogen atmosphere. Lastly, the material was washed and dried at 35 ºC.[42]

Sanchez-Cantu *et al.* (2013) synthesized CaAl-LDH by coprecipitation but modifying the procedure described by López-Salinas *et al*. Calcium and aluminium nitrate were dissolved in deionized water. Separately, a solution containing KOH and deionized water was prepared. Afterwards, the solution of salts was placed in a glass reactor and the KOH solution was added dropwise into the slurry until a pH of 12.5. The slurry was aged at 60 ºC for 12 h under vigorous stirring. The precipitate was washed with hot deionized water and dried at 100 ºC overnight.[26] Linares *et al*. (2014) also used the methodology of Lopez-Salinas for the synthesis of hydrocalumites to be applied as antacids.[30]

In the last decade microwaves have been used as a heating source in the synthesis of several materials, such as zeolites, saponites, hectorites, etc. It is mainly because the use of microwaves considerably reduces the synthesis time and modifies the samples properties (e.g. higher crystallinity of the samples at a shorter aging time), that it can be of interest for catalysis.[18,54–57]

The hydrothermal treatments are among the most interesting applications of the microwaves radiation. The fast heating of the suspension or solution within the autoclave leads to significant advantages compared to high pressure steel autoclaves used in conventional hydrothermal heating processes.[58] Several authors have studied the application of microwaves radiation in the synthesis of LDHs,[58–69] but there is only one paper about the synthesis of hydrocalumites with microwaves. Perez-Barrado *et al*. (2013) synthesized hydrocalumites by the coprecipitation method following the methodology by Vieille *et al*. but using microwaves during the aging treatment. The authors reported that the hydrocalumites aged using microwave irradiation showed larger crystallite sizes along the stacking direction than those aged by conventional heating under the same conditions.[70]

The ultrasonic-assisted synthesis is another interesting technique to modify the properties of materials. The use of ultrasounds for the mixing of reagents leads to materials with more homogeneous composition, smaller particles sizes and higher specific surface areas than conventional samples.[17,18,56,57] Ultrasounds have been extensively used in the synthesis and modification of LDHs materials[71–75] but only some references report the use of this technique in the preparation of hydrocalumites. Li *et al*. (2013) prepared CaAl-LDH using the co-precipitation method under ultrasounds. They added quickly $Al(NO_3)_3 \cdot 9H_2O$ solutions to CaO solutions, which were in the ultrasonic washer for 10 min, and aged for 30 min by ultrasonic oscillation at 55 ºC. The pure LDH slurry was separated through washing and vacuum filtering, and then dried at 80 ºC.[76]

LDHs have been widely characterized by Infrared and Raman spectroscopy.[77–86] Aditionally, many studies in the last decades used nitriles as probe molecules in heterogeneous catalysts to analyze their acid and basic strength.[87–96] However, in the case of hydrocalumites there are very few

spectroscopic studies and the adsorption of probe molecules to study their acidity-basicity has not been performed yet.

In this section we present the results obtained in the study of the effect of microwaves, ultrasounds and interlayer anion on the synthesis of hydrocalumite-type materials through the classical techniques of characterization of solids (i.e. X-ray diffraction, nitrogen physisorption, elemental analysis, SEM and TEM); as well as a detailed Raman and Infrared spectroscopy chacterization of several prepared samples in order to study the influence of microwaves and ultrasounds in the synthesis of hydrocalumites. Finally, we study the acidity and basicity strength of several hydrocalumites by the adsorption of nitriles compounds as probe molecules.

4.1.1 Effect of microwaves, ultrasounds and interlayer anion on the hydrocalumites synthesis

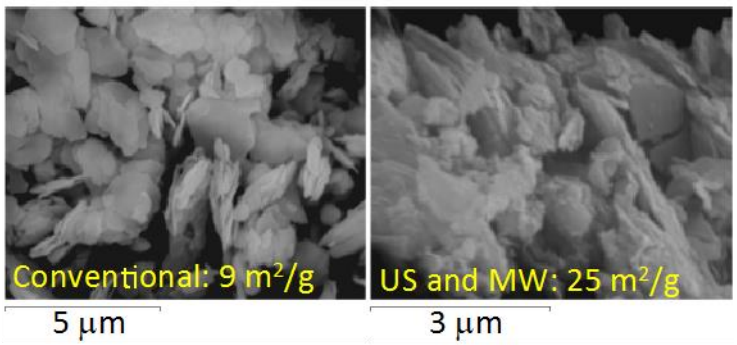

Abstract

Several hydrocalumites were precipitated from nitrate or chloride salts with and without ultrasounds, and aged hydrothermally in autoclave or by refluxing with and without microwaves. The use of ultrasounds during coprecipitation led to more crystalline hydrocalumites whereas the use of autoclave and microwaves during aging, favoured the formation of a secondary phase, katoite, in addition to hydrocalumite. The presence of katoite affected the crystallization of hydrocalumite. Hydrocalumites with nitrates as interlayer anions were slightly less crystalline than those prepared with chloride anions. Additionally, the synthesis with nitrates resulted in the formation of higher amounts of katoite in autoclave conditions. Hydrocalumites exhibited thin regular hexagonal layers, as observed by SEM and TEM, with lower particle size for the samples aged with microwaves. Interestingly, the hydrocalumite prepared from nitrates by coprecipitation in ultrasounds and aged under microwaves resulted in the highest surface area measured (25 m^2/g) according to the additional mesoporosity observed by N_2 physisorption.

Introduction

Hydrocalumite-type compounds (HC) belong to the layered double hydroxides (LDH) family. LDHs are anionic clays with general formula $[M^{II}_{1-x}M^{III}_{x}(OH)_2][X^{q-}_{x/q}\cdot nH_2O]$ where $[M^{II}_{1-x}M^{III}_{x}(OH)_2]$ cation represents the layer composition, and $[X^{q-}_{x/q}\cdot nH_2O]$ the interlayer composition. In the particular case of hydrocalumites, the layers are formed by $[Ca_2Al(OH)_6]^+$ whereas the interlayers are composed of water molecules and anions (e.g. OH^-, NO_3^-, SO_4^{2-}, CO_3^{2-}, or Cl^-).[13,15,22,32,36,37,39,41,44] For hydrocalumite, Ca^{2+} and Al^{3+}, fixed in a molar ratio of two, are seven and six-fold coordinated, respectively, being the seventh ligand of the Ca-polyhedron a water molecule from the interlayer.[13] Hydrocalumites have been extensively used in the immobilization of toxic cations,[13,32,36,37,39–41,97] the optimization of concrete properties,[15,44–47] and, in less extent, for catalysis due to their basic properties.[24] The structure of hydrocalumites collapses at temperatures between 400 ºC and 600 ºC due to the dehydroxylation of their octahedral layers, giving rise to the formation of an amorphous, basic Ca-Al mixed oxide, $Ca(Al)O_x$, which may be also used as catalyst for organic reactions such as the Meerwein-Ponndorf-Verley reaction,[25] the isomerization of 1-butene[49] or the transesterification of castor bean oil and methanol.[26]

In the existing literature, hydrocalumites are usually prepared by the co-precipitation of calcium and aluminium salts (typically chlorides or nitrates) with NaOH at controlled pH in an inert atmosphere, to avoid the presence of carbonates, and with temperature (60-80 ºC), using conventional heating. Then, the coprecipitated gel is aged by refluxing at temperatures between 60-80 ºC for long times (24-48 h).[24,37,98] On the other hand, for the preparation of OH^- containing hydrocalumites, a direct method based on the controlled hydrolysis of Ca^{2+} and Al^{3+} alkoxides has been reported.[25] Other hydrocalumites preparation methods are the sol-gel methods and the homogeneous precipitation with urea.[24]

In recent years, the use of microwaves for the synthesis or modification of materials is becoming an important tool to decrease the synthesis time, with the subsequent energy saving, and to modify the sample properties, which can be of

interest for catalysis.[18,54,55,57,99] Additionally, ultrasounds is another interesting technique to improve the synthesis of materials since, when used for the mixing of reagents, allows obtaining materials with more homogeneous composition.[17,57,99] In a previous work, we synthesized hydrocalumites from chloride salts faster by using microwaves during the aging treatment (3 h) than by conventional heating (24 h).[70]

The aim of this work was to study the effect of using ultrasounds during the coprecipitation step, and microwaves during the aging treatment of several hydrocalumites, on their surface and basic properties. Hydrocalumites were synthesized from nitrate or chloride salts, and during the aging treatment autoclave or refluxing conditions were used. Several hydrocalumites were also prepared by conventional heating (with and without ultrasounds) for comparison.

Experimental

Samples preparation

Two series of hydrocalumites were synthesized by the co-precipitation method from different starting salts, chlorides (serie HC1) or nitrates (serie HC2), at 60 ºC under vigorous magnetic stirring using deionized/decarbonated water as well as nitrogen atmosphere. In a typical synthesis, two different aqueous solutions containing $CaCl_2 \cdot 2H_2O$ (sigma-Aldrich) and $AlCl_3 \cdot 6H_2O$ (Riedel-de Haën) or $Ca(NO_3)_2 \cdot 4H_2O$ (sigma-Aldrich) and $Al(NO_3)_3 \cdot 9H_2O$ (sigma-Aldrich) were prepared with a 2:1 molar ratio of Ca^{2+}/Al^{3+}. The solutions were added dropwise to a 500 ml four neck round-botton flack in an oil bath at 60 ºC previously filled with 250 ml of a mixture of water/ethanol in a 2:3 volumetric ratio. The pH was kept constant at 11.5 ± 0.1, by the simultaneous addition of an aqueous solution of 2 M NaOH (Panreac). After complete addition of the metallic salts, the two mother solutions were aged by several treatments.

Four samples were aged under refluxing, two at 60 °C for 24 h under conventional heating ($HC1R_{24}$ and $HC2R_{24}$) and the other two using microwave irradiation (Milestone ETHOS-TOUCH CONTROL) at 60 ºC for 6 h ($HC1RMw_6$ and $HC2RMw_6$). Other six samples were prepared using an autoclave. Two of them were aged in an oven at 180 °C for 1 h ($HC1AC_1$ and $HC2AC_1$) and other four were

aged in a microwave oven at 180 °C for 1 and 3 h ($HC1AMw_1$, $HC1AMw_3$, $HC2AMw_1$ and $HC2AMw_3$). Two more samples were prepared by aging the mother solution obtained from the coprecipitation of the nitrate salts in autoclave by conventional heating and with microwaves at 100 °C for 1 h (HC2AC100 and HC2AMw100).

Finally, four hydrocalumites were prepared by co-precipitation of chlorides salts and nitrates salts in the same conditions than those commented above, but using ultrasounds instead of magnetic stirring during coprecipitation. The ultrasound device was heated until 60 ºC. Once reached the temperature, we started the precipitation of salts under ultrasounds stirring, inert atmosphere and pH constant of 11.5. After coprecipitation, two samples were aged by refluxing under conventional heating at 60 ºC for 24 h ($HC1USR_{24}$, $HC2USR_{24}$) and two more were aged by refluxing with microwaves at 60 ºC for 6 h ($HC1USRMw_6$, $HC2USRMw_6$).

All samples were filtered at room temperature, washed with deionized water and then dried in an oven at 80 ºC overnight. . Table 1 summarizes the preparation conditions used.

Table 1. Aging treatments of hydrocalumites.

Sample	Ultrasound [a]	Aging			
		Heating	Technique	T (ºC)	Time (h)
$HC1R_{24}$	No	conventional	refluxing	60	24
$HC1RMw_6$	No	microwaves	refluxing	60	6
$HC1AC_1$	No	conventional	autoclave	180	1
$HC1AMw_1$	No	microwaves	autoclave	180	1
$HC1AMw_3$	No	microwaves	autoclave	180	3
$HC1USR_{24}$	Yes	conventional	refluxing	60	24
$HC1USRMw_6$	Yes	microwaves	refluxing	60	6
$HC2R_{24}$	No	conventional	refluxing	60	24
$HC2RMw_6$	No	microwaves	refluxing	60	6
$HC2AC_1$	No	conventional	autoclave	180	1
$HC2AMw_1$	No	microwaves	autoclave	180	1
$HC2AMw_3$	No	microwaves	autoclave	180	3
HC2AC100	No	conventional	autoclave	100	1
HC2AMw100	No	microwaves	autoclave	100	1
$HC2USR_{24}$	Yes	conventional	refluxing	60	24
$HC2USRMw_6$	Yes	microwaves	refluxing	60	6

a During precipitation

X-ray diffraction (XRD)

Powder X-ray diffraction patterns of the samples were obtained with a Siemens D5000 diffractometer using nickel-filtered CuKα radiation and detecting between 2θ values of 5º-70º. Crystalline phases were identified using the Joint Committee on Powder Diffraction Standards (JCPDS) files (035-0105- Calcium aluminium hydroxide chloride hydrate-$Ca_2Al(OH)_6Cl{\cdot}2H_2O$, 089-6723- Calcium Aluminun Nitrate Hydroxide Hydrate- $Ca_2Al(OH)_6NO_3{\cdot}2H_2O$ and 089-0217- Katoite- $Ca_3Al_2(OH)_{12}$).

Cell parameter *c* was calculated from (006) for hydrocalumites type chlorides and (002) for hydrocalumites type nitrates whereas cell parameter *a* was calculated from (110) for both. The Rietveld method was used to perform quantitative phase analysis of multicomponent mixtures from the X-ray powder

diffraction data. To apply this method it is only necessary to know the crystal structure of each phase of interest.[19]

Inductively Coupled Plasma- Optical Emission Spectroscopy (ICP-OES)

Elemental analysis of the samples was obtained with an ICP-OES analyser (Induced Coupled Plasma – Optical Emission Spectroscopy) from Spectro Arcos. The digestion of all hydrocalumites was carried out with concentrated HNO_3. Analyses were performed by triplicate.

Scanning electron microscopy (SEM)

Scanning electron micrographs were obtained with a JEOL JSM-35C scanning microscope operating at an accelerating voltage in the range 15-30 kV, work distance of 14 mm and magnification values between 5000 and 30000x.

Transmission electron microscopy (TEM)

Transmission electron microscopy of the samples was performed using a JEOL electron microscope Model 1011 with an operating voltage of 80 kV. Samples were dispersed in acetone and a drop of the suspension was poured on to a carbon coated cooper grip and dried at room temperature before measurements. The magnification values used were between 20 and 100 k.

Nitrogen Physisorption

BET areas were calculated from the nitrogen adsorption isotherms at -196 ºC using a Quadrasorb *SI.* Automated surface area & Pore Size Analyzer and a value of 0.164 nm^2 for the cross-section of the nitrogen molecule. Brunauer, Emmett and Teller (BET) theory were applied to calculate the total surface area of the samples. Samples were degassed at 90 ºC, to avoid degradation of the hydrocalumites.

Thermogravimetric analysis (TGA)

Thermogravimetric analyses were carried out in a Perkin Elmer TGA 7 microbalance equipped whit a 20-1100 ºC programmable temperature furnace. The accuracy was ± 1μg. Each sample was heated in an N_2 flow (80 cm^3) from 25 °C to 1100 °C at a rate of 5 °C/min.

Results and discussion

X-ray diffraction (XRD)

XRD patterns of the samples obtained from chloride salts (HC1) presented only one crystalline phase corresponding to hydrocalumites (Fig. 15), except for the samples aged in autoclave with microwaves (Fig. 15d and e), and the samples coprecipitated under ultrasounds (Fig. 15f and g), where we also observed additionally the presence of katoite in low amounts (Table 2). Katoite is a non-layered double hydroxide with formula $Ca_3Al_2(OH)_{12}$.[100]

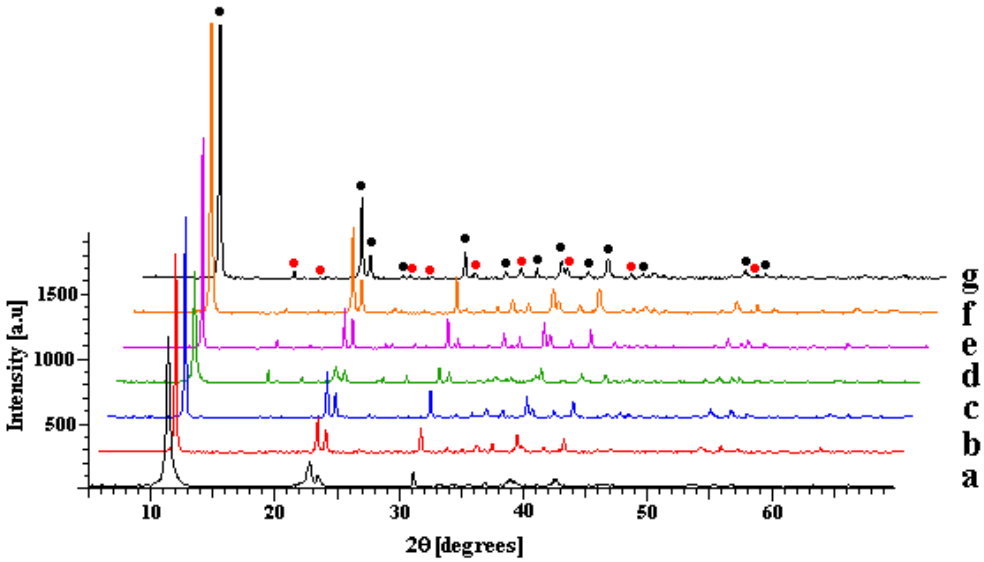

Figure 15. XRD patterns of the samples obtained from chlorides salts a) $HC1R_{24}$, b) $HC1RMw_6$, c) $HC1AC_1$, d) $HC1AMw_1$, e) $HC1AMw_3$ f) $HC1USR_{24}$ and g) $HC1USRMw_6$. (●) Calcium aluminium hydroxide chloride hydrate phase (●) katoite phase.

Table 2 summarizes some characterization data obtained from XRD patterns. The full width at half maximum (FWHM) of the basal reflection plane (006) is usually taken to evaluate the crystallinity in the stacking direction. The sample aged by refluxing with microwaves ($HC1RMw_6$) showed higher crystallinity than that prepared by conventional refluxing ($HC1R_{24}$). Therefore, the use of microwaves allowed us to obtain one hydrocalumite with higher crystallinity at much shorter time (6 h in front of 24 h). However, when comparing the sample aged

in autoclave under microwaves at 180 ºC for 1 h ($HC1AMw_1$) with that obtained in autoclave by conventional heating at the same temperature and time ($HC1AC_1$), we observed higher stacking order for the sample aged by conventional heating. This can be related to the presence of an additional phase (katoite) for the sample aged with microwaves (Fig. 15d). Precipitation of katoite could affect the crystal growth in the stacking direction of the hydrocalumite phase, which is forming simultaneously. At longer aging time in autoclave under microwaves ($HC1AMw_3$), crystallinity of hydrocalumite increased, as expected. Regarding the samples coprecipitated under ultrasounds ($HC1USR_{24}$, $HC1USRMw_6$), they showed lower FWHM values, and consequently higher cristallinity, than their corresponding samples coprecipitated without ultrasounds ($HC1R_{24}$, $HC1RMw_6$) in spite of the presence of very low amounts of katoite (Table 2), and independently of the heating used during aging. Therefore, the use of ultrasounds during precipitation favours crystallization in stacking direction.

The crystallinity of the lamellas can be evaluated by comparing the FWHM values measured for the (110) plane (Table 2). For the samples aged by refluxing, the tendency was the same than that observed in the stacking direction since the sample aged with microwaves ($HC1RMw_6$) had lower FWHM value than that of the sample aged by conventional heating ($HC1R_{24}$). However, for the samples aged in autoclave, the use of microwaves led to an increase in the crystallinity of the layers, contrarious to the behaviour observed in the stacking direction. Therefore, the presence of katoite during the formation of hydrocalumite affects more the crystallinity order in the stacking direction than in the layers. For the samples aged with ultrasounds, the crystallinity of the layers was higher than that of the corresponding samples aged without ultrasounds independently of the heating source used for aging. This tendency was the same than that observed in the stacking direction.

Table 2. Characterization results of the samples**.**

Samples	c (Å)	a (Å)	FWHM (002/006) (°)	FWHM (110) (°)	Ca/Al	BET Area (m^2g^{-1})	Average Pore Diameter (Å)	Pore Volume (cm^3g^{-1})
$HC1R_{24}$	46.71	5.75	0.30	0.18	1.98	13	248	0.09
$HC1RMw_6$	47.15	5.76	0.16	0.17	1.87	10	282	0.07
$HC1AC_1$	46.92	5.75	0.14	0.15	1.96	7	200	0.04
$HC1AMw_1$	46.72	5.75	0.20	0.14	1.93	10	190	0.05
$HC1AMw_3$	46.93	5.75	0.11	0.14	2.12	10	290	0.07
$HC1USR_{24}$	47.00	5.75	0.15	0.14	1.97	6	364	0.05
$HC1USRMw_6$	46.94	5.75	0.15	0.15	1.88	7	230	0.04
$HC2R_{24}$	17.54	5.74	0.28	0.17	1.79	9	308	0.07
$HC2RMw_6$	16.75	5.75	0.41	0.19	1.63	9	184	0.04
$HC2AC_1$	17.24	5.74	0.23	0.19	1.76	10	224	0.04
$HC2AMw_1$	17.12	5.74	0.35	0.18	1.42	11	236	0.06
$HC2AMw_3$	-	-	-	-	1.38	12	266	0.07
$HC2USR_{24}$	17.25	5.75	0.23	0.17	1.78	16	238	0.11
$HC2USRMw_6$	17.25	5.74	0.19	0.17	1.85	25	254	0.16

FWHM: Full width at half maximum

The structure of hydrocalumite $[Ca_2Al(OH)_6]Cl{\cdot}2H_2O$ is indexed in the rhomboedral lattice system belonging to the group *R3c* (Nº 161) with theroretical *a* and *c* parameter values of 5.75 Å and 46.85 Å, respectively.[15] Cell parameters (*a* and *c*) were calculated from the interplanar distances (110) and (006), respectively (Table 1). Lattice parameter *a* is related to the isomorphic substitution between Ca^{2+} and Al^{3+} whereas *c* parameter depends on the charge and size of the anion between the brucite layers. Cell parameter a was very similar for all the hydrocalumites, with values around 5.75 Å, in agreement with the theoretical value. This should be related to a similar stoichiometry for all samples. For cell parameter *c*, with the same type and number of anions, the slight differences observed between the samples can be attributed to some differences in the hydration degree.

Fig. 16 shows the XRD patterns of the samples prepared from nitrate salts (HC2 samples). On the whole, a mixture of hydrocalumite and katoite crystalline phases was observed for all samples in different relative proportions depending on the aging performed (Table 2). The formation of katoite was more favoured in

autoclaved samples, and using microwaves at longer aging times. Actually, katoite practically became the only one phase (85 %) for the sample aged in autoclave with microwaves at longer aging time ($HC2AMw_3$) (Fig. 16e).

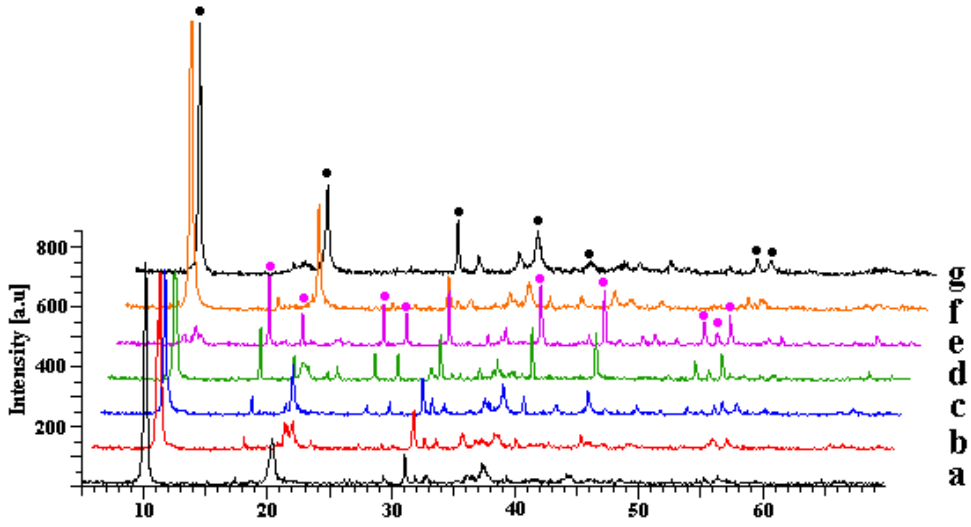

Figure 16. XRD patterns of the samples prepared from nitrate salts a) $HC2R_{24}$, b) $HC2RMw_6$, c) $HC2AC_1$ d) $HC2AMw_1$, e) $HC2AMw_3$ f) $HC2USR_{24}$ and g) $HC2USRMw_6$. (●)Calcium Aluminun Nitrate Hydroxide Hydrate phase (●) katoite phase.

In order to confirm the effect of microwaves, two more samples were synthesized from nitrate salts and aged in autoclave by microwaves or conventional heating at lower temperature (100 ºC) for 1 h (HC2AMw100 and HC2A100, respectively). Figure 17 depicts the XRD patterns of these two new samples. Crystalline katoite phase was clearly detected for the sample aged with microwaves at 100 ºC but no for the sample aged by conventional heating at the same temperature. From these results we can conclude that microwaves have a kinetic effect accelerating the formation of the katoite phase in front of hydrocalumite. The layer construction of hydrocalumite probably has lower rate of formation than katoite, a nonlayered compound. It is well known that microwaves can accelerate organic reactions (oxidation, polymerization, reduction),[101] and inorganic synthesis (zeolites, clays),[18,54,55,57,99] among others.

Hydrocalumites with nitrates as interlayer anions (Fig. 16, Table 1) were slightly less crystalline than those prepared with chloride anions at the same conditions (Fig. 15, Table 1). Therefore, the interlayer anion affects the way to construct the stacking of the hydrocalumite layers. This can be related to the higher repulsion of the larger nitrate anions in the interlayers, as previously reported.[97] In fact, both hydrocalumites present different crystalline system (rombohedral with chlorides and hexagonal with nitrates).

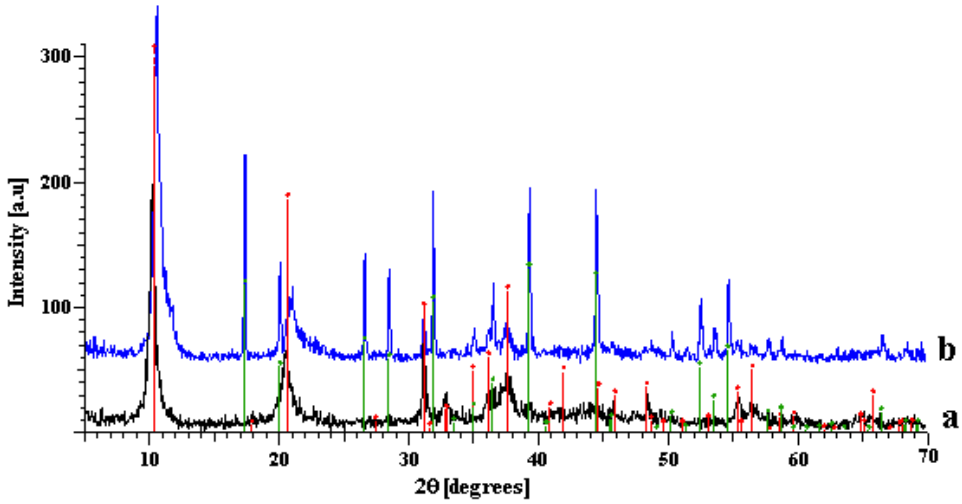

Figure 17. XRD patterns of the samples prepared from nitrate salts a) HC2AC100, b) HC2AMw100. (red line) Calcium Aluminun Nitrate Hydroxide Hydrate phase, (green line) katoite phase.

Table 2 shows the results obtained for the full width at half maximum (FWHM) and of the hydrocalumite phase calculated from the reflections (002) and (110), and cell parameters *a* and *c*, calculated from the interplanar distances (110) and (002), respectively, for HC2 samples. These data were not calculated for $HC2AMw_3$ because its XRD practically did not show the hydrocalumite phase (Fig. 16e). By comparing the samples obtained by refluxing by conventional heating ($HC2R_{24}$) or under microwaves ($HC2RMw_6$), crystallinity of the hydrocalumite phase in the stacking direction and in the lamellar plane was higher for the sample aged by conventional heating (Fig. 16a and b). Taking into account that XRD pattern of $HC2R_{24}$ practically only had the hydrocalumite phase, whereas that of

HC2RMw$_6$ clearly showed the presence of a mixture of hydrocalumite and katoite phases, we can conclude that, again, the presence of katoite seems difficult the crystallization of the hydrocalumite phase. The same tendency was observed in the stacking direction when comparing HC2AC$_1$ and HC2AMw$_1$, aged in autoclave by conventional heating and with microwaves, respectively (Table 2). However, in the lamellar plane, the crystallinity of the sample aged with microwaves was higher than that of the sample aged by conventional heating. Therefore, the presence of katoite affects more the crystallinity of the hydrocalumites in the stacking direction, as observed in samples HC1. Regarding the samples coprecipitated under ultrasounds (HC2USR$_{24}$, HC2USRMw$_6$), we observed lower FWHM values in the stacking direction, and in the layer direction than those corresponding to the samples prepared without ultrasounds (HC2R$_{24}$, HC2RMw$_6$), especially for the sample aged with microwaves (HC2USRMw$_6$) (Table 1). From these results, we can confirm that the use of ultrasounds favoured crystallinity of the resulting hydrocalumites, as previously observed for samples HC1.

The structure of hydrocalumite $[Ca_2Al(OH)_6]NO_3{\cdot}2H_2O$ is indexed in the hexagonal lattice system belonging to the group *P-3c1* (Nº 165) with theroretical *a* and *c* parameter values of 5.74 Å and 17.23 Å, respectively. Cell parameters values of samples HC2 follow the same tendencies than those observed for samples HC1. Cell parameter *a* was practically the same for all samples in agreement with the theoretical value (Table 2) whereas the slight differences observed for cell parameter *c* can be related to some differences in the hydration degree since the type and number of anions should be similar.

Inductively Coupled Plasma- Optical Emission Spectroscopy (ICP-OES)

The analysis of the atomic composition of the samples synthesized from HC1 samples (Table 2) led to a Ca/Al molar ratio of about 2, in agreement with the Ca/Al molar ratio of the starting solutions used for co-precipitation, except for the sample aged at longer time in autoclave with microwaves (HC1AMw$_3$), which had slight higher Ca/Al molar ratio. Longer aging times in autoclave with microwaves could involve some dealumination of the hydrocalumite layers, explaining the

higher Ca/Al molar ratio of HC1AMw$_3$. This effect was previously observed in the preparation of hydrotalcites with microwaves.[18]

Ca/Al molar ratio values of the samples prepared from HC2 samples were lower than those obtained for the samples synthesized from chloride salts (Table 2). There is a correlation between the amount of katoite phase and the decrease in the Ca/Al molar ratio observed for the HC2 samples. Thus, the sample with the highest amount of katoite showed the lowest Ca/Al ratio (Table 2). This can be associated with the lower Ca/Al molar ratio of katoite ($Ca_3Al_2(OH)_{12}$), which is 1.5.

Scanning electron microscopy (SEM) and Transmission electron microscopy (TEM)

Figure 18 shows the SEM images of several HC1 and HC2 samples, synthesized by different aging treatments from chloride and nitrate salts, respectively. All samples showed the formation of thin regular hexagonal crystals corresponding to the hydrocalumite-type compound with some overlay of the layers except the sample HC2AMw$_3$ (Fig. 18j), where non-layered particles were observed since this sample is composed by katoite, a non-layered calcium aluminium hydroxide compound. On the whole, the samples aged with microwaves (by refluxing or in autoclave) exhibited lower particle sizes than those aged by conventional heating. Interestingly, samples prepared from nitrate salts using ultrasounds during coprecipitation showed different particle size distribution (Fig. 18k and 18l) than those synthesized at the same conditions but from chloride salts (Fig. 18e and 18f). This can be again related to the presence of larger nitrate anions in the interlayers, which should affect the construction of the hydrocalumite structure, as commented above.

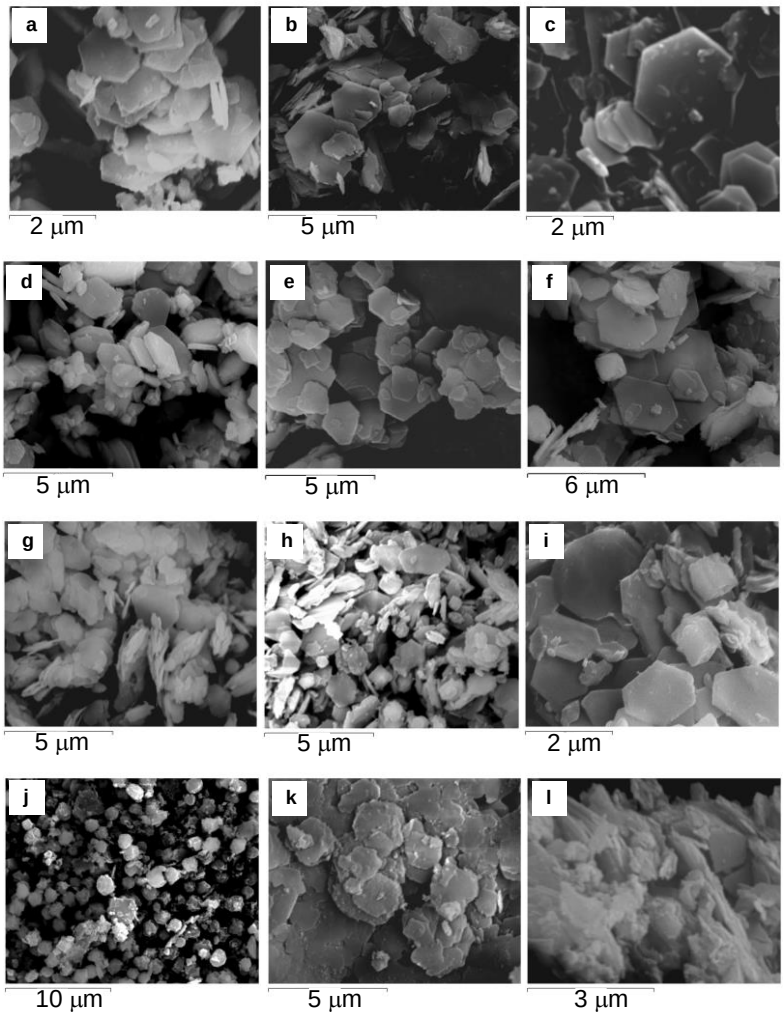

Figure 18. SEM images of a) $HC1R_{24}$ (x20000) b) $HC1RMw_6$ (x10000) c) $HC1AC_1$ (x20000) d) $HC1AMw_3$ (x10000) e) $HC1USR_{24}$ (x10000) f) $HC1USRMw_6$ (x5000) g) $HC2R_{24}$ (x10000) h) $HC2RMw_6$ (x10000) i) $HC2AC_1$ (x20000) j) $HC2AMw_3$ (x9000) k) $HC2USR_{24}$ (x11000) l) $HC2USRMw_6$ (x19000).

TEM images allowed us to confirm the observation of well-formed hexagonal sheets corresponding to the hydrocalumite phase for all samples (Figure 19). The average size of the particles was, in general, 0.5-2 μm. The micrographies of the samples $HC2USR_{24}$ (Fig. 19g) and $HC2USRMw_6$ (Fig. 19h) showed more aggregated layers, probably because of the presence of particles with different size.

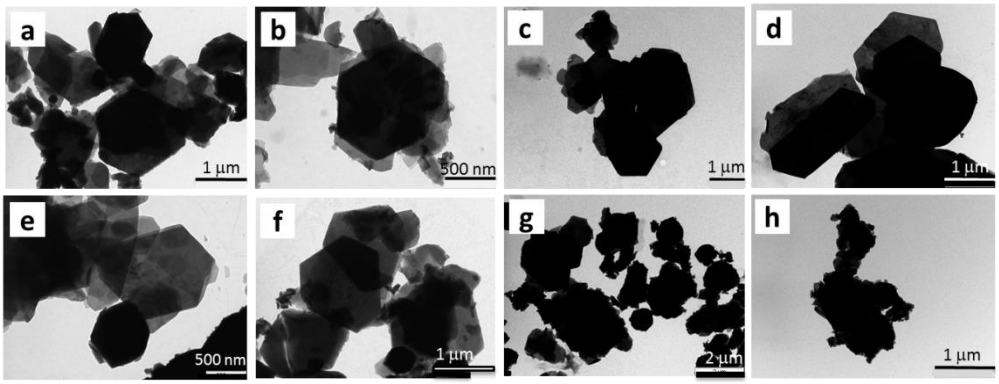

Figure 19. TEM images of a) $HC1R_{24}$ (x50000) b) $HC1RMw_6$ (x20000) c) $HC1USR_{24}$ (x15000) d) $HC1USRMw_6$ (x25000) e) $HC2R_{24}$ (x40000) f) $HC2RMw_6$ (x30000) g) $HC2USR_{24}$ (x12000) h) $HC2USRMw_6$ (x30000).

Nitrogen Physisorption

HC1 and HC2 samples exhibited nitrogen adsorption-desorption isotherms of type IV, according to IUPAC classification, with average pore diameters in the range of mesopores (Table 2). On the whole, all samples showed low surface areas and low pore volumes. This agrees with the results reported by other authors for conventionally prepared hydrocalumites.[26,49] Interestingly, samples HC2 precipitated from nitrate salts using ultrasounds for stirring had the highest surface areas values (Table 2). It is important to remark that the sample $HC2USRMw_6$ achieved the highest surface area (25 m^2/g) found in the literature for hydrocalumites compounds.

For HC1 samples, the slight differences observed between the surface areas measured could be explained taking into account two main contributions: higher crystallinity of hydrocalumite led to low surface area whereas the presence of katoite in low amounts contributed to a slight surface area increase. This effect of katoite was confirmed regarding the results of the samples HC2 prepared without ultrasounds, where the highest surface area corresponded to the sample $HC2AMw_3$, which was mainly composed of katoite (Fig. 16). The higher surface area measured for the samples HC2 precipitated under ultrasounds, especially for that aged under microwaves ($HC2USRMw_6$), could be attributed to a interparticle mesoporosity between larger and smaller particles, as confirmed by comparing the pore size

distribution graphic of samples HC2RMw$_6$ and HC2USRMw$_6$, in which additional mesoporosity of higher diameter size was observed for the sample coprecipitated with ultrasounds (Figure 20). This behaviour also agrees with the differences observed by SEM and TEM for this sample with respect to the rest of hydrocalumites prepared.

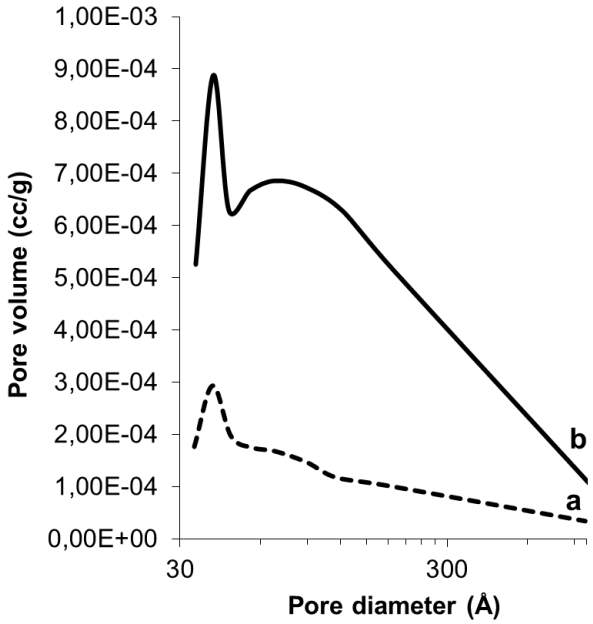

Figure 20. Pore size distribution graphic of samples a) HC2RMw$_6$ and b) HC2USRMw$_6$.

Thermogravimetric analysis (TGA)

TGA curves of samples HC1 showed the three-weight losses characteristic of hydrocalumite-type samples prepared from chloride salts, [49] with a total weight losses between 42 and 48.5%, as observed for a representative sample (Figure 21a). The temperature range of the three weight losses were 90 ≤ T ≤ 200 ºC, 200 ≤ T ≤ 400 °C and 400 ≤ T ≤ 1000 °C. The first weight loss can be related to the loss of physically adsorbed water and the two water molecules computed according to the hydrocalumite formula whereas the second and third weight losses can be mainly associated with dehydroxylation of the Ca-Al hydroxide layer, with the formation of water, and the release of chloride anions as hydrogen chloride, respectively.[49] The

presence of small amounts of katoite in samples $HC1AMw_1$, $HC1AMw_3$, $HC1USR_{24}$ and $HC1USRMw_6$ did not affect the profile of the TGA curve.

On the other hand, TGA curves of samples HC2 showed different profiles depending on the composition of the samples. Thus, TGA curves of samples $HC2R_{24}$, $HC2RMw_6$, $HC2USR_{24}$ and $HC2USRMw_6$, mainly composed of hydrocalumite phase (Figure 16), exhibited four weight losses (e.g. Figure 21b) with total weight losses between 40.3 % and 47.4 %. The first step (between $90 \leq T \leq 200$ ºC) corresponds to the removal of physisorbed water and water molecules from the interlayer space. The second step, between $200 \leq T \leq 400$ ºC can be associated with the dehydroxylation of the Ca-Al hydroxide layer, with the corresponding formation of water. Finally, the third and fourth steps can be related to the release of $[NO_3]^-$, as NO_x, in two consecutive steps between $400 \leq T \leq 800$ ºC. In contrast, sample $HC2AMw_3$, which was practically katoite (Figure 16), also had a profile with four weight losses (Figure 21c) but the loss weight for each step was clearly very different compared with those observed for the samples mainly composed of hydrocalumite (e.g. Figure 21b). Therefore, the main weight loss observed in the TGA of $HC2AMw_3$ (the second weight loss) should be attributed to the decomposition of the katoite phase, whereas the first, third and four weight losses should be related to some physisorbed water, and some nitrate anions, respectively, probably due to the presence of small amounts of hydrocalumite in this sample.

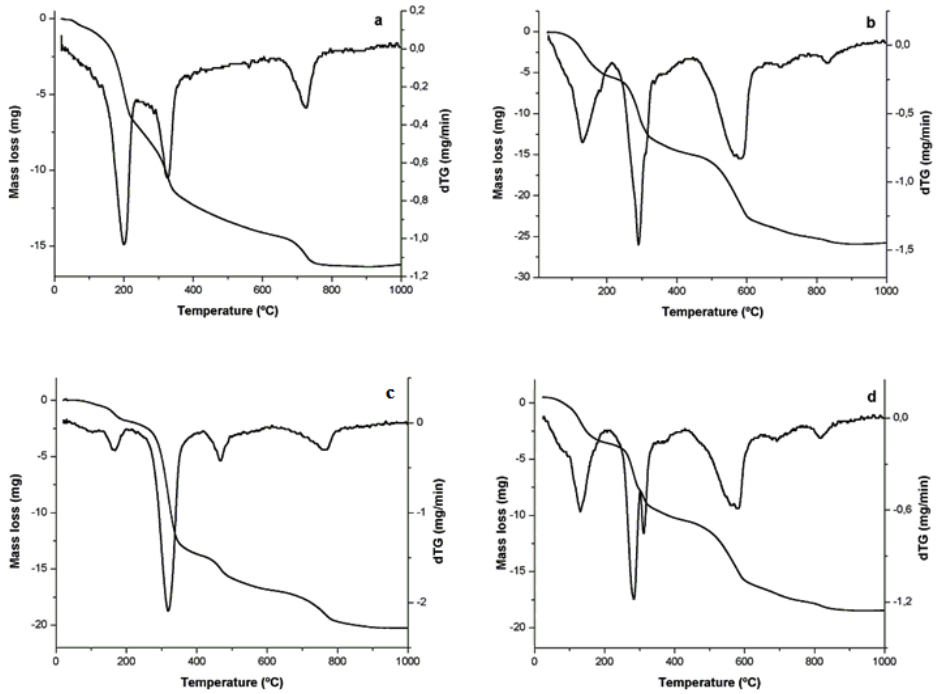

Figure 21. TGA curves and derivatives of several representative samples a) $HC1AC_1$, b) $HC2USR_{24}$, c) $HC2AMw_3$, and d) $HC2AMw_1$.

Finally, samples $HC2AC_1$, and $HC2AMw_1$, the XRD patterns of which showed the presence of a mixture of hydrocalumite and katoite phase (Figure 16), exhibited also TGA curves with four weight losses, and interestingly the second weight loss had two contributions (e.g. Figure 21d). The main contribution of the second weight loss for these two samples could be associated to the decomposition of the Ca-Al layers of the hydrocalumite phase whereas the second contribution could be attributed to the katoite phase, since the maximum of the derivative appeared practically at the same temperature than that observed for the sample identified as katoite (see Figures 21c and 21d).

Table 3 and Table 4 depict the values of the initial temperature of each weight loss for HC1 and HC2 samples, respectively. These values were very similar between the samples. Samples $HC2AC_1$ and $HC2AMw_1$ had two initial temperatures corresponding to the second weight loss since two contributions were observed for this peak, as previously commented. The slight higher values of the initial

temperature of the dehydration step corresponded to the most crystalline samples. A higher order in the stacking direction can suppose higher interactions for the interlamellar water, and consequently, higher temperatures should be necessary to be removed. Respect to the second weight loss, due to dehydroxilation of the layers, again slight higher values of the initial temperature were observed for the samples with higher crystallinity.

Table 3. Data obtained from the thermogravimetric analysis of the samples HC1.

Sample	Temperature First weight loss (ºC) [a]	Temperature Second weight loss (ºC) [a]	Temperature Third weight loss (ºC) [a]
$HC1R_{24}$	102	276	623
$HC1RMw_6$	104	280	625
$HC1AC_1$	108	283	649
$HC1AMw_1$	107	281	657
$HC1AMw_3$	111	287	627
$HC1USR_{24}$	105	281	635
$HC1USRMw_6$	109	283	642

a Initial temperature of the corresponding weight loss.

Table 4. Data obtained from the thermogravimetric analysis of the samples HC2.

Sample	Temperature First weight loss (ºC) [a]	Temperature Second weight loss (ºC) [a]	Temperature Third weight loss (ºC) [a]	Temperature Fourth weight loss (ºC) [a]
$HC2R_{24}$	91	203	478	694
$HC2RMw_6$	88	201	472	689
$HC2AC_1$	102	208, 287	489	784
$HC2AMw_1$	104	212, 291	482	775
$HC2AMw_3$	108	275	447	701
$HC2USR_{24}$	101	206	481	692
$HC2USRMw_6$	105	207	484	688

[a] Initial temperature of the corresponding weight loss.

Conclusions

Several hydrocalumites were synthesized by coprecipitation of nitrate or chloride salts with and without ultrasounds, and aged hydrothermally in autoclave or by refluxing with and without microwaves. The presence of nitrates as interlayer anions resulted in hydrocalumites slight less crystalline than those prepared with chlorides, and favour the formation of katoite, whereas the use of ultrasounds during coprecipitation led to more crystalline hydrocalumites. The use of autoclave and microwaves during aging, especially at longer times, also favoured the formation of katoite, in addition to hydrocalumite.

On the whole, all samples showed low surface areas and low pore volumes. Interestingly, the hydrocalumite prepared from nitrates by coprecipitation in ultrasounds and aged under microwaves resulted in the highest surface area measured (25 m^2/g). This sample also showed an additional mesoporosity consequence of the different particle size distribution observed by SEM and TEM with respect to the rest of samples.

Acknowledgments

Authors acknowledge Ministerio de Economía y Competitividad of Spain and Feder Funds (CTQ2011-24610), and Catalan Government for FI grant (2012FI_B00564). We thank Dr. Francesc Gispert Guirado for his help in the calculation of the percentages of the crystalline phases obtained by XRD.

4.1.2 Raman and infrared spectroscopy studies about the influence of microwaves and ultrasounds in the synthesis of hydrocalumites

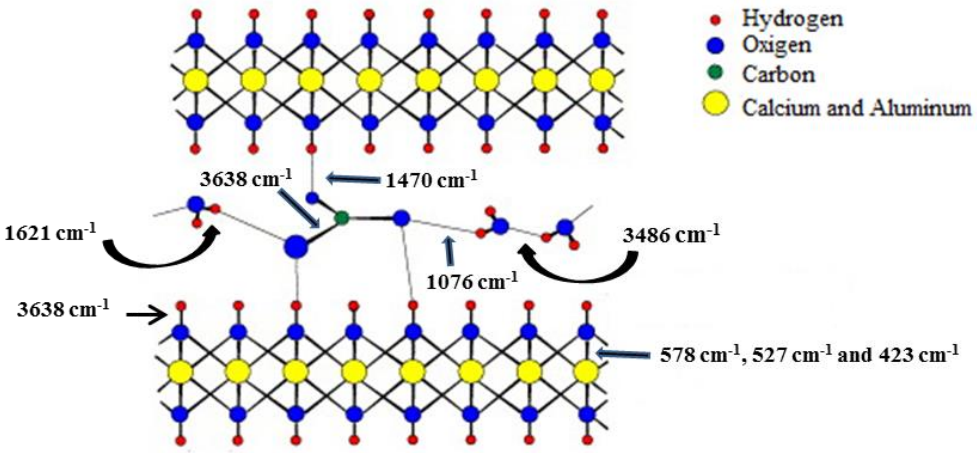

Abstract

We performed the Raman, near infrared, mid-infrared and far infrared spectra for four hydrocalumites prepared by different methods (ultrasounds or magnetic stirring, and microwave or conventional heating). The mid-infrared and Raman results show the characteristic bands of the hydrocalumites, as well as the formation of the calcite phase in low amounts. Moreover, far infrared spectra confirm the presence of the Cl^- anion in the interlayer space. These results also agree with those obtained by near infrared spectroscopy, in which the characteristic overtone bands due to the hydrocalumites were observed.

Introduction

In recent years, the family of layered double hydroxides (LDHs) has attracted much interest in research studies due to its multiple applications in catalysis, in the pharmaceutical industry, in water treatment plants, among other uses.[29,98]

LDHs exhibit a structure similar to brucite, $Mg(OH)_2$. However, some trivalent metal cations may partially substitute the Mg^{2+}. This creates a positive charge on the brucite layers that is compensated by the presence of interlayer anions. LDHs have the general formula $[M^{2+}_{1-x}\ M^{3+}_{x}(OH)_2][X^{q-}_{x/q}\cdot nH_2O]$, where $[M^{2+}_{1-x}M^{3+}_{x}(OH)_2]$ is the cation composition of the layers, M^{2+} is a divalent ion (Mg^{2+}, Ca^{2+}, Mn^{2+}, Co^{2+}, Cu^{2+}, Ni^{2+}, etc), and M^{3+} is a trivalent ion (Al^{3+}, Fe^{3+}, Ni^{3+}, Mn^{3+}, etc.) whereas $[X^{q-}_{x/q}\cdot nH_2O]$ represents the interlayer composition.[102]

LDHs family is mainly represented by the natural mineral hydrotalcite, with the formula $Mg_6Al_2(OH)_{16}CO_3\cdot 4H_2O$. Hydrotalcites have characteristic properties, such as anion exchange. Additionally, calcined hydrotalcites present high surface areas, high thermal stability, basic properties and memory effect; which make them useful in the synthesis of catalyst supports, flame-retardants, ions exchangers and absorbents, controlled drug delivery devices and gene therapy. [45,77,78]

Other less-known LDHs are the hydrocalumites-type compounds, whose general formula is $Ca_2M^{3+}(OH)_6\ X\cdot H_2O_x$, in which M^{3+} is usually Al^{3+}, X represents a charged anion (e.g. OH^-, NO_3^-, CO_3^{2-}, or Cl^-).[22] Specifically, the hydrocalumite name is used when the anion is chloride. The structure of hydrocalumite $[Ca_2Al(OH)_6]Cl\cdot 2H_2O$ is indexed in the rhomboedral lattice system belonging to the group *R3c* with theoretical *a* and *c* parameter values of 5.75 and 46.85 Å, respectively.[15] These Ca/Al compounds are used in the immobilization of toxic cations,[13,32,34] in the optimization of concrete properties,[46,47] and in catalysis due to their basic properties.[103]

In the literature, numerous studies about the structure and composition of the LDHs by Infrared and Raman spectroscopy can be found in the field of catalysis,[77,78] to study the effect of the anions in the interlaminar space,[79–81] to

confirm the anion exchange,[82,83] and to observe the thermal behavior in hydrotalcite-like materials.[84–86]

In the case of the hydrocalumites, some authors used spectroscopy characterization to identify the characteristic bands of this material as complementary techniques of their studies, without going into depth in the spectroscopic analysis. To our knowledge, there are very few spectroscopy studies of Ca/Al-LDHs so far. Frost *et al*. (2010) studied the synthesis and Raman spectroscopic characterization of Ca/Al-CO_3 with different molar ratio.[104] Zhang *et al*. (2011) studied the Na-dodecylbenzenesulfate intercalated into Ca/Al-Cl by near-infrared and mid-infrared.[38] Mora *et al*. (2011) studied the synthesis of Ca/Al-NO_3 LDH obtained by coprecipitation, sol-gel and urea methods by near and mid-infrared.[48] However, the effect of using different stirring and aging techniques in the salts coprecipitation method referred to the synthesis of hydrocalumite-type materials has not been reported yet.

In this research work, we study the differences between hydrocalumites prepared by stirring during the salts precipitation, with ultrasounds vs. magnetic stirring; and by aging with a conventional oil bath vs. microwaves. Samples were characterized through a detailed spectroscopic analysis using the following techniques: Raman, near infrared, mid-infrared and far infrared spectroscopies.

Experimental

Synthesis of hydrocalumites

Hydrocalumites were synthesized by the co-precipitation method (for details of the methodology please refer to Granados-Reyes *et al*.[105] chapter 4.1.1). An aqueous solution containing $CaCl_2 \cdot 2H_2O$ (sigma-Aldrich) and $AlCl_3 \cdot 6H_2O$ (Riedel-de Haën) was prepared with a 2:1 Ca^{2+}/Al^{3+} molar ratio under nitrogen atmosphere. This solution was added to 250 ml of a mixture of water/ethanol in a 2:3 volumetric ratio in an oil bath or ultrasounds, depending on the samples, at 60 ºC. The pH was kept constant at 11.5 ± 0.1, by the simultaneous addition of an aqueous solution of 2 M NaOH (Panreac). Magnetic stirring or ultrasounds were used for mixing during precipitation. After complete addition of the metallic salts, the mother solutions were

aged by several treatments (Table 5): by refluxing with conventional heating at 60 ºC for 24 h (HCR_{24} and $HCUSR_{24}$) and by refluxing with microwaves (Milestone ETHOS-TOUCH CONTROL) at 60 ºC for 6 h ($HCRMw_6$ and $HCUSRMw_6$). Finally, all samples were filtered at room temperature, washed with deionized and decarbonated water and then dried in an oven at 80 ºC overnight.

Table 5. Aging treatments of hydrocalumites.

Sample	Ultrasound[a]	Aging		
		Heating	T (ºC)	Time (h)
HCR_{24}	No	conventional	60	24
$HCRMw_6$	No	microwave	60	6
$HCUSR_{24}$	Yes	conventional	60	24
$HCUSRMw_6$	Yes	microwave	60	6

a during precipitation

Raman microspectroscopy

Synthesized samples were analyzed by Raman spectroscopy using a RENISHAW Via Raman Microscope, equipped with a Leyca microscope with 50x objective. Spectra were obtained by excitation with a laser of 514 nm of wavelength, (for the range of 3000-4000 cm^{-1}); and with a laser of 785 nm (for the range of 100-2000 cm^{-1}). In both cases, the laser power was set to 10 %. The exposure time was of 60 s in 2 scans per spectrum, in order to improve the signal-to-noise ratio.

Mid-infrared spectroscopy

Infrared spectra were recorded on a NICOLET 380 FI-IR spectrometer. Spectra were acquired by accumulating 100 scans at 2 cm^{-1} resolution in the range of 400–4000 cm^{-1}. Samples were prepared by mixing the powdered solids with pressed KBr disks in a mass ratio of 1:100.

Near-infrared spectroscopy

Near-IR spectra were recorded on a Jasco V570 spectrometer, in Diffuse Reflectance, using an integration sphere, in air. Spectra were obtained from 800 to 2500 nm.

Far-infrared spectroscopy

Far IR spectra were recorded on a Thermofisher 6700 spectrometer. Spectra were acquired by accumulating 100 scans at 4 cm^{-1} resolution in the range of 50–400 cm^{-1}. For the Far IR experiments the sample powders were deposited on a polyethylene film.

Results and discussion

In this section we start with a preliminary characterization section, in which the results from elementary analysis and X-ray diffraction are described. Results from this section serve as a starting point for the core results of this study, followed by the section where the main outcomes of the Raman and mid-infrared spectroscopy are presented. After, the results of far-infrared spectroscopy are presented, and the last section shows the results of near-infrared spectroscopy.

Preliminary characterization

Table 6 shows some of the characterization results obtained for these samples, which have been previously reported by Granados-Reyes *et al*.[105] (chapter 4.1.1). XRD of the samples stirred during the precipitation with ultrasounds exhibited, in addition to the hydrocalumite phase, the presence of katoite in low amounts. Katoite is a non-layered double hydroxide with formula $Ca_3Al_2(OH)_{12}$.

Table 6. Preliminary characterization results of the samples*

Sample	Crystalline phases (XRD)	FWHM (006) (°)	Ca^{2+}/Al^{3+}
HCR_{24}	HC	0.300	1.98
$HCRMw_6$	HC	0.155	1.87
$HCUSR_{24}$	HC (94 %) + K (6%)	0.145	1.97
$HCUSRMw_6$	HC (93 %) + K (7 %)	0.148	1.88

*Values reported in Granados-Reyes et al. (2014).[105] HC: Hydrocalumite; K: Katoite; FWHM: Full width at half maximum.

The full width at half maximum (FWHM) values of the basal reflection plane (006), obtained by XRD, was used to evaluate the crystallinity of the samples in the stacking direction. The sample aged by refluxing with microwaves

(HCRMw$_6$) showed higher crystallinity than that prepared by conventional refluxing (HCR$_{24}$). Therefore, the use of microwaves favors the hydrocalumite crystallinity at shorter aging time (6 h against 24 h). In spite of the low amounts of katoite observed in the samples coprecipitated under ultrasounds (HCUSR$_{24}$, HCUSRMw$_6$), they showed lower FWHM values, and consequently higher crystallinity, than the corresponding samples coprecipitated by magnetic stirring (HCR$_{24}$, HCRMw$_6$) (see Table 6) independently on the type of heating used during aging. This means that the use of ultrasounds during precipitation favors crystallization of the hydrocalumite in the stacking direction.

Samples had a Ca/Al molar ratio of about 2 (Table 6), in agreement with the Ca/Al molar ratio of the starting solutions used for co-precipitation. Samples aged with microwaves showed slight lower Ca/Al ratio than those aged by conventional heating.

Raman and mid-infrared spectroscopy

In this section, the main IR and Raman bands related to the hydrocalumite phase are assigned. For the sake of clarity, spectra are presented and discussed considering three main spectral regions: 4000- 3000 cm^{-1}, 2000-1000 cm^{-1} and 1000-400 cm^{-1}.

Raman and infrared spectroscopy of the 4000-3000 cm^{-1} region

Figure 22 shows the Mid-IR spectra in the region of 4000-3000 cm^{-1}, in which the bands characteristic of the hydroxyl stretching region can be observed.

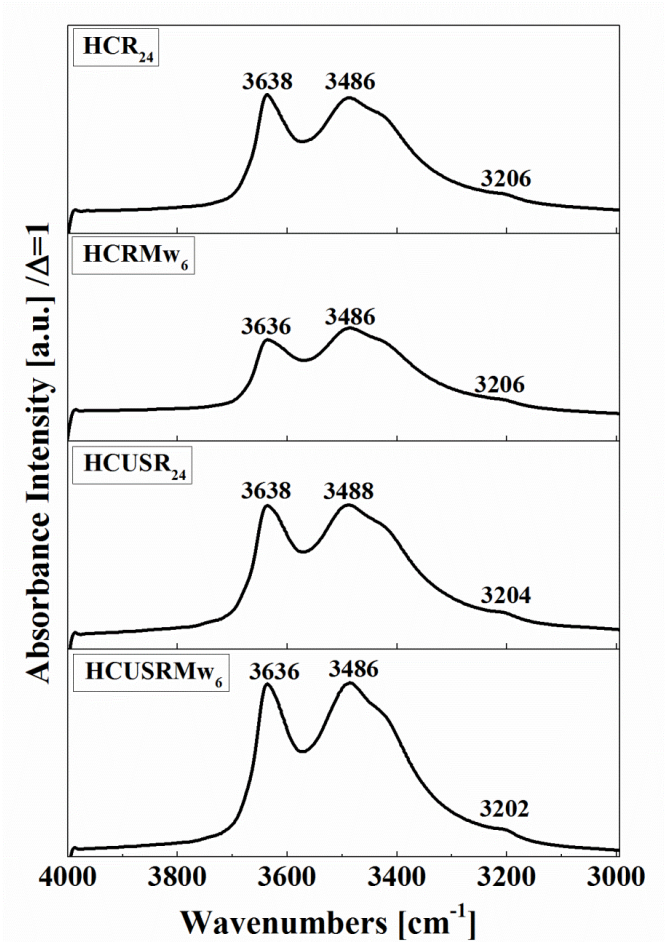

Figure 22. Mid-infrared spectra of the hydrocalumites in the 4000-3000 cm^{-1} region.

All samples presented similar IR spectra. The samples aged under microwaves had a band at 3636 cm^{-1} whereas for those conventionally aged this band appeared at 3638 cm^{-1}, slightly tailing towards lower frequencies, in both cases. Additionally, all samples exhibited two bands, one around 3486 cm^{-1} complex, and another weak band around 3205 cm^{-1}. According to Frost *et al.* [104] the band at the highest wavenumber can be assigned to O-H stretching vibrations of hydroxyl groups in octahedral layer bonded to the cations in mixed species, such as $CaAl_2OH$ and Ca_2AlOH. The bands around 3486 cm^{-1} can be attributed to water molecules within the interlayer interacting through H-bonds, while the assignation of the band at 3205 cm^{-1} is not straight forward. Frost *et al*. suggested that a band at

3365 cm^{-1} could be due to water molecules bonded to exposed hydroxyl groups at the surface of the interlayer. Alternatively, such a low frequency band could be assigned to water molecules bound to carbonate ions.[104] The Raman spectra of these samples reveal differences between them, depending on the preparation process (Figure 23).

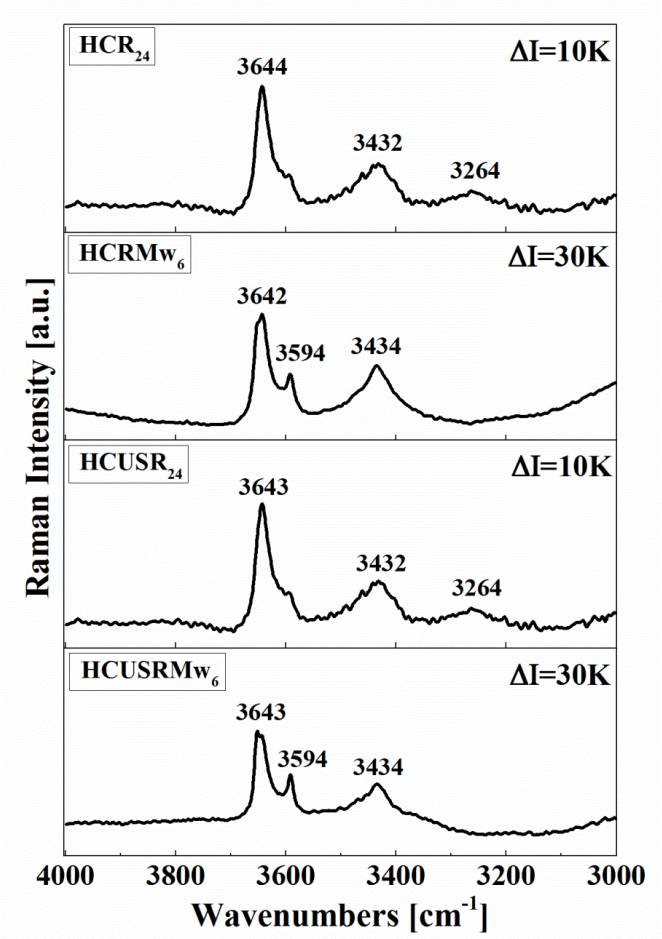

Figure 23. Raman spectra of the hydrocalumites in the 4000-3000 cm^{-1} region.

The samples aged by conventional heating (HCR_{24} and $HCUSR_{24}$) presented similar spectra, with bands around 3644 cm^{-1}, 3432 cm^{-1} and 3265 cm^{-1} with a weak shoulder at 3595 cm^{-1}. These Raman bands correspond to the IR bands observed at 3638 cm^{-1}, 3486 cm^{-1} and 3205 cm^{-1}, respectively. In contrast, the samples aged with microwaves ($HCRMw_6$ and $HCUSRMw_6$) showed two bands around 3643 cm^{-1} and

3434 cm^{-1}, and a sharp, although weak peak, at 3594 cm^{-1}. This small peak can be attributed to the stretching mode of OH groups bonded to Ca^{2+} cations.[104] It is worth to emphasize that the band at 3264 cm^{-1}, related to water forming hydrogen bonds with the OH groups of the layer, was not observed for the microwaved samples.

Raman and infrared spectroscopy of the 2000-1000 cm^{-1} region

In the region between 2000-1100 cm^{-1} the Raman spectrum presented very low resolution. Therefore, the results in this region will be only explained by infrared spectroscopy (figure 24).

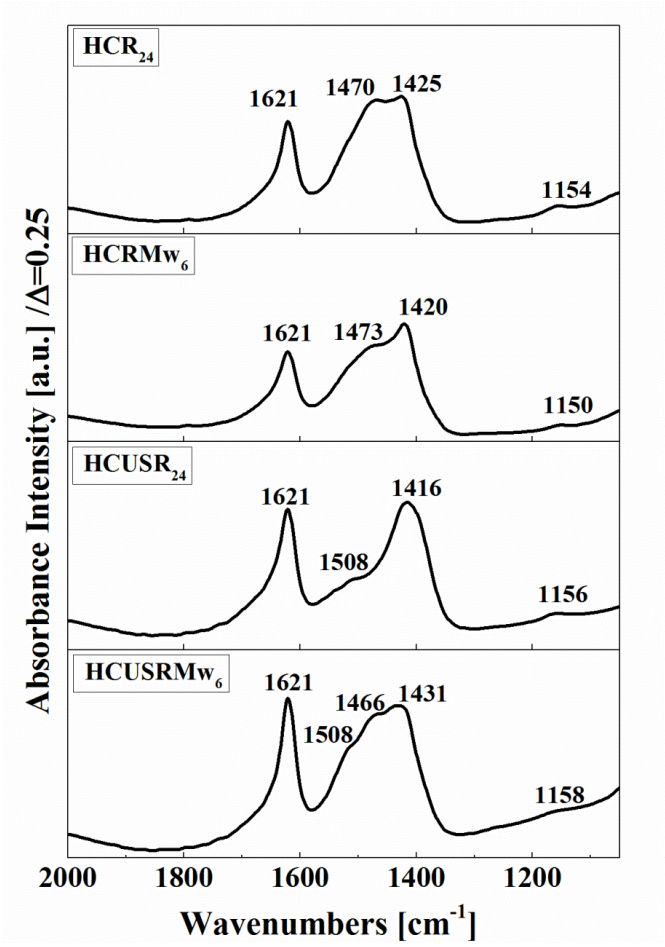

Figure 24. Mid-infrared spectra of the hydrocalumites in the 2000-1050 cm^{-1} region.

The most characteristic vibrations of CO_3^{2-} and H_2O molecules can be observed in this region for all samples. The first band, around 1470 cm^{-1}, corresponds to the antisymmetric stretching vibration mode of carbonate (υ_3) bonded hydroxyl from the brucite-like surface while the second band, around 1423 cm^{-1}, can be attributed to antisymmetric stretching vibration of carbonate in calcite. However, the band at 1470 cm^{-1} disappears in $HCUSR_{24}$, evidencing another component at 1508 cm^{-1}, which was masked by the stronger absorption, whereas in sample $HCUSRMw_6$ all these components are detectable, possibly due to carbonate in several different coordination at the interlayer surface. Additionally, a sharp peak at 1621 cm^{-1} appeared for all samples. This can be assigned to the HOH bending mode of the interlayer water

Figure 25 shows a band at 1085 cm^{-1} in Raman spectrum, for all the samples, that can be attributed to the symmetry stretching vibrations mode of carbonate anion in calcite (υ_1). In the samples in which the starting salts were precipitated with ultrasounds ($HCUSR_{24}$ and $HCUSRMw_6$) a shoulder was also observed at 1076 cm^{-1},[104] which can be related to the interlayer carbonate bonded to the water. This peak was only present in the samples with katoite phase. Since the katoite has a rhombic structure, it could be inferred that the katoite affects the laminar system so that a small amount of atmospheric carbonate inlays in the interlayer space. The bands at 1085 cm^{-1} and 1076 cm^{-1} were not observed in the IR spectra.

These results confirm the presence of carbonates in the materials since bands were very weak. Moreover, the calcite ($CaCO_3$) phase was not detected in any of the samples by XRD.[105] Thus, low amounts of carbonates were in the samples despite of using decarbonated/deionized water and an inert atmosphere during preparation to prevent the formation of carbonates in the materials.

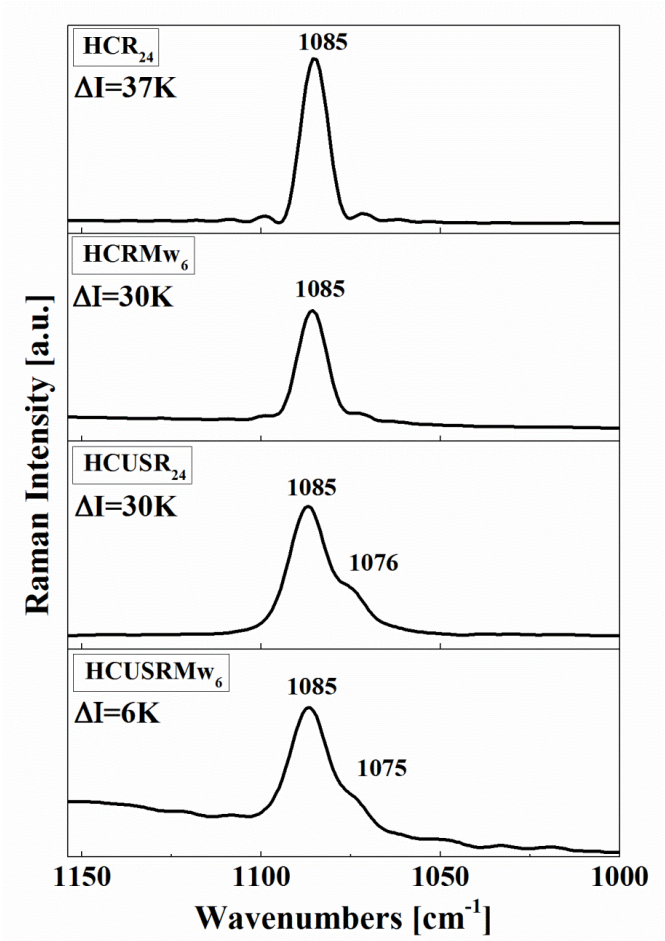

Figure 25. Raman spectra of the hydrocalumites in the 1150-1000 cm^{-1} region.

Raman and infrared spectroscopy of the 1000-400 cm^{-1} region

Figure 26 shows the infrared spectra obtained for all samples in the range of 1000 to 400 cm^{-1}. This figure exhibits a very weak peak at 876 cm^{-1} for all samples except for the $HCUSR_{24}$, in addition to a weak peak around 853 cm^{-1}. These peaks correspond to the carbonate symmetric vibration out of plane bending (υ_2). The band of υ_2 is inactive in Raman when the CO_3^{2-} ion has its ideal geometry (D_{3h}). When a reduction in the geometry of the carbonate anion occurs, it is possible to observe a weak band in Raman, as in this case we observed around 863 cm^{-1} (Figure 27).[104]

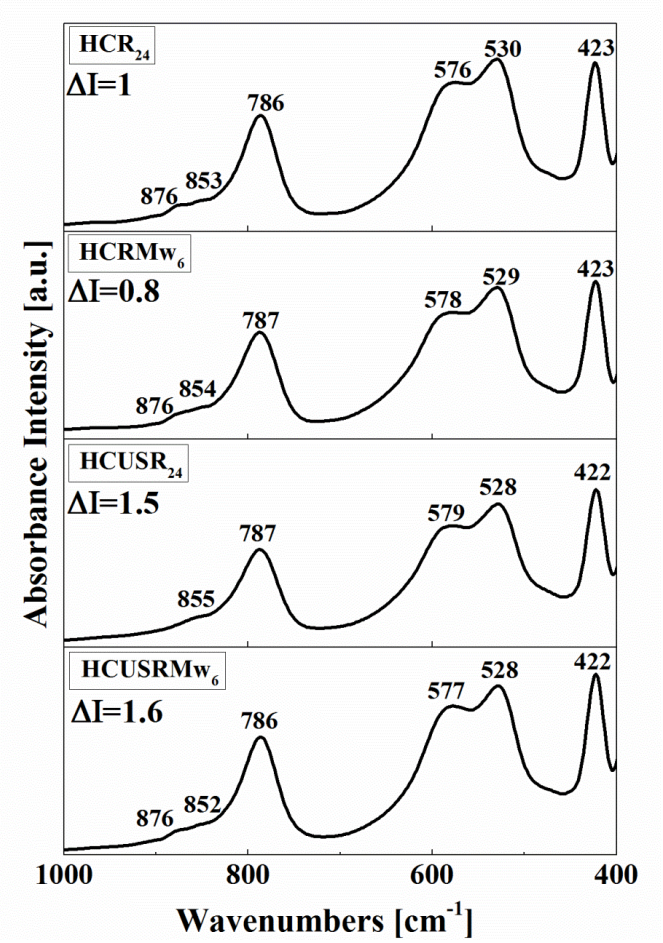

Figure 26. Mid-infrared and spectra of the hydrocalumites in the 1000-400 cm^{-1} region.

Additionally, the infrared spectra shows a weak band around 783 cm^{-1} that can be attributed to water vibrational mode, which can be observed in Raman at 787 cm^{-1} for samples HCR_{24} and $HCUSR_{24}$ (aged by conventional heating) and at 783 cm^{-1} for samples $HCRMw_6$ and $HCUSRMw_6$ (aged by microwaves). Another important carbonate bending mode observed in this region is the vibration mode υ_4 (symmetric vibration in the plane bending). This appeared in Raman at 710 cm^{-1} and can be assigned to the calcite phase.

In the Raman spectra, a very sharp band was observed at 530 cm^{-1}, which can be related to stretching vibrations of the Al-O-Al bonds linked to the layer

structure. The Metal-OH bands were recorded in the infrared region between 700 cm^{-1} and 400 cm^{-1}. Figure 27 shows three bands around 578 cm^{-1}, 527 cm^{-1} and 423 cm^{-1} for all samples that are assigned to Metal-O lattice vibrations ($\upsilon_{M\text{-}OH}$, $\upsilon_{M\text{-}O\text{-}M}$ and $\upsilon_{O\text{-}M\text{-}O}$).

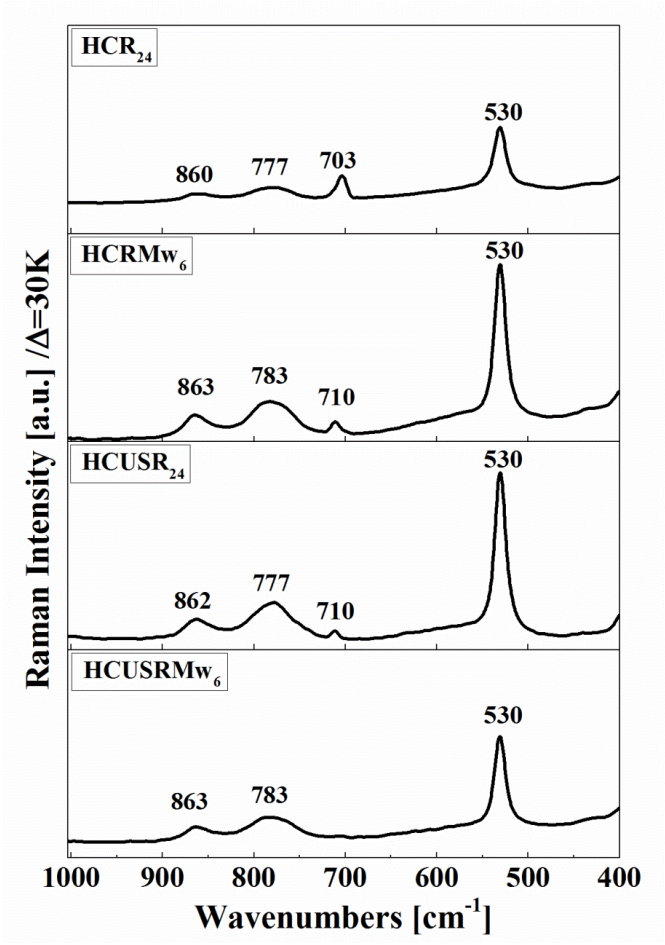

Figure 27. Raman spectra of the hydrocalumites in the 1000-400 cm^{-1} region.

Far-infrared spectroscopy

The Far-IR study provides information about the cations located in the interlayer space of the material.

Figure 28 shows the results for the four samples analyzed in the region of 400-50 cm^{-1}. According to Wang *et al*. (2003),[79] the weak bands observed at 307 cm^{-1}, for the samples aged by conventional heating, and at 306 $cm^{-1,}$ for those aged

by microwaves, can be attributed to OH vibrations in the plane of the layer and in the stacking direction of the layer. Other band, observed for all samples around 257 cm^{-1} was assigned to the Ca and Al vibrations in the direction of the layer, with OH also cooperatively moving parallel to this plane.

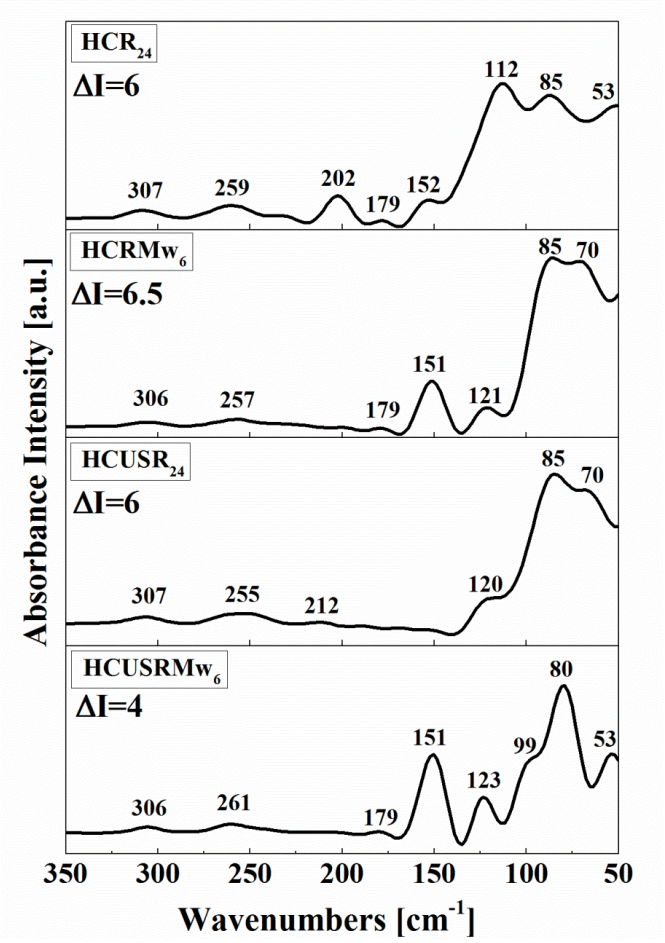

Figure 28. Far-infrared spectra of the hydrocalumites in the 400-50 cm^{-1} region.

Additionally, the samples aged by conventional heating showed a band between 200 and 212 cm^{-1}, which can be related to water motions (hydrogen bond stretching) in the direction perpendicular to the layer, and with the contribution of the Cl^- ions with translational motions parallel of the layers, respectively. The samples also exhibited a weak band at 179 cm^{-1} and a band around 151 cm^{-1}, except the sample $HCUSR_{24}$. The weak first band can be related to Al^{3+} vibrations in the

stacking direction with a lower contribution of Ca^{2+} and OH whereas the band at lower value can be assigned to OH of the layer bending mode vibrations in the direction of the layer.

A band at 120 cm^{-1} was also observed, except in HCR_{24} sample although in this case, the lower frequency band could overlap it. This band is mainly due to Cl^- motions in the stacking direction. The HCR_{24} and $HCUSRMw_6$ samples present a band at 112 cm^{-1} and 99 cm^{-1}, which correspond to Ca^{2+} moving in the perpendicular direction of the layer overlapped with Al^{3+} and OH motions in the layer direction.

All samples show a band around 85 cm^{-1}. This band is a contribution of the Cl^- in all directions (in the stacking direction and in the layer direction), as well as interlayer water vibrations in the layer direction. The band observed at 53 cm^{-1} in the HCR_{24} and $HCUSRMw_6$ samples can be assigned to Cl^- contribution in the direction of the layer and some of interlayer water translations (hydrogen bond bending) in the direction of the layer. In the $HCRMw_6$ and $HCUSR_{24}$ samples, we observed the contribution of the interlayer water translations (hydrogen bond bending) parallel to the layer, at 70 cm^{-1}.

Near-infrared spectroscopy

In the Near-IR region the overtones bands related to the hydroxyl groups observed in the Mid-IR, can appear. Thereby, the presence of different O-H bonds in the samples was confirmed. Near IR region study was located in the range of the infrared spectrum between 20000 cm^{-1} to 4000 cm^{-1} (500-2500 nm). To facilitate the presentation of the results, this section is presented in nm.

Figure 29 shows the results of the Near-IR study. All samples had a broad weak band in the region of 900-1020 nm with two maximum peaks around 957 nm and 991 nm, corresponding to the second overtone of O-H stretching vibrations of hydroxyl groups in octahedral layers bonded to metal atoms. These bands appeared at 3638 cm^{-1} in the Mid-IR. Furthermore, it is possible to observe a small shoulder at 1017 nm, which can be assigned to the third overtone of O-H stretching vibrations of hydroxyl groups in interlayer water (in mid-IR this can be observed around 3205 cm^{-1}).[106]

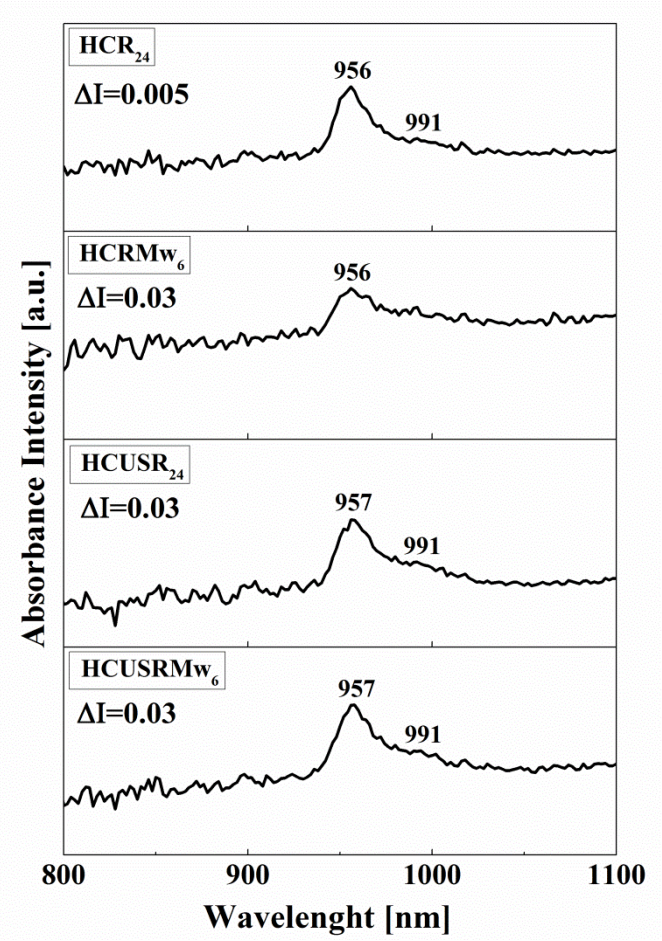

Figure 29. Near-infrared spectra of the hydrocalumites in the 800-1100 nm (12500 cm^{-1} to 9000 cm^{-1}) region.

In Figure 30 we can observe the spectra of the hydrocalumites in the 1200-2400 nm (8300 cm^{-1} to 4100 cm^{-1}) region. The spectral region between 1100 and 1600 nm showed a broad band for all samples, with 3 peaks around 1404 nm, 1438 nm and 1494 nm. These peaks correspond to the first overtone of the hydroxyl groups. The most intense peak at 1404 and 1438 nm can be related to the first overtone of the stretching vibrations of O-H groups bonded to metal atoms. The shoulder around 1494 nm can be attributed to the first overtone of O-H stretching vibrations of hydroxyl groups in interlayer water.

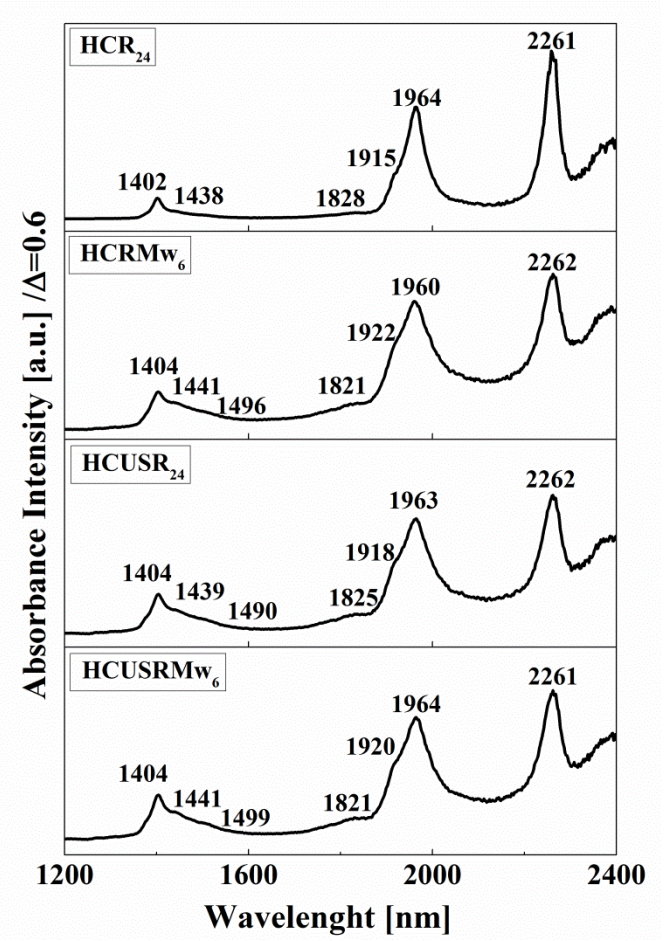

Figure 30. Near-infrared spectra of the hydrocalumites in the 1200-2400 nm (8300 cm^{-1} to 4100 cm^{-1}) region.

Finally, in the range of 1667-2500 nm, two intense bands were observed at 1963 nm and 2263 nm. The band at 1963 nm can be related to the overtones of OH vibrations of the water, and the band at 2263 nm corresponds to overtones of vibrational modes of carbonate ion.

Conclusions

Hydrocalumite-type materials were studied by Raman, near infrared, mid-infrared and far infrared spectroscopies. The mid-infrared results showed the characteristic bands of the hydrocalumites, as well as the formation of the calcite in low amounts. Moreover, the samples stirred by ultrasounds ($HCUSR_{24}$ and

HCUSRMw$_6$) exhibited a band at 1508 cm^{-1} due to a higher adsorption of the carbonate. Raman results confirm the presence of carbonate in these samples since the band at 1076 cm^{-1} can be attributed to interlayer carbonate bonded to the water due to the presence of the katoite phase. The Far-IR spectra provide information about the cations located in the interlayer space, and confirm the presence of the Cl^- anion in the interlayer space. Finally, near infrared spectra showed the characteristic overtones bands of the hydrocalumites. However, it was not possible to observe significant differences between the samples because of the similar composition of the hydrocalumites.

Acknowledgments

Authors acknowledge Ministerio de Economía y Competitividad of Spain and Feder Funds (CTQ2011-24610), Catalan Government for FI grant (2012FI_B00564) and to a mobility grant (2013AEE-34) from the Universitat Rovira i Virgili.

4.1.3 Nitriles compounds as probe molecules to study the acidity and basicity strength of hydrocalumites prepared with ultrasounds and microwaves

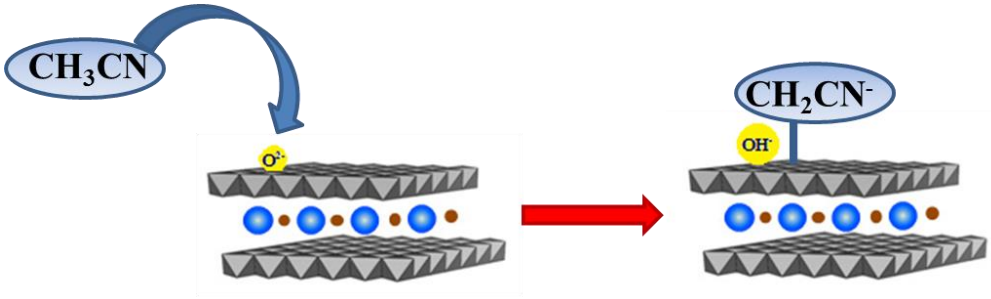

Abstract

Four hydrocalumites were synthesized by coprecipitation of chloride salts with and without the use of ultrasounds. All the samples were aged by refluxing with and without microwaves. We next studied the decomposition of the hydrocalumites, as well as their acidity and basicity by infrared spectroscopy. Pivalonitrile and acetonitrile were used as probe molecules to be adsorbed on the samples. Results confirmed that the thermal decomposition of hydrocalumites occurs in successive steps.

After pivalonitrile adsorption, the samples outgassed at room temperature evidenced very weak Brønsted acidity. The amount of Lewis acid sites increased after activation of the samples at 100 °C and after outgassing at 400 °C, stronger Lewis acid sites were detected. Moreover, these samples had strong basicity due to the O^{2-} anions, evidenced by the formation of $(CH_2CN)^-$ anions after acetonitrile adsorption at high temperature.

Introduction

Infrared spectroscopy of adsorbed probe molecules is extensively used to study the acid and basic sites in solids. Some of the most commonly used probe molecules are pyridine, carbon monoxide, carbon dioxide, methanol, ethanol, chloroform, ammonia, among others. Nitrile compounds, in particular, are the most used probe molecules in the characterization of acid and basic sites.[107–109]

The adsorption of pivalonitrile (PN) is often used for surface acidity tests.[110] Pivalonitrile is a very weak base, sterically hindered by the ramification of the alkylic chain, whose IR spectrum is characterized by a strong band observed in the liquid phase at 2235 cm^{-1}. This band is due to the stretching of the υC≡N bond, and shifts to higher frequency when pivalonitrile interacts with electron-withdrawing centers through its nitrogen electrons lone pair.[110]

On the other side, acetonitrile (AN) can be used to characterize both the acidity and basicity of the materials, due to the hydrogen atoms of the methyl group that present a proton-donor character. The rupture of the C-H bond in the methyl groups of acetonitrile at the surface of very basic materials lead to the formation of $(CH_2CN)^-$ carbanion and/or the corresponding dimeric compound, whose IR features have been reported to fall below 2200 cm^{-1}.[88,111]

Many studies in the last decades used nitriles as probe molecules for zeolites, oxides and mixed oxides, to analyze their acid strength.[87–91] Busca *et al*. (2008) studied the adsorption and desorption of acetonitrile in different inorganic solids (e.g. silicas, aluminas, metal oxides, protonic zeolites and clays).[92] Aboulayt *et al*. (1995) studied the mechanism of acetonitrile hydrolysis on hydroxylated zirconium dioxide;[93] and Morterra *et al*. (2002) studied the acetonitrile adsorption at room temperature in several ZnO_2-based systems for their surface characterization.[94] There are fewer studies focused on the characterization of basic sites as well as acidic sites. Koubowetz *et al*. (1980) studied the adsorption of acetonitrile to analyze its interactions with the atoms of MgO.[95] Prinetto *et al*. (2004) also investigated the acid-basic properties and nature of Pd phases and the metal-support interactions in Pd/Mg(Al)O catalysts obtained from hydrotalcites and

in Ni-LDH based catalysts. These studies were performed by FTIR spectroscopy using acetonitrile and carbon monoxide as probe molecules.[96,112]

Hydrotalcites are part of the family of Layered double hydroxides (LDHs), being the most common compounds. Hydrocalumites (Ca/Al-LDH) are also LDHs compounds with formula $Ca_2Al(OH)_6Cl{\cdot}2H_2O$.[22] These materials are used in catalysis due to their basic properties,[24,27,28] and are frequently applied for environmental applications such as the immobilization of toxic cations or surfactants.[13,32,34,35]

Many studies used nitriles as probe molecules to analyse the acid or basic strength in solid catalysts.[87–96] However, the acidic and basic properties of the hydrocalumites have not been deeply studied although these properties are of major interest for understanding of catalytic reactions.[91]

The aim of this paper is to study the acidity and basicity of several hydrocalumite-type materials by infrared spectroscopy, through the adsorption of pivalonitrile and acetonitrile as probe molecules. Special attention will paid to study the effect of using ultrasounds during precipitation and microwaves for aging compared with conventional stirring and heating methods.

Experimental

Preparation of materials

Hydrocalumites were synthesized by the co-precipitation method. For details of the methodology please refer to Granados-Reyes *et al*.[105] (chapter 4.1.1). An aqueous mother solution containing $CaCl_2{\cdot}2H_2O$ (sigma-Aldrich) and $AlCl_3{\cdot}6H_2O$ (Riedel-de Haën) was prepared with a 2:1 Ca^{2+}/Al^{3+} molar ratio. The pH and the temperature were kept constant at 11.5 ± 0.1 and 60 ºC, respectively. Magnetic stirring or ultrasounds were used for mixing during precipitation. After complete addition of the metallic salts, the mother solution was aged by several treatments (described in Table 7) using microwaves or conventional heating, under refluxing at different conditions.

Finally, all samples were filtered at room temperature, washed with deionized and decarbonated water and then dried in an oven at 80 ºC overnight.

Table 7. Aging treatments of hydrocalumites.

Sample	Ultrasound[a]	Aging		
		Heating	T (ºC)	Time (h)
HCR_{24}	No	conventional	60	24
$HCRMw_6$	No	microwave	60	6
$HCUSR_{24}$	Yes	conventional	60	24
$HCUSRMw_6$	Yes	microwave	60	6

a during precipitation

FT-IR in situ study of thermal decomposition.

Pure powder disks of the hydrocalumite materials have been outgassed at increasing temperatures up to 400 °C in the IR cell directly connected to oven and gas manipulation apparatus. Spectra were recorded at room temperature immediately after the heating step by means of on a NICOLET 380 FT-IR spectrometer, DTGS detector, KBr beamsplitter. Spectra were acquired by accumulating 100 scans at 4 cm^{-1} resolution (OMNIC software).

FT-IR study of the acid strength of hydrocalumites-type materials by pivalonitrile adsorption

Pivalonitrile (PN) was used as probe molecule adsorption to study the acid strength in the samples. Pressed disks of pure material were prepared with weights among 16 and 22 mg of sample. These were activated at 400 ºC for 1 h under vacuum into the IR cell connected to a gas manipulation apparatus. Pivalonitrile (0.09 Torr at equilibrium) was introduced at room temperature and evacuated at the same temperature to eliminate physisorbed species. Stepwise adsorption and desorption was continued at 100 °C and 400 °C. The infrared spectra of the adsorption and desorption of pivalonitrile were subtracted, once at a time using the OMNIC software.

FT-IR Study of the basic strength of hydrocalumites-type materials by acetonitrile adsorption

Acetonitrile (AN) was used to study the basic strength of hydrocalumites by adsorption at increasing temperatures. Pressed disks were prepared of pure catalyst powder and activated by outgassing at 400 °C for 1 h in the IR cell. Once activated

the sample, the acetonitrile was adsorbed on the surface of the material at room temperature. Stepwise acetonitrile adsorption was continued to 400 °C, and spectra of both adsorbed species and gas phase species were recorded. In the last step, the sample was evacuated at 400 ºC to evidence strongly adsorbed species at the catalytic surface.

Results and discussion

In situ thermal decomposition studies of hydrocalumite-based materials.

In figure 31 we depict the spectra of pure powder HCR_{24} sample submitted to outgassing at increasing temperature as an example of the hydrocalumite thermal evolution spectra.

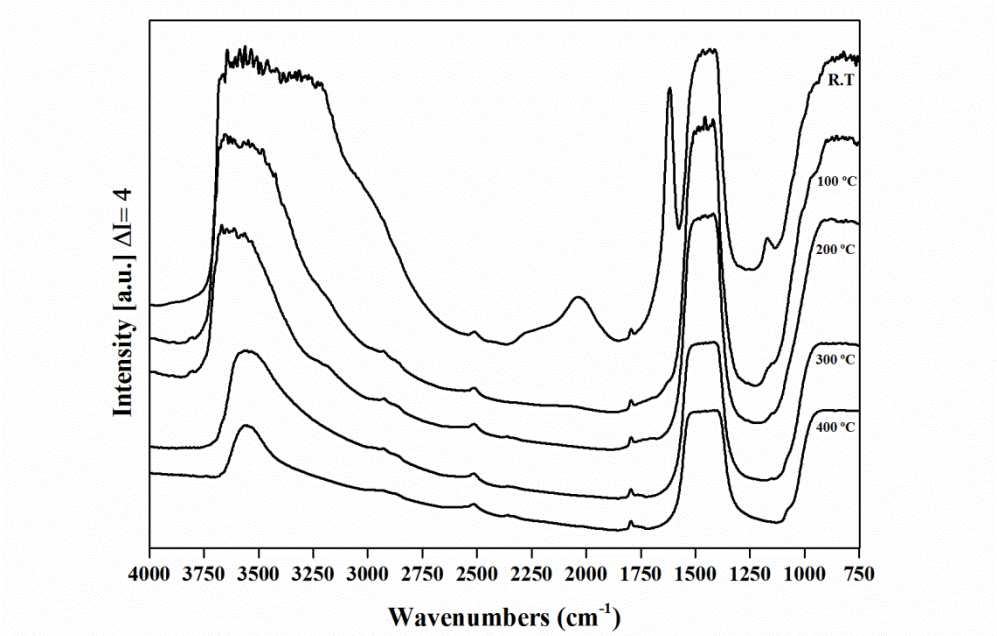

Figure 31. FT-IR spectra of pure powder HCR_{24} recorded at increasing temperatures (from top to bottom: room temperature, 100 °C, 200 °C, 300 °C, 400 °C)

Clearly, the spectrum recorded at room temperature showed as main features bands those due to carbonate bulk species, characterized by strong and ill-resolved absorption about 1450-1400 cm^{-1}, and corresponding overtones at about 1800 and 2500 cm^{-1}, and bands due to adsorbed water, characterized by the sharp and strong deformation mode at 1630 cm^{-1} and by a broad and weaker band in the range 2200-

2000 cm^{-1}, due to overtones. Correspondingly, the OH stretching region was composed by a broad absorption extending from 3750 to 3000 cm^{-1}, due to surface OH groups and adsorbed water interacting through H-bonds. A very weak and diffuse absorption centred at 3000 cm^{-1} has been previously assigned to stretching vibrational modes of water molecules in the interlayer, interacting with the chloride anions.[113] Increasing the pretreatment temperature at 100 °C resulted in the desorption of molecularly adsorbed water, thus to the disappearance of the band at 1630 cm^{-1} and the weakening of the broad bands in the range 3750-3000 cm^{-1}. This step should correspond to the first weight loss recorded by TG analysis for these materials, therefore, to the loss of physically adsorbed water and the loss of almost all interlayer water molecules, which was complete around 200 °C.[105] Correspondingly in the high frequency region of the spectrum we were able to discriminate several components in the OH absorption band, also detectable after heating at 200 °C. Maxima can be detected at 3180 cm^{-1} ca, 3550 cm^{-1}, and 3650 cm^{-1}, assigned to H-bound interlayer water, strongly bonded to M-OH groups of the hydrocalumite structure.

Further heating in the 200-400 °C range led to the disappearance of all the high frequency components and to the formation of a weak and broad band centred at 3550 cm^{-1}. This interval corresponds to the second weight loss detected by TG and assigned to the dehydroxylation of the Ca–Al hydroxide layer. At 400 °C the collapse of the lamellar structure of hydrocalumite to oxide phases (CaO and mayenite) is likely to occur.

Nevertheless, bands due to carbonate species were still the main features of the spectrum at all the temperatures considered. Indeed decarbonation of similar materials has been reported to occur at temperatures higher than 700 °C.[114]

The comparison of several materials after the same treatment in vacuum at 400 °C arose some differences (Figure 32).

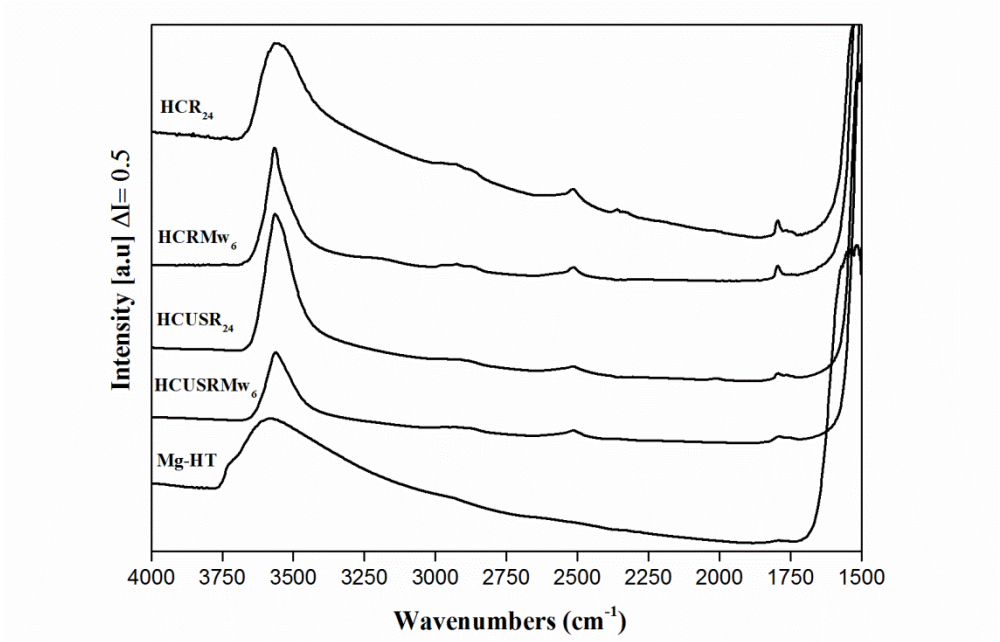

Figure 32. FT-IR spectra of pure powder hydrocalumites recorded after outgassing at 400 °C. Bottom spectrum: reference Mg-HT

After the analysis of the IR spectra recorded at increasing temperatures, we chose to carry out PN adsorption over the catalyst surfaces pretreated in vacuum at three significant temperatures: i) prolonged outgassing at room temperature (i.e. in the presence of physisorbed water and carbonates); ii) outgassing at 100 °C (i.e. removal of physisorbed water and mostly of interlayer water); iii) outgassing at 400 °C (i.e. deep dehydroxylation and likely loss of lamellar structure). Results are discussed in the following paragraph.

Analysis of the νC≡N modes of pivalonitrile (PN) with acid sites.

In Figs. 33 and 34 the spectra of pivalonitrile adsorbed on the hydrocalumite samples in the C≡N stretching region are reported. For each sample the upper spectra were those recorded in contact with PN gas (the gas-phase spectrum was subtracted) while the lower one (dotted line) was recorded after outgassing.

First, we studied the pivalonitrile adsorption at room temperature. Figure 33 shows the IR subtraction spectra of adsorbed PN at room temperature for all samples in the range of frequency from 2300 to 2200 cm^{-1}. Samples aged by conventional

heating (HCR_{24} and $HCUSR_{24}$) exhibited a broad and complex band with two maxima at 2247 and 2238 cm^{-1} in HCR_{24}, and at 2253 and 2240 cm^{-1} in $HCUSR_{24}$. The bands at 2238 cm^{-1}, in HCR_{24}, and 2240 cm^{-1}, in $HCUSR_{24}$ were only very slightly shifted by the interaction with the surface in comparison with the liquid PN spectrum and can be assigned to H-bonded species over non-acidic OHs. The band at 2247 cm^{-1}, only observed in HCR_{24}, corresponded to PN interacting with weakly Brønsted acid sites whereas the band at 2253 cm^{-1}, only appeared in $HCUSR_{24}$, can be related to the formation of medium-weak Lewis acidity sites, which may be due to exposed Ca^{2+} ions in surface defects.

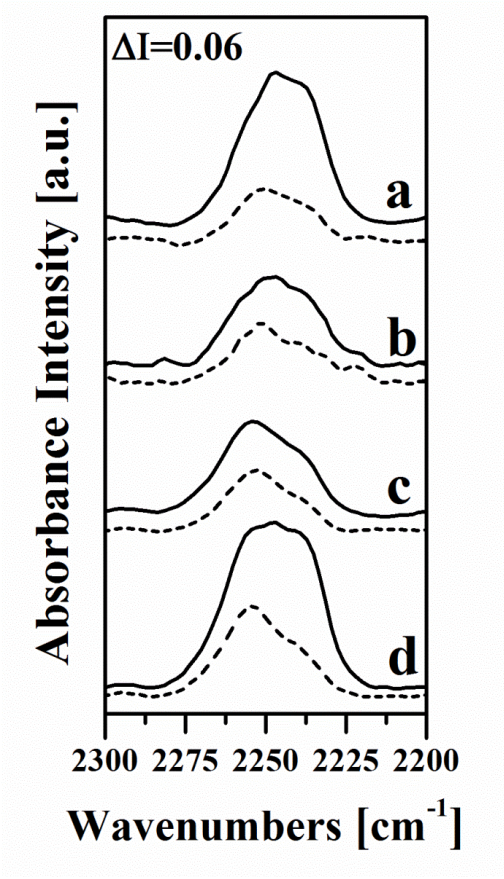

Figure 33. FT-IR subtraction spectra of the surface species arising from room temperature PN adsorption (black line) and desorption (dotted line) over samples: (a) HCR_{24}, (b) $HCRMw_6$, (c) $HCUSR_{24}$ and (d) $HCUSRMw_6$. C≡N stretching region.

Samples aged by microwaves ($HCRMw_6$ and $HCUSRMw_6$) showed a broad band composed by three maxima. The first maximum was observed at 2238 cm^{-1}, in $HCRMw_6$ and at 2240 cm^{-1} in $HCUSRMw_6$ (as for its corresponding conventional heated sample); the second maximum at 2247 cm^{-1}, as in HCR_{24}; and the third maximum around 2254 cm^{-1}, as in $HCUSR_{24}$. Additionally, a weak band at 2281 cm^{-1} can be observed in the $HCRMw_6$ sample. This band can be assigned to PN that interacts with medium-strong Lewis acid sites.

Moreover, it is important to note that the first maximum, related to H-bonded species over non-acidic OHs, shifted to higher frequency values for the samples prepared with ultrasounds ($HCUSR_{24}$ and $HCUSRMw_6$) when compared with those synthesized by magnetic stirring (HCR_{24} and $HCRMw_6$).

After evacuation at room temperature, all the IR bands significantly reduced in intensity and slightly changed in shape and position. In detail, bands below 2250 cm^{-1} (i.e. the band at 2247 cm^{-1} as well as the bands around 2238-2240 cm^{-1}) almost disappeared or were strongly weakened for all samples while the band above 2250 cm^{-1} remained but shifted to lower frequencies. This behavior of the low frequency bands is in agreement with the assignation to nitrile species weakly bound. On the other side, the shift of the high frequency band, more resistant to outgassing as expected for nitriles coordinated over Lewis sites, could be due to the low PN coverage consequent to outgassing of the sample. The band around 2281 cm^{-1}, only detected in the $HCRMw_6$ sample spectrum at room temperature, also weakened.

Next, we proceed to study the pivalonitrile adsorption at 100 ºC. Figures 34-A and 34-B, show the corresponding spectra for the samples stirred with magnetic stirrer, HCR_{24} and $HCRMw_6$, respectively. The two spectra were similar to those obtained when the pivalonitrile was adsorbed at room temperature (Figure 33) but they presented a new shoulder at 2273 cm^{-1}, which was indeed assigned to PN interacting with medium-strong Lewis sites, likely surface Al^{3+} exposed by the activation of the sample at 100 °C (or Ca^{2+} ions in a different coordination). By degassing the HCR_{24} sample, the intensity of the band around 2238 cm^{-1} decreased, the band at 2247 cm^{-1} disappeared, and a new band appeared at higher frequency (2252 cm^{-1}). In addition, the shoulder at 2273 cm^{-1} remained. These results indicate

that higher amounts of PN were preferentially coordinated on Lewis acid sites than interacting with Brønsted acid sites. For the sample aged with microwaves, $HCRMw_6$, after degassing, all bands shifted to lower frequencies and decreased their intensity, except for that at 2251 cm^{-1}, which increased its relative intensity with respect to the other peaks. This behavior confirms that at 100 °C, the amount of weak Brønsted acidic sites decreased while the amount of Lewis acidic sites increased. Additionally, after degassing, the shoulder at 2273 cm^{-1} was still detected, confirming its assignation to PN more strongly adsorbed on Lewis acid sites.

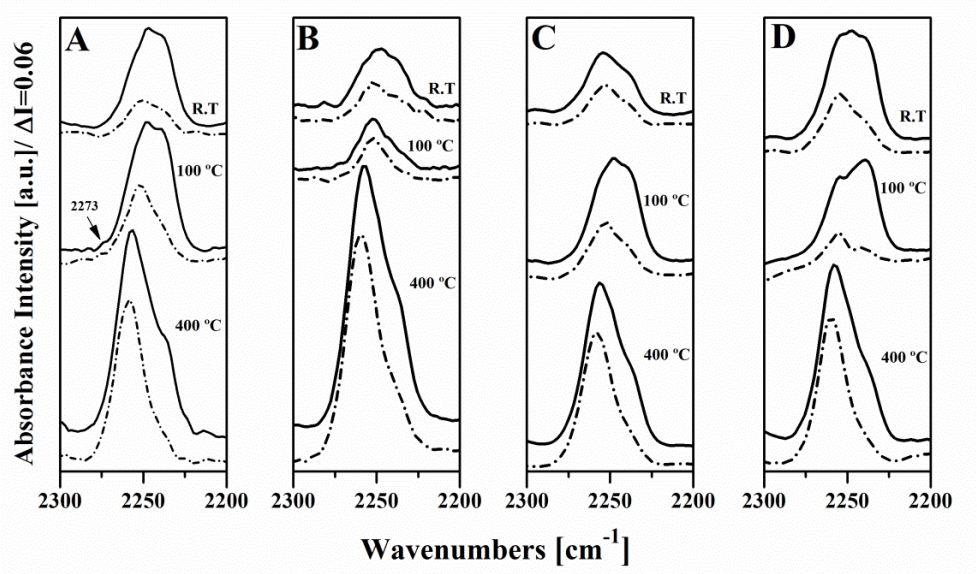

Figure 34. FT-IR subtraction spectra of the adsorbed species arising from PN adsorption (black line) and desorption (dotted line) over the samples: (A) HCR_{24}, (B) $HCRMw_6$, (C) $HCUSR_{24}$ and (D) $HCUSRMw_6$. C≡N stretching region.

In the case of the $HCUSR_{24}$ sample, stirred with ultrasounds and aged by conventional heating, after adsorbing PN at 100 ºC, a broad band with three maxima at 2240 cm^{-1}, 2248 cm^{-1} and 2255 cm^{-1} was observed (Figure 34-C). The band at 2248 cm^{-1} was not evident in the spectrum recorded at room temperature. After degassing, this sample presented the same behavior than HCR_{24}, thus, the band at 2248 cm^{-1} became the main one of the spectrum, with a shoulder at 2240 cm^{-1}.

The $HCUSRMw_6$ sample, stirred with ultrasounds and aged with microwaves, after adsorbing PN at 100 ºC, presented two bands at 2239 cm^{-1} and

2254 cm^{-1} (Figure 34-D). The relative intensity of the band at 2239 cm^{-1} increased with respect to the band at 2254 cm^{-1}, when compared to the spectrum of this sample at room temperature (Figure 33). This indicates that the Lewis-to-Brønsted acid sites ratio decreased, obtaining a higher contribution of Brønsted acidity due to the OH groups. After degassing, the intensity of both bands decreased (Figure 34-D) and the highest frequency band was predominant, according to its assignation to PN on Lewis sites.

When performing the adsorption of PN at 400 °C, the same behavior was observed for all samples. The spectra showed one main band in the range 2256-2258 cm^{-1} and a shoulder around 2237 cm^{-1} (Figure 34). A significant increase of intensity and a shift to higher frequencies was observed for the band appearing at 2256-2258 cm^{-1} when compared to the results obtained by adsorbing PN at 100 ºC (Figure 34). This effect can be explained by the high activation temperature of the samples. As a matter of fact, thermogravimetry,[105] as well as IR thermal analysis, have shown that at this temperature decomposition of the hydrocalumite structure occurs, therefore exposing Ca and Al cations acting as Lewis acid sites.

The samples aged by microwaves exhibited bands at higher frequencies than those aged by conventional heating. After outgassing, the band at 2237 cm^{-1} disappeared whereas the band around 2257 cm^{-1} remained. These results indicate that at 400 ºC the Lewis-to-Brønsted acid site ratio increased for all samples, although strong Lewis acid sites were not observed.

Table 8 shows a summary of the wavenumber (cm^{-1}) for PN adsorption at different temperatures.

Table 8. Wavenumber (cm^{-1}) of PN adsorption at different temperatures

Sample	r.t				100 ºC				400 ºC	
HCR_{24}	-	-	2247	2238	2273	-	2247	2239	2256	2237
$HCRMw_6$	2281	2257	2247	2238	2273	2251	2242	2234	2257	2240
$HCUSR_{24}$	-	2253	2240	-	-	2253	2248	2240	2256	2240
$HCUSRMw_6$	-	2254	2247	2240	-	2254	-	2239	2258	2241

r.t: room temperature

Analysis of the υC≡N modes of acetonitrile (AN) with basic sites.

In this section, we present the results of acetonitrile adsorption at different temperatures on the hydrocalumite samples. For each sample the spectra were recorded in contact with AN gas at the reported temperature (the corresponding gas-phase spectra were subtracted).

Figure 35 exhibits the spectra of the acetonitrile adsorption at different temperatures in the C≡N stretching region for the HCR_{24} sample. In the spectra recorded from room temperature up to 200 °C the characteristic bands due to the formation of carbanions, were not observed. Only the characteristic peaks of acetonitrile at 2272 and 2305 cm^{-1}, with a shoulder at 2255 cm^{-1} appeared. The peak at 2255 cm^{-1} corresponds to C≡N vibrational modes due to the formation of physisorbed species. The bands at higher frequencies are generated by the Fermi resonance between the C≡N stretching and a δCH_3 + υC-C combination. This doublet can be related to AN coordinated to Lewis acid sites on Al^{3+} ions [115] partially overlapped with the doublet corresponding to AN weakly interacting with OH groups, in agreement with results from PN adsorption reported in the previous section.

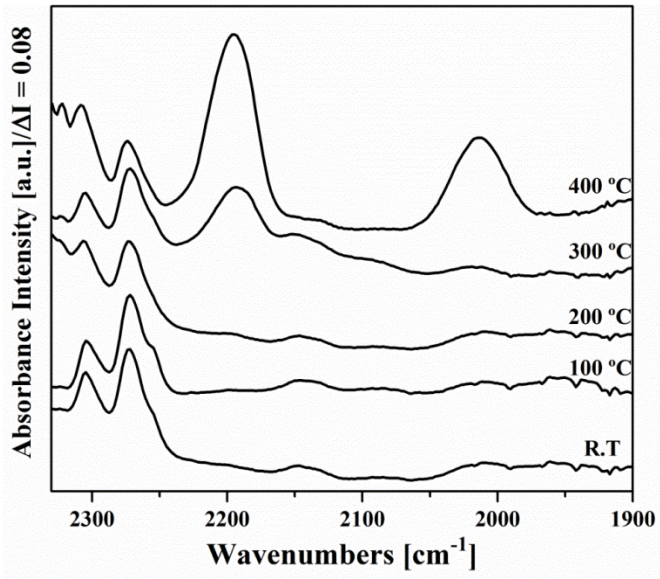

Figure 35. FT-IR subtraction spectra of Acetonitrile adsorption on the sample HCR_{24} at increasing temperatures (2350 to 1900 cm^{-1}).

However, at 300 °C a new band at 2196 cm^{-1} was formed, indicating a reaction between acetonitrile and the catalyst surface (Figure 35). At 400 °C this band was even more intense and a second band appeared around 2016 cm^{-1}. These bands must be assigned to adsorbed species different than AN. According to Lavalley (1996), the band at 2016 cm^{-1} could correspond to the $(CH_2CN)^-$ carbanion formation at the catalyst surface, stabilized by resonance, whose C≡N stretching band should fall at about 2050 cm^{-1} depending on the exposed cations.[88] The band appearing at higher frequency (2196 cm^{-1}) could be related to the anion formed by dimerization of AN, through the reaction of the same carbanion discussed above. The υC≡N frequency of such species has been reported at about 2110 cm^{-1} and the corresponding υNH frequency was around 3260 cm^{-1}. [88] Prinetto *et al.* (2004) also detected similar species after AN adsorption at room temperature over Mg(Al)O mixed oxides MgAl layered double hydroxides, and assigned the band at 2088 cm^{-1} to $(CH_2CN)^-$ anions coordinated over Mg ions whereas the band characteristic of polyanions was reported at 2161 cm^{-1}, with a shoulder at lower frequencies.[96,112] They also suggested that the preferential formation of anions or polyanions depends on the AN partial pressure at the catalyst surface, i.e. on the AN coverage, polyanions forming only in the presence of an excess of AN. This effect will explain the detection of dimeric species as first adsorbed species in our experimental conditions, where the catalyst surface is saturated with AN.

It is worth noting that the $HCUSR_{24}$ sample presented the same behavior (Figure 36) as that observed for the HCR_{24} sample (Figure 35). The adsorption contact time at 400 °C was rised up to 1 h to observe possible changes in the spectrum. In fact, a reduction in the intensity of the band around 2200 cm^{-1} was recorded while the band around 2000 cm^{-1} maintained, as shown in Figure 36. Probably, the dimeric species (those firstly detected in the spectrum) are less stable (more reactive) than the adsorbed $(CH_2CN)^-$ anions. This could be explained by some decomposition of the sample due to the high temperature used. The above discussion indicates the high basicity of these materials. Moreover, the sample $HCUSR_{24}$ exhibited more intense peaks assigned to adsorbed anions than the HCR_{24}

sample at 400 ºC. Therefore, the precipitation of the starting salts in ultrasonic helps obtaining of a higher basicity in the final material.

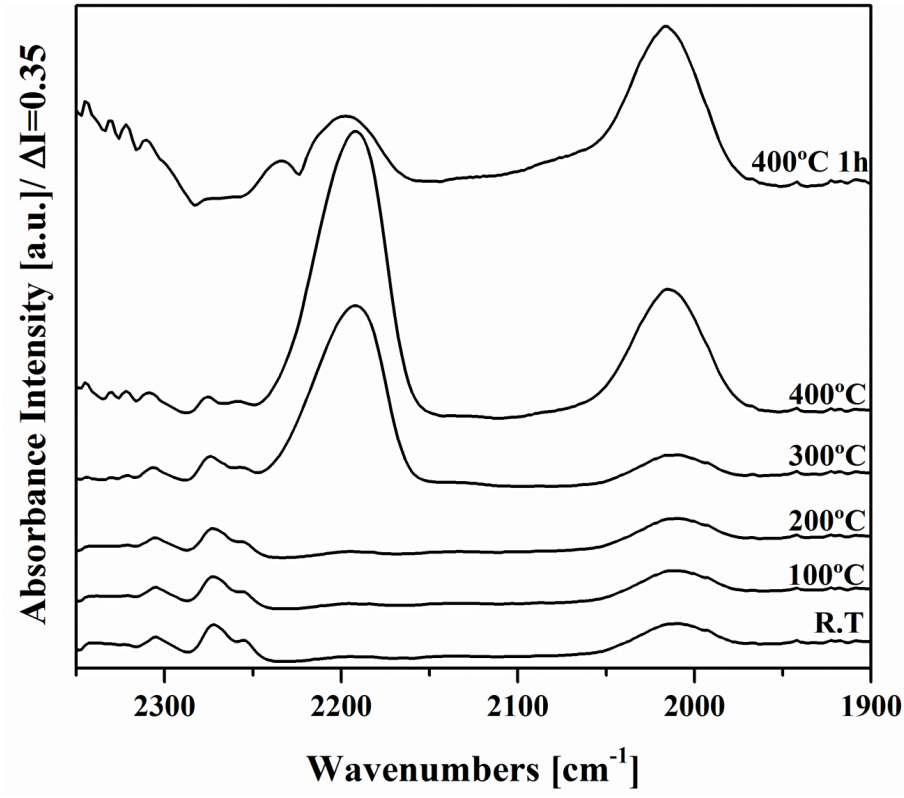

Figure 36. FT-IR subtraction spectra of Acetonitrile adsorption on the sample $HCUSR_{24}$ at increasing temperatures (2350 to 1900 cm^{-1}).

The spectra of the sample magnetically stirred and aged by microwaves ($HCRMw_6$) presented a decrease in the intensity of the peaks at 400 ºC with respect to the $HCUSR_{24}$ sample (aged by conventional heating). However, the $HCRMw_6$ sample presents an increase in the acetonitrile adsorption with respect to the $HCUSR_{24}$ sample (Figure 37). This could point out a higher reactivity towards acidic probe molecules. In these spectra we also detected a shoulder at 2065 cm^{-1} of the main band at 2016 cm^{-1}. The complexity of this band suggests an increase in the heterogeneity of the surface, exposing different cationic sites available to the carbanion coordination.

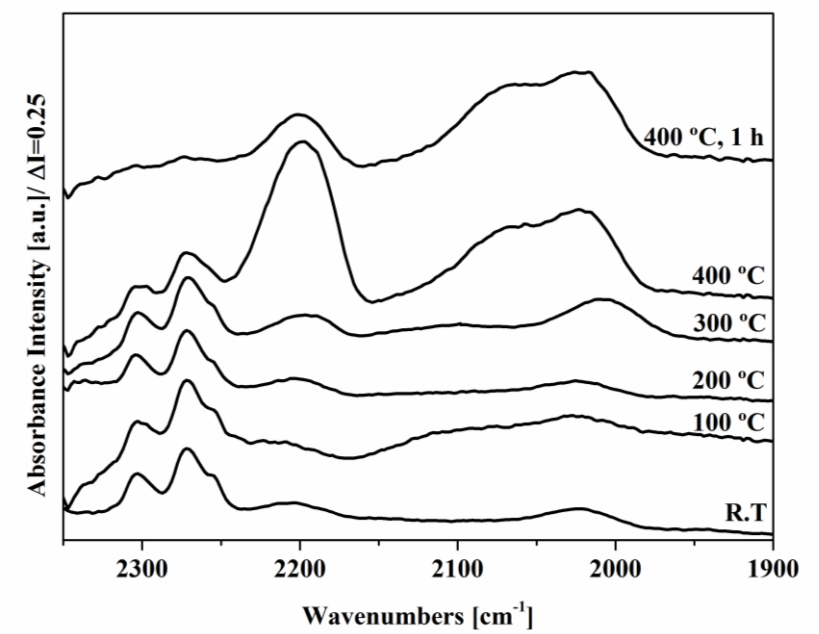

Figure 37. FT-IR subtraction spectra of Acetonitrile adsorption on the sample $HCRMw_6$ at increasing temperatures (2350 to 1900 cm^{-1}).

Finally, the sample stirred by ultrasounds and aged by microwaves ($HCUSRMw_6$) presented a different behavior in comparison to the previous samples since there was no formation of new bands at 300 °C or 400 °C (Figure 38). After 1 h of adsorption at 400 °C, the formation of a very weak peak was observed at 2200 cm^{-1} (characterizing the dimerization of the CH_3CN). Despite maintaining the adsorption up to 3 h at 400 °C, the formation of the band around 2000 cm^{-1} was not observed. However, an increase in the intensity of the bands at 1794 cm^{-1} and 1075 cm^{-1} was recorded on longer adsorption at 400 °C (Figure 38). This could be related to the formation of acetamide type species due to nucleophilic attack of $CH_3C{\equiv}N$ with hydroxyls groups present at the surface.[88] The formation of acetamide species by hydrolysis can be also responsible for the decrease of the υOH band intensity (around 3562 cm^{-1}). Therefore, the use of microwaves and ultrasounds during hydrocalumite preparation resulted in different surface characteristics of the $HCUSRMw_6$.

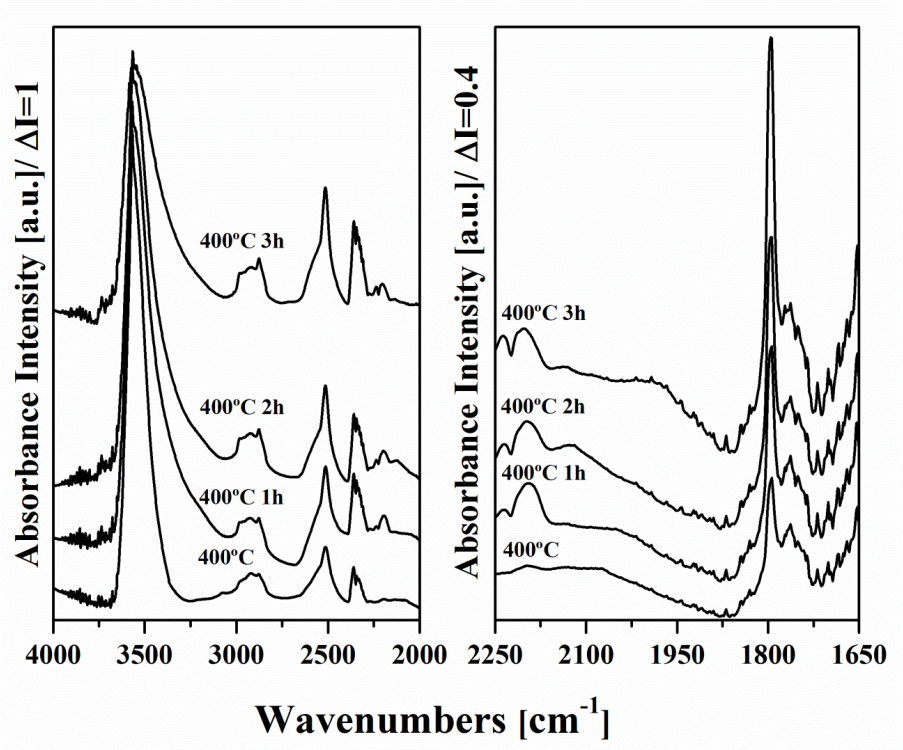

Figure 38. FT-IR subtraction spectra of Acetonitrile adsorption over the sample $HCUSRMw_6$ at different temperatures in the range from 4000 to 1650 cm^{-1}.

These results confirm the formation of adsorbed anions, which evidences the strong basicity of O^{2-} sites in these materials. Figure 39 shows the spectra of the four hydrocalumites recorded after adsorbing AN at 400 ºC. The band around 2200 cm^{-1}, characteristic of the CH_3CN dimerization, increased in wavenumber in the following order: $HCUSR_{24}$ < HCR_{24} <$HCRMw_6$<$HCUSRMw_6$. The same effect was observed with the band around 2000 cm^{-1} (characteristic of $(CH_2CN)^-$) where the variations in wavenumber were $HCUSR_{24}$ < HCR_{24}<$HCRMw_6$<$HCUSRMw_6$.

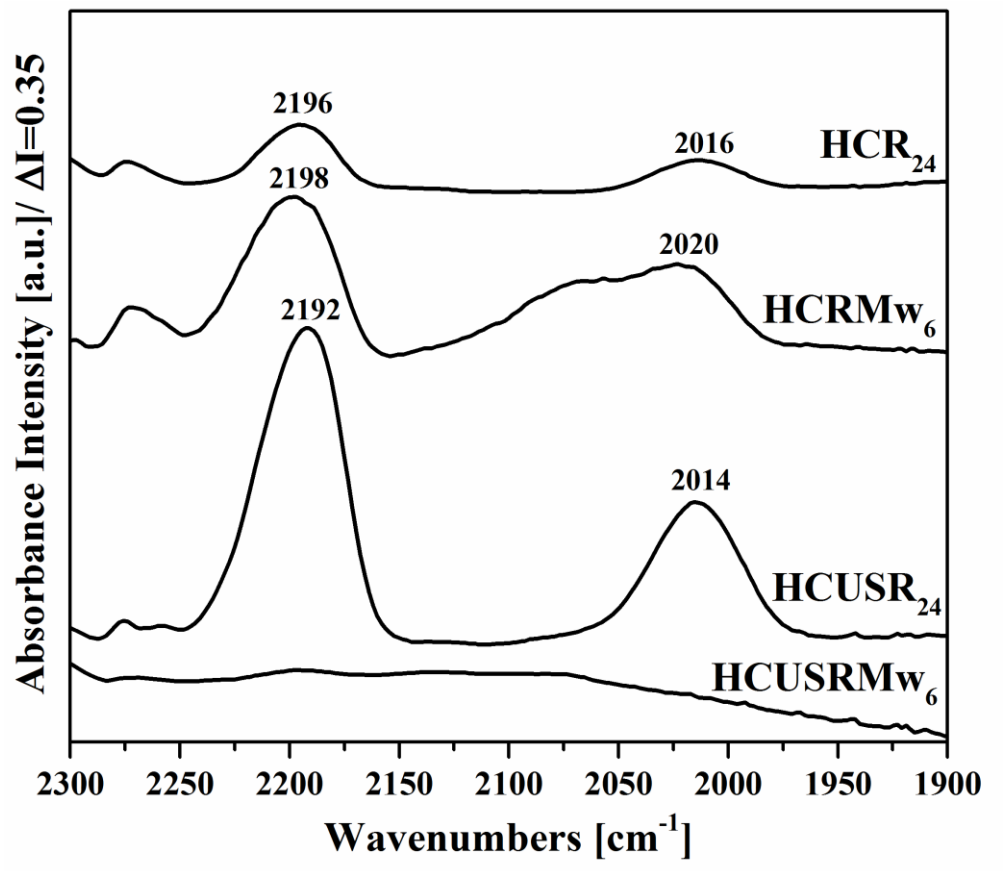

Figure 39. FT-IR subtraction spectra of surface species arising from Acetonitrile adsorption on the samples at 400 ºC in the range from 2300 to 1900 cm^{-1}.

The intensity of the band is another important factor to characterize basicity since the higher intensity involves the presence of higher amounts of basic sites. The samples show the following order regarding the $(CH_2CN)^-$ peak intensity: $HCUSR_{24}$ >$HCRMw_6$ > HCR_{24}. $HCUSR_{24}$ had the highest relative intensity of the $(CH_2CN)^-$ peak, which is also complex and possibly detectable already at room temperature. It seems that oxygen basic sites are more active in C-H bond breaking, while, at the same time, different cations are exposed at the surface, available for anions coordination.

Conclusions

By TF-IR spectroscopy we checked that the thermal decomposition of these samples occurs through successive steps of dehydration, dehydoxylation and layered structure decomposition. Moreover, PN adsorption over the samples outgassed as such at room temperature mainly evidenced very weak Brønsted acidity, possibly increased by the magnetic stirring. Ultrasounds technique during precipitation appears to increase the amount of weak Lewis acid sites, likely Ca ions, characterized by bands at 2253-2255 cm^{-1}. The amount of Lewis acid sites increased after activation of the samples at 100 °C (i.e. over dehydrated surface) and after outgassing at 400 °C, stronger Lewis sites were detected (CN stretching bad at 2258-2259 cm^{-1}). However, at this temperature the lamellar structure was practically lost. All these samples are characterized by strong basicity of the O^{2-} anions, evidenced by the formation of $(CH_2CN)^-$ anions after AN adsorption at high temperature.

Acknowledgments

Authors acknowledge Ministerio de Economía y Competitividad of Spain and Feder Funds (CTQ2011-24610), Catalan Government for FI grant (2012FI_B00564) and to a mobility grant (2013AEE-34) from the Universitat Rovira i Virgili.

UNIVERSITAT ROVIRA I VIRGILI
HYDROCALUMITE-BASED CATALYSTS FOR GLYCEROL REVALORIZATION.
Judith Cecilia Granados Reyes
Dipòsit Legal: T 1362-2015

CHAPTER 4

Results and discussion

Catalytic transesterification of glycerol with dimethyl carbonate to obtain glycerol carbonate

UNIVERSITAT ROVIRA I VIRGILI
HYDROCALUMITE-BASED CATALYSTS FOR GLYCEROL REVALORIZATION.
Judith Cecilia Granados Reyes
Dipòsit Legal: T 1362-2015

4.2. Background about the catalytic transesterification of glycerol with dimethyl carbonate to obtain glycerol carbonate.

Glycerol carbonate (4-hydroxymethyl-1,3-dixolan-2-one) is an important and interesting derivative from glycerol due to its low toxicity, good biodegradability and low boiling point. Because of these properties, this compound has many applications in different industrial sectors, especially as non-volatile polar solvent, as intermediate in organic synthesis (e.g. monomer in the synthesis of polycarbonates, polyurethanes and polyglycerols), as precursor in biomedical applications or as protector in the carbohydrates chemistry. Also, it is used as component of gas separation membranes, a component in coatings, and in the production of polyurethane foams and surfactants.[12,116,117] (its molecular structure shown in Figure 40)

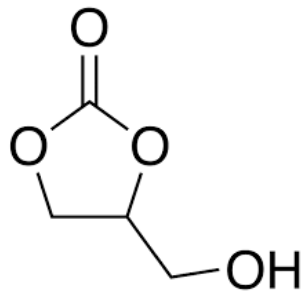

Figure 40. Molecular structure of glycerol carbonate.

Traditionally, glycerol carbonate has been prepared in the industry by reacting glycerol with phosgene but due to the high toxicity and corrosive nature of this reagent, new alternative routes have been investigated.[118]

At middle 90s, several methods for glycerol carbonate manufacture were patented, such as the reaction of glycerol with CO and oxygen at high pressure using Cu(I) salts as catalysts[119] or by reacting glycerol with organic carbonates in the presence of homogeneous or heterogeneous catalysts with the aim to favour the heterocyclation of two neighbours hydroxyls of glycerol, and thus, to form the glycerol carbonate.[120] In the studies performed by Mouloungui *et al* (1996), they observed that transcarbonatation of glycerol takes place directly by using cyclic

organic carbonates (ethylene carbonate, propene carbonate) as well as by using non-cyclic carbonates (dimethyl carbonate, diethyl carbonate) as sources of carbonates. These authors postulated that the diol radicals are formed on the basic sites of catalysts: basic oxides, basic forms of X and Y zeolites or bicarbonated or hydroxylated anionic-exchange resins. The best results were achieved with ethylene carbonate as carbonate source and using macroporous resins with basic properties as catalysts, obtaining yields of 86-88 % at 30 min in a discontinuous reactor, and at 7 min in a continuous reactor.[120]

Other method for the synthesis of glycerol carbonate, initially published in patents, consists of the catalytic carbonylation of glycerol with urea (Figure 41).[121–127] The reaction is carried out in 2 consecutive steps of carbamilation and carbonatation using mainly heterogeneous catalysts such as ZnO, MgO or $ZnSO_4$ at temperatures of 140-180 ºC. Thus, the final reaction system is formed by 3 phases: liquid (glycerol/glycerol carbonate), solid (catalyst) and gaseous (NH_3 released during reaction).

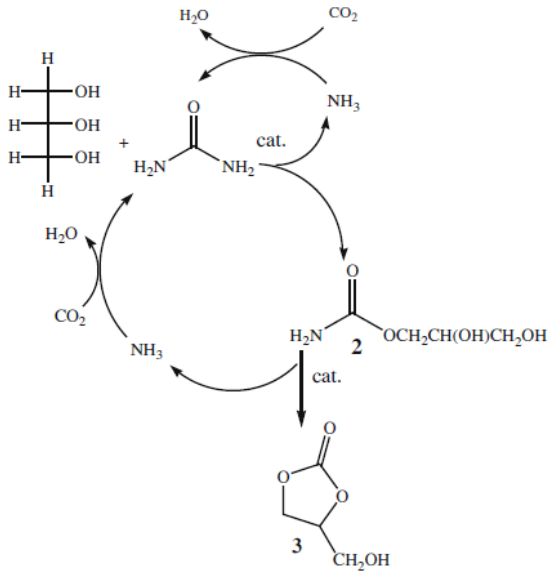

Figure 41. Synthesis of glycerol carbonate by glycerolysis of urea.[128]

Mouloungui *et al*. concluded that the nucleation of $ZnSO_4$ catalyst and the production “in situ” of gaseous ammonia modify the equilibrium state favouring the

formation of glycerol carbonate. They reported, as best result, a yield of 90 % in a batch reactor of 25 l at 140 ºC with pressures of 30 mbar to 5 mbar with a reaction time of 6.5 h.[121–123] Okutsu and Kitsuki prepared glycerol carbonate by reacting glycerol with urea using ZnO as catalyst in the presence of a dehydrating agent ($MgSO_4$) at 120 ºC. After 6 h of reaction, the conversion of glycerol was of 62-65 % with selectivity to glycerol carbonate of 92 %.[124–127] Aresta *et al*. published yields of 80 % at 145 ºC after 3 h of reaction using equimolar amounts of glycerol and urea with γ-zirconium phosphate as catalyst.[128–130]

Many authors have reported the use of urea and glycerol as a method of synthesis of glycerol carbonate. Climent *et al*. (2010) studied the transesterification of ethylene carbonate with glycerol and urea, catalyzed by basic oxides derived from hydrotalcites to obtain glycerol carbonate. Their results showed that balanced bifunctional acid-base catalysts were the most active and selective catalysts.[131] Fujita *et al*. (2013) studied inorganic zinc salts as catalysts to produce glycerol carbonate from glycerol and urea under solvent-free conditions (at 130 °C and at a reduced pressure of 3 kPa). These homogeneous catalysts presented a correlation between the carbonate yield and the amount of zinc species dissolved into the liquid phase.[132] More recently, Ryu *et al*. (2015) used a mixture of ZnO and $ZnAl_2O_4$, obtaining a yield to glycerol carbonate of 82 % and a conversion of 83 %. They found a correlation between the highest yield to glycerol carbonate and the acid base sites ratio.[133] Chem *et al*. (2015) published their studies using acidic, basic and neutral ionic liquids as catalysts for the carbonylation of glycerol with urea. Results showed that neutral ionic liquids had high catalytic activity for this reaction.[134] A Zn/MCM-41 catalyst, reported by Kondawar *et al*. (2015), exhibited an excellent activity for the reaction of glycerol and urea, with 75 % glycerol conversion and 98 % of selectivity to glycerol carbonate. The excellent activity of such catalyst was explained based on the presence of both basic and acidic sites on the same catalyst, which activated the glycerol and urea molecules, respectively.[135] Other heterogeneous catalysts (e.g. gold and palladium supported nanoparticles) have shown to be effective catalysts for the transformation of glycerol into glycerol carbonate.[136] Tin-tungsten mixed oxide catalysts were highly active for the

selective formation of glycerol carbonate (about 52 % of glycerol conversion with >95 % selectivity towards glycerol carbonate).[137] Lanthanum oxide exhibited high catalytic activity with 49 % of glycerol conversion and 82 % selectivity to glycerol carbonate at 150 °C after 4 h reaction.[138,139]

High glycerol conversion and high glycerol carbonate selectivity values were achieved with the reaction of glycerol with urea. However, this reaction must be conducted at pressures below 20-30 mbar in order to separate gaseous ammonia and avoid the formation of undesirable products such as isocyanic acid and biuret.

Another alternative process is the carbonylation of glycerol with CO_2 to obtain glycerol carbonate. George *et al*. (2009) prepared glycerol carbonate from glycerol and CO_2 in methanol, by using nBu_2SnO as catalyst. The reaction was completed in 4 h and the yield of glycerol carbonate obtained was around 35 %.[140] Li *et al*. (2013) studied the transformation of CO_2 and glycerol into glycerol carbonate using acetonitrile as coupling agent, over $La_2O_2CO_3$-ZnO. The best result was achieved with the catalyst whose La/Zn molar ratio was 4 and was calcined at 500 °C.[141] Zhang *et al*. (2014) obtained glycerol carbonate and monoacetin from glycerol and CO_2 in the presence of CH_3CN and Cu/La_2O_3 as catalysts, with glycerol conversion of 33 %, selectivity to glycerol carbonate of 45 % and selectivity to monoacetin of 53 % at 150 °C for 12 h and 7 MPa.[142] Also, Liu *et al*. (2014) synthesized glycerol carbonate from glycerol and CO_2 over a cobalt acetate catalyst at 180 °C for 6 h, with a molar ratio of solvents to glycerol 4:1. The conversion of glycerol was 37 % and the selectivity to GC was 12 %.[143] More recently, Li *et al*. (2015) presented the direct carbonylation of glycerol with CO_2 to glycerol carbonate over Zn/Al/La/X (X=F, Cl, Br) catalysts (mixed oxides derived from calcination of re-constructed hydrotalcites).[144] The addition of propilene oxide to the reaction improved the yield. Thus, Ma *et al*. (2012) studied the simultaneous transformation of CO_2 and glycerol to value-added products using propylene oxide as coupling agent, catalyzed by alkali metal halides. The effects of the reaction temperature, CO_2 pressure, reaction time, amount of catalyst were investigated, finding that, the reaction was very effectively using KI as catalyst.[145] Yu *et al*. (2014) evaluated the catalytic activity of $KI/\gamma\text{-}Al_2O_3$ by the reaction of CO_2, propylene oxide and glycerol

to synthesize glycerol carbonate, at 130 °C for 2 h and 5 MPa of pressure, obtaining a conversion of glycerol of 58 % and yield to glycerol carbonate of 55 %.[146] However, the catalytic results in the carbonylation reaction of glycerol with CO_2 to obtain glycerol carbonate are not highly significant.

The transesterification reaction of glycerol with dimethyl carbonate (DMC) has taken great strength in the last years as one of the most direct and industrial feasible pathways to produce glycerol carbonate. DMC is one of the most used, since its co-product, methanol, can be easily separated and the reaction can be performed at milder conditions.

Biocatalysts have been used in the transesterification reaction of glycerol with dimethyl carbonate to obtain glycerol carbonate. However, this method need long reaction times.[147] In the last year, Waghmare *et al*. (2015) studied the transesterification of glycerol to glycerol carbonate using commercial immobilized lipase (Novozym 435) under ultrasonic irradiation. They found that ultrasounds reduces up the reaction time using Novozym 435 as catalyst to 4 h, compared to conventional stirring method (14 h).[148]

Some studies have been carried out using zeolites as catalysts for the transesterificaión reaction of glycerol with dimethyl carbonate.[149–151] Additionally, Ochoa-Gomez *et al*. (2009) studied different reaction conditions with different basic and acid homogeneous and heterogeneous catalysts. The best results were achieved using a basic heterogeneous catalyst (CaO). The CaO showed 100 % of conversion and >95 % yield after 1.5 h of reaction at 95 °C. Moreover, CaO catalyst led to 70 % of conversion and 70 % of yield to glycerol carbonate at 75 ºC in 15 min of reaction. Ochoa-Gómez *et al*. (2009) also proposed one mechanism for this reaction, in which two conditions are required: close contact between basic catalytic sites and glycerol, and catalyst base strength must be high enough to abstract a proton from the primary hydroxyl group of glycerol (Figure 42).[12]

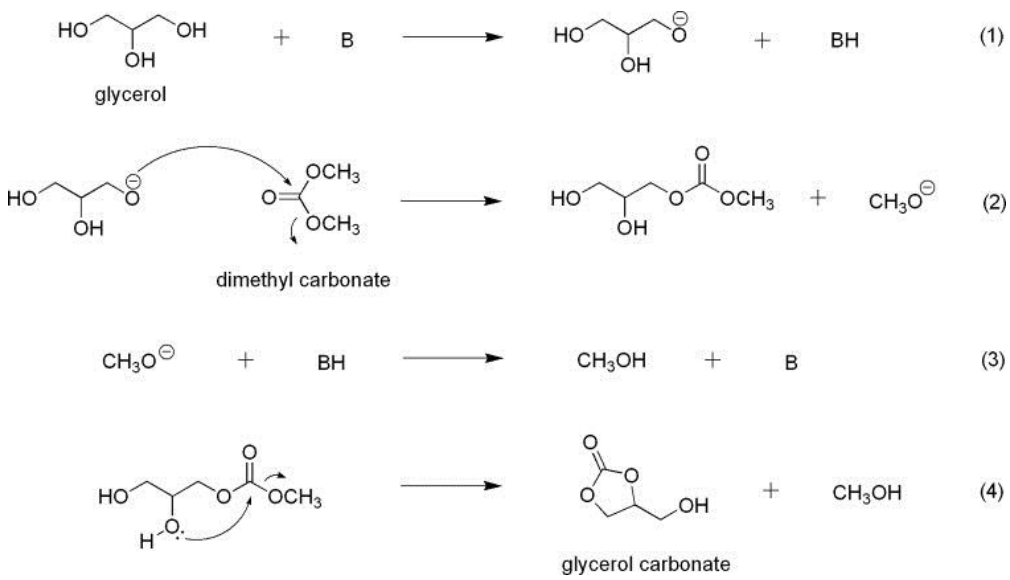

Figure 42. Base-catalyzed transesterification mechanism. B: base.[12]

Hydrotalcite-based catalysts have been widely employed for this reaction; Álvarez *et al.* (2012) used MgAl hydrotalcites supported on α- and γ-Al_2O_3,[152] and also prepared hydrotalcite-like compounds containing a Mg/Al molar ratio of 4, activated by calcination, followed by rehydratation under ultrasounds.[153] or by anion exchange (F^-, Cl^-, CO_3^{2-}).[154] Also Zheng *et al*. (2014) studied the transesterification reaction of glycerol using MgAl hydrotalcites with different Mg/Al ratios. The sample with ratio equal to 2 showed 97 % of selectivity to GC and 67 % of glycerol conversion at 70 °C for 3 h.[155] Yadav *et al*. (2014) studied the effects of various hydrotalcites with different Mg/Al composition loaded on hexagonal mesoporous silica (HMS) for the transesterification reaction of glycerol, in autoclave at 230 ºC for 3 h. They obtained a glycerol conversion of 85 % and selectivity to glycerol carbonate between 84-88 %.[156] Other authors have studied this reaction with ZnO/La_2O_3 mixed oxides,[157] Mg/Al/Zr calcined at different temperatures,[158] and Mg/Zr/Sr mixed oxide base catalysts.[159]

The first studies using uncalcined Mg/Al hydrotalcites were found to be active catalysts for this reaction. Unfortunately it required the use of a harmful solvent (N,N-dimethyl formamide).[160] Doping transition metals cations into Mg/Al hydrotalcites have been also tested as catalysts for this reaction, resulting in yields to

glycerol carbonate between 55-94 % at reaction temperatures in the range 75-100 ºC. [161] More recently, Liu *et al.* (2015) synthetized MgAl hydrotalcite, which was calcined to produce $Mg_4AlO_{5.5}$ mixed oxides. These oxides were modified by introducing $LiNO_3$ and applied to the synthesis of glycerol carbonate from glycerol and dimethyl carbonate. Full conversion of glycerol and 96 % yield of glycerol carbonate at 80 ºC for 1.5 h was obtained with this catalyst.[162] On the other hand, although there are numerous studies about the use of microwaves to transform glycerol into high value-added products,[163–173] there are no references about its application for the transesterification reaction of glycerol to obtain glycerol carbonate.

In this section we present the results obtained by testing several Ca/Al hydrocalumite-type compounds, synthesized by using microwaves and ultrasounds, for the transesterification of glycerol with dimethyl carbonate to obtain glycerol carbonate. Additionally, we will study the effect of the preparation conditions on the catalytic activity of the oxides derived from the calcination of these hydrocalumite-type compounds as well as the effect of using microwaves as heating source during reaction.

4.2.1 CaAl-layered double hydroxides as active catalysts for the transesterification of glycerol to glycerol carbonate

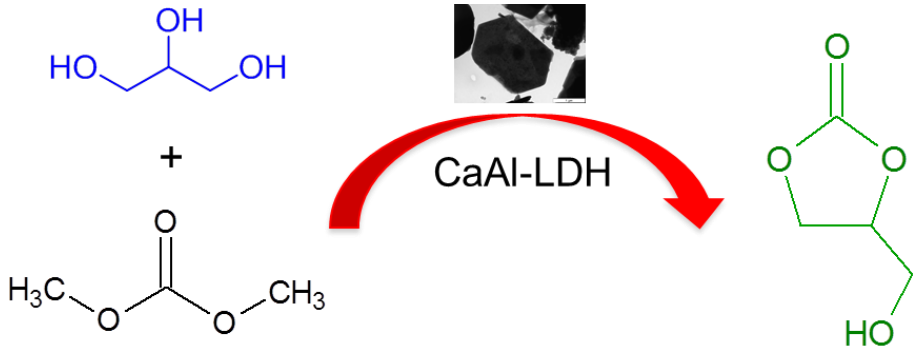

Abstract

Several hydrocalumite-type materials (CaAl-LDHs) were prepared by precipitation using nitrate or chloride salts with and without ultrasounds, and aged hydrothermally in autoclave or by refluxing with and without microwaves. These samples were tested as catalysts for the transesterification of glycerol with dimethyl carbonate to glycerol carbonate. After 3 h of reaction, all catalysts showed high glycerol conversion (70-84 %) and moderate selectivity values to glycerol carbonate (52-65 %) accompanied by the formation of low amounts of glycidol (7-15 %). These results are very interesting taking into account the low surface area of these catalysts (7-25 m^2/g). No significant catalytic differences were observed between the catalysts. This can be due to the similar surface and basic characteristics observed for all of them. By increasing the reaction time, an increase of conversion was observed arriving practically to total conversion after 24 h of reaction, with selectivity to glycerol carbonate in the range 65-75 %. Several catalytic reuses favoured the decarboxylation of glycerol carbonate resulting in the formation of higher amounts of glycidol (30 %) but still maintaining high selectivity values to glycerol carbonate (70 %).

Introduction

Biofuels, derived from renewable raw materials, have emerged as an alternative to overcome the environmental problems associated with the use of fossil fuels. During biodiesel manufacture, by transesterification of vegetable oils with methanol in the presence of basic catalysts, glycerol is formed as by-product in high amounts (10 wt % of the total product).[8] The price of glycerol is falling as fast as biodiesel plants are being built. Thus, it is necessary to find new outlets to convert the surplus of glycerol into high-added value products that improve the economy of the whole process.[5,7,8,174–177]

One challenging option is the obtention of glycerol carbonate, (4-hydroxymethyl-1,3-dioxolan-2-one), which is a relatively new product in the chemical industry with a large potential due to its low toxicity, good biodegradability and high boiling point.[118] Glycerol carbonate is a green substitute for important petro-derivative compounds such as ethylene carbonate or propylene carbonate.[178] Additionally, this compound has many applications in different industrial sectors, such as intermediate in organic synthesis (e.g. monomer in the synthesis of polycarbonates, polyurethanes and polyglycerols),[5,11] biolubricant owing to its adhesion to metallic surfaces and resistance to oxidation, hydrolysis, and pressure,[8] protector in the carbohydrates chemistry, component of gas separation membranes, in coatings, or in the production of polyurethane foams[179] and surfactants.[180] Glycerol carbonate could also serve as a source of glycidol,[181] which is employed in textile, plastics, pharmaceutical and cosmetics industries.

Traditionally, glycerol carbonate has been industrially produced by reacting glycerol with phosgene but due to the high toxicity and corrosive nature of this reagent, new alternative routes have been investigated.[118] Studies have been carried out on the synthesis of glycerol carbonate from glycerol and urea over zinc-containing homogeneous catalysts,[132] and over heterogeneous catalysts, such as gold,[182] lanthanum oxide,[139] hydrotalcite,[131] tin-tungsten mixed oxides[137] and, more recently, polymer-supported metal containing ionic liquid catalysts.[183] High glycerol conversion and high glycerol carbonate selectivity values were achieved.

However, the reaction of glycerol with urea must be conducted at pressures below 20-30 mbar in order to separate gaseous ammonia and avoid the formation of undesirable products such as isocyanic acid and biuret.

An alternative catalytic route to obtain glycerol carbonate is the transesterification reaction of glycerol with organic cyclic carbonates (ethylene carbonate or propene carbonate) or with non-cyclic carbonates (diethyl carbonate or dimethyl carbonate). Dimethyl carbonate is preferred since the reaction can be performed at milder conditions and the co-product methanol can be easily separated. Ochoa-Gomez *et al*.(2009) studied the influence of 12 different basic and acid homogeneous and heterogeneous catalysts at different reaction conditions. The best results were obtained using basic heterogeneous catalysts.[12] CaO catalyst led to 70 % of conversion and 70 % of yield to glycerol carbonate at 75 ºC after 15 min of reaction.[184] Hydrotalcite-based catalysts have been widely employed for this reaction.[156,158–161,185,186] In the first studies, uncalcined Mg/Al hydrotalcites with co-existent hydromagnesite phase were found to be active catalysts for this reaction but the use of a harmful solvent (N,N-dimethyl formamide) was necessary.[160,185] Calcined Mg/Al/Zr,[158] calcined Mg/Zr/Sr [159] and doping transition metals cations into Mg/Al hydrotalcites[161] have been also tested as catalysts for this transesterification reaction resulting in yields to glycerol carbonate between 55-94 % at reaction temperatures in the range 75-100 ºC. More recently, Z. Liu *et al*. (2015) reported full conversion of glycerol and 96 % yield of glycerol carbonate at 80 ºC for 1.5 h in the presence of $Li/Mg_4AlO_{5.5}$ obtained by impregnating calcined Mg/Al hydrotalcite with $LiNO_3$.[186] Finally, Yadav et al. performed this reaction in autoclave at 170 ºC for 3 h obtaining conversion values around 85 % and selectivity to glycerol carbonate values between 84-88 % when using Mg/Al hydrotalcites supported on hexagonal mesoporous silica as catalysts.[156]

Hydrocalumite-type compounds belong to the layered double hydroxides family (LDHs) with formula $[M(II)_{1-x}M(III)_x(OH)_2][X_q^{-x/q}\bullet nH_2O]$ where $[Ca_2Al(OH)_6]^+$ represents the hydrocalumite layer composition, and $[X_q^{-x/q}\bullet nH_2O]$ the interlayer composition.[13] Especifically, the hydrocalumite name is used when the anion is chloride. Hydrocalumites have been widely used in the immobilization

of toxic cations,[36] optimization of concrete properties,[47] but in less extent, for catalysis[103] although the presence of Ca^{2+} instead of Mg^{2+} into the layers can provide interesting basic properties. In recent years, the use of microwaves for the synthesis or modification of materials is becoming an important tool to decrease the synthesis time, with the subsequent energy saving, and to modify the sample properties, which can be of interest for catalysis.[18,54,55,57,99] Additionally, ultrasounds is another interesting technique to improve the synthesis of materials since, when used for the mixing of reagents, allows obtaining materials with more homogeneous composition.[17,57,99]

The aim of this work was to test several Ca/Al hydrocalumite-type compounds, synthesized using microwaves and ultrasounds, as catalysts for the transesterification of glycerol with dimethyl carbonate to obtain glycerol carbonate.

Experimental

Preparation of catalysts

Hydrocalumite-type compounds were synthesized by the co-precipitation method from different starting salts: chlorides (series HC1) or nitrates (series HC2). Two different aqueous solutions containing $CaCl_2 \cdot 2H_2O$ (Sigma-Aldrich) and $AlCl_3 \cdot 6H_2O$ (Riedel-de Haën) or $Ca(NO_3)_2 \cdot 4H_2O$ (Sigma-Aldrich) and $Al(NO_3)_3 \cdot 9H_2O$ (Sigma-Aldrich) were prepared with a 2:1 Ca^{2+}/Al^{3+} molar ratio. These solutions were added dropwise to a 500 ml four neck round-botton flack in an oil bath at 60 ºC previously filled with 250 ml of a mixture of water/ethanol in a 2:3 volumetric ratio. The pH was kept constant at 11.5 ± 0.1, by the simultaneous addition of an aqueous solution of 2 M NaOH (Panreac). Magnetic stirring or ultrasounds were used for mixing during precipitation (Table 9). After complete addition of the metallic salts, the mother solutions were aged by several treatments using microwaves or conventional heating, refluxing or autoclave at different conditions (Table 9). Finally, all samples were filtered at room temperature, washed with deionized and decarbonated water and then dried in an oven at 80 ºC overnight.

Table 9. Aging treatments of hydrocalumites.

Sample	Ultrasound[a]	Aging			
		Heating	Technique	T (ºC)	Time (h)
$HC1R_{24}$	No	conventional	refluxing	60	24
$HC1RMw_6$	No	microwaves	refluxing	60	6
$HC1AC_1$	No	conventional	autoclave	180	1
$HC1AMw_1$	No	microwaves	autoclave	180	1
$HC1AMw_3$	No	microwaves	autoclave	180	3
$HC1USR_{24}$	Yes	conventional	refluxing	60	24
$HC1USRMw_6$	Yes	microwaves	refluxing	60	6
$HC2R_{24}$	No	conventional	refluxing	60	24
$HC2RMw_6$	No	microwaves	refluxing	60	6
$HC2AC_1$	No	conventional	autoclave	180	1
$HC2AMw_1$	No	microwaves	autoclave	180	1
$HC2AMw_3$	No	microwaves	autoclave	180	3
HC2AC100	No	conventional	autoclave	100	1
HC2AMw100	No	microwaves	autoclave	100	1
$HC2USR_{24}$	Yes	conventional	refluxing	60	24
$HC2USRMw_6$	Yes	microwaves	refluxing	60	6

[a] during precipitation

$HC2R_{24}$ sample was modified with a KOH solution, with the purpose of modify the amount of basic centers in the catalyst. 1 g of sample was mixed (dropwise) with 0.047 g of KOH contained in a 1.5 ml of aqueous solution. The resulting sample was dried at 80 ºC overnight.

Characterization methods

Powder X-ray diffraction patterns of the samples were obtained with a Siemens D5000 diffractometer using nickel-filtered CuKα radiation and detecting between 2θ values of 5º-70º. Crystalline phases were identified using the Joint Committee on Powder Diffraction Standards (JCPDS) files (035-0105- Calcium aluminium hydroxide chloride hydrate-$Ca_2Al(OH)_6Cl•2H_2O$, 089-6723- Calcium Aluminun Nitrate Hydroxide Hydrate- $Ca_2Al(OH)_6NO_3•2H_2O$, 089-0217- Katoite-$Ca_3Al_2(OH)_{12}$ and 086-2341- calcite -$CaCO_3$).

Elemental analysis of the samples was obtained with an ICP-OES analyser (Induced Coupled Plasma – Optical Emission Spectroscopy) from Spectro Arcos. The digestion of all hydrocalumites was carried out with concentrated HNO_3. Analyses were performed by triplicate.

Scanning electron micrographs were obtained with a JEOL JSM-35C scanning microscope operating at an accelerating voltage in the range 15-30 kV, work distance of 14 mm and magnification values between 5000 and 30000x.

Transmission electron microscopy of the samples was performed using a JEOL electron microscope Model 1011 with an operating voltage of 80 kV. Samples were dispersed in acetone and a drop of the suspension was poured on to a carbon coated cooper grip and dried at room temperature before measurements. The magnification values used were between 20 and 100 k.

BET surface areas were calculated from the nitrogen adsorption isotherms at -196 ºC using a Quantachrome Quadrasorb SI surface analyzer and a value of 0.164 nm^2 for the cross-section of the nitrogen molecule. Samples were degassed at 90 ºC.

Basicity of the catalysts was evaluated using Hammett indicators: phenolphthalein (pKa = 8.2), nile blue A (pKa = 10.1), tropaeolin O (pKa = 11), thyazole yellow G (pKa = 13.4) and 2,4-dinitroaniline (pKa = 15). 25 mg of catalyst was taken along with 2.5 ml dry methanol and 1 ml of indicator, and kept in a shaker for 2 h.

Catalytic Tests

For the catalytic tests, dimethyl carbonate and glycerol were mixed in a 3.5:1 weight ratio in a 50 ml round bottom 3-neck jacketed glass reactor fitted with a magnetic stirrer, a reflux condenser and a thermometer. The mixture was heated at 90 ºC with constant stirring at 1000 rpm under N_2. Then, 0.15 g of catalyst was added to start the reaction. After 1, 3, 6, 12 or 24 h of reaction, the mixture was filtered and evaporated in a rotatory evaporator. 1 µl of the concentrated residue was analysed by gas chromatography.

Gas chromatography analyses were performed in a ZHIMADSU GC-2010 apparatus, equipped with a split injection mode and a flame ionization detector. The

column was a 60 m length SUPRAWAX-280 with a film thickness of 50 μm and an internal diameter of 0.25 mm. Glycerol conversion and selectivity to glycerol carbonate and glycidol were determined from calibration lines obtained from commercial products.

Results and discussion

Catalysts characterization

Table 10 summarizes the main characterization results of the catalysts. More detailed characterization of the samples can be found in a chapter 4.1.1.

Table 10. Characterization of the catalysts

Samples	Crystalline phases (XRD)	Ca/Al (ICP)	BET Area (m^2/g)	Basicity (Hammett Indicators)
$HC1R_{24}$	$Ca_2Al(OH)_6Cl{\cdot}2H_2O$	1.98	13	10.1<H_>13.4
$HC1RMw_6$	$Ca_2Al(OH)_6Cl{\cdot}2H_2O$	1.87	10	10.1<H_>13.4
$HC1USR_{24}$	$Ca_2Al(OH)_6Cl{\cdot}2H_2O$[a]	1.97	6	10.1<H_>13.4
$HC1USRMw_6$	$Ca_2Al(OH)_6Cl{\cdot}2H_2O$[a]	1.88	7	10.1<H_>13.4
$HC1AC_1$	$Ca_2Al(OH)_6Cl{\cdot}2H_2O$	1.96	7	10.1<H_>13.4
$HC1AMw_1$	$Ca_2Al(OH)_6Cl{\cdot}2H_2O$[a]	1.93	10	10.1<H_>13.4
$HC1AMw_3$	$Ca_2Al(OH)_6Cl{\cdot}2H_2O$[a]	2.12	10	10.1<H_>13.4
$HC2R_{24}$	$Ca_2Al(OH)_6NO_3{\cdot}2H_2O$[a]	1.79	9	10.1<H_>13.4
$HC2RMw_6$	$Ca_2Al(OH)_6NO_3{\cdot}2H_2O$[a]	1.63	9	10.1<H_>13.4
$HC2USR_{24}$	$Ca_2Al(OH)_6NO_3{\cdot}2H_2O$[a]	1.78	16	10.1<H_>13.4
$HC2USRMw_6$	$Ca_2Al(OH)_6NO_3{\cdot}2H_2O$[a]	1.85	25	10.1<H_>13.4
$HC2AC_1$	$Ca_2Al(OH)_6NO_3{\cdot}2H_2O$[a]	1.76	10	10.1<H_>13.4
$HC2AMw_1$	$Ca_2Al(OH)_6NO_3{\cdot}2H_2O$ + katoite	1.42	11	10.1<H_>13.4
$HC2AMw_3$	Katoite[b]	1.38	12	10.1<H_>13.4

[a] Katoite phase was detected in low amounts (5-23 %) [105]
[b] Hydrocalumite phase was detected in low amounts (15 %) [105]

XRD patterns of the samples obtained from chloride salts (HC1) presented only one crystalline phase corresponding to hydrocalumite, except for the samples aged in autoclave with microwaves, and the samples coprecipitated under

ultrasounds where we observed additionally the presence of katoite in very low amounts.[105] Katoite is a non-layered double hydroxide with formula $Ca_3Al_2(OH)_{12}$. For HC2 samples, a mixture of the CaAl-LDH structure and katoite phase was observed for all samples in different relative proportions depending on the aging performed.[105] The formation of katoite was more favoured in autoclaved samples, and using microwaves at longer aging times. Actually, katoite practically became the only one phase for the sample aged in autoclave with microwaves at longer aging time ($HC2AMw_3$).

Ca/Al molar ratio of HC1 samples were around 2, in agreement with the Ca/Al molar ratio of the starting solutions used for coprecipitation, except for the sample aged at longer time in autoclave with microwaves ($HC1AMw_3$), which had slight higher Ca/Al molar ratio (Table 10). Longer aging times in autoclave under microwaves could involve some dealumination of the hydrocalumite layers, explaining the higher Ca/Al molar ratio of $HC1AMw_3$. This effect was previously observed in the preparation of hydrotalcites with microwaves.[18] Ca/Al molar ratio values of the samples prepared from nitrates (HC2) were lower than those obtained for the samples synthesized from chloride salts (Table 10). There is a clear correlation between the amount of katoite phase and the decrease in the Ca/Al molar ratio observed for the HC2 samples. Thus, the sample with the highest amount of katoite showed the lowest Ca/Al ratio (Table 10). This can be attributed to the lower Ca/Al molar ratio of katoite ($Ca_3Al_2(OH)_{12}$), which is 1.5.

All the HC1 and HC2 samples exhibited nitrogen adsorption-desorption isotherms type IV according to IUPAC classification, corresponding to solids with mesoporous contribution. On the whole, all samples had low surface areas (Table 10). This agrees with the results reported by other authors for conventionally prepared hydrocalumite-type compounds.[49] Interestingly, samples precipitated from nitrate salts using ultrasounds for stirring had the highest surface areas values (Table 10). This has been attributed to the presence of interparticle mesoporosity between larger and smaller particles, as confirmed by comparing the pore size distribution of the samples.[105]

All samples showed the formation of thin regular hexagonal crystals corresponding to the hydrocalumite-type compound with some overlay of the layers (e.g. Fig. 43a) except the sample HC2AMw$_3$, where non-layered particles were observed since this sample is composed of katoite, a non-layered calcium aluminium hydroxide compound (Fig. 43b). TEM images allowed us to confirm the observation of well-formed hexagonal sheets corresponding to the hydrocalumite phase (Figure 43c).

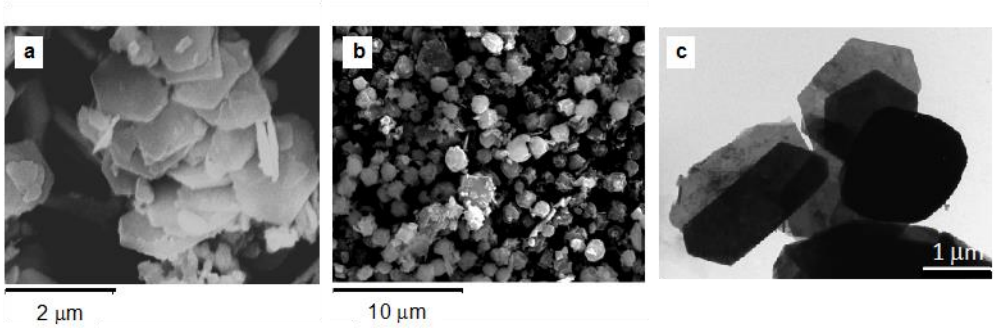

Figure 43. a) SEM image of HC1R$_{24}$ (x 20000), b) SEM image of HC2AMw$_3$ (x 9000) and c) TEM image of HC1USRMw$_6$ (x 25000).

All catalysts had similar basicity strength (10.1< H_ <13.4), as deduced from the results obtained by using Hammett indicators (Table 10).

Catalytic Tests

Figure 44-A and 44-B show the catalytic results obtained for HC1 and HC2 catalysts for the transesterification of glycerol with dimethyl carbonate after 3 h of reaction. All catalysts exhibited high glycerol conversion (70-84 %) and moderate selectivity values to glycerol carbonate (52-65 %). These results are very interesting taking into account the low surface area of these catalysts, and the lower reaction time used compared with other hydrotalcite-type catalysts previously reported.[158,159,161] Additionally, low amounts of glycidol (7-15 %) were detected for all of them. The formation of glycidol during this reaction, by decarboxylation of glycerol carbonate, has been previously reported by other authors over catalysts with high basicity strength.[186] No other reaction products were detected by gas chromatography at the conditions used. The formation of condensation products

from glycerol or glycidol could round off the total products obtained. It is well known that glycerol can polymerize in the presence of basic sites. By comparing these catalytic activity results, there are no great differences between HC1 and HC2 catalysts. This can be due to the similar surface and basic characteristics observed for these catalysts (Table 10). Therefore, there is not effect of using ultrasounds during mixing of the reagents, microwaves during hydrothermal treatment or different interlayer anion (chloride or nitrate). Additionally, the presence of katoite in higher amounts ($HC2AMw_1$ and $HC2AMw_3$) did not modify significantly the catalytic results.

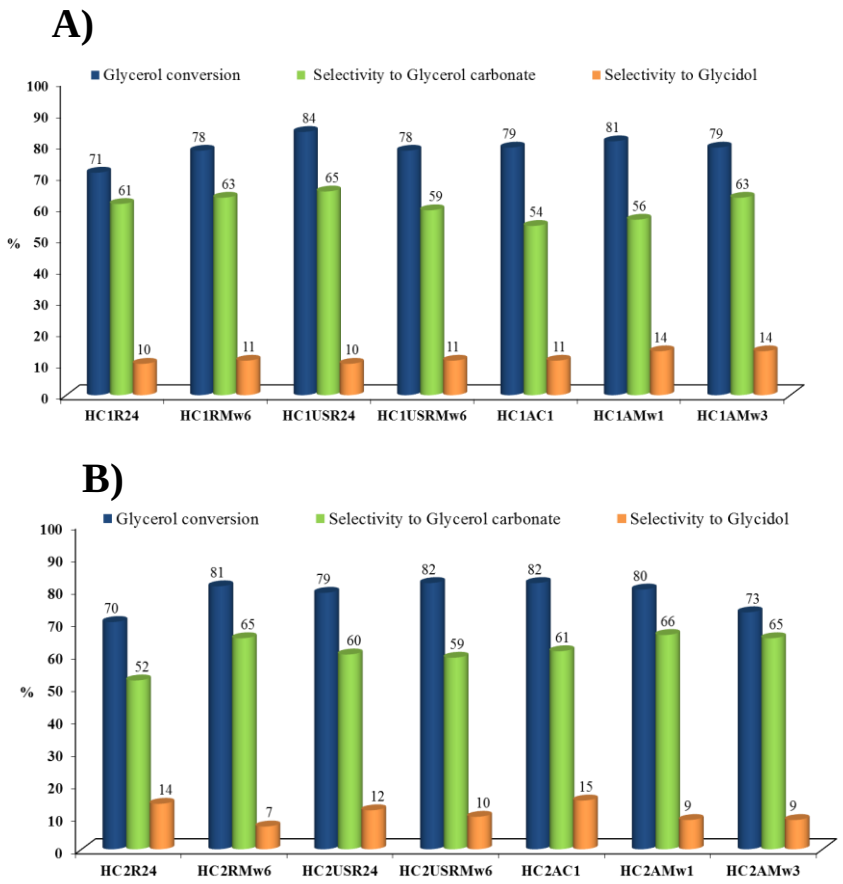

Figure 44. Catalytic activity of the catalysts A) HC1 and B) HC2 after 3 h of reaction. Reaction conditions: dimethyl carbonate/glycerol = 3.5:1 weight ratio; stirring 1000 rpm; N_2 atmosphere; 0.15 g of catalyst; temperature: 90 ºC; time: 3 h.

The sample modified with KOH showed a glycerol conversion of 80 % and selectivity to glycerol carbonate of 61 % after 3 h of reaction. These values were higher than those obtained with the starting sample ($HC2R_{24}$: 70 % of conversion and 52 % of selectivity). The selectivity to glycidol was also higher for the modified sample (20 % in front of 14 %).

In order to study the catalytic behaviour of the hydrocalumite-type catalysts with time, several HC1 and HC2 samples were tested at different reaction times maintaining the rest of reaction conditions (Fig. 45).

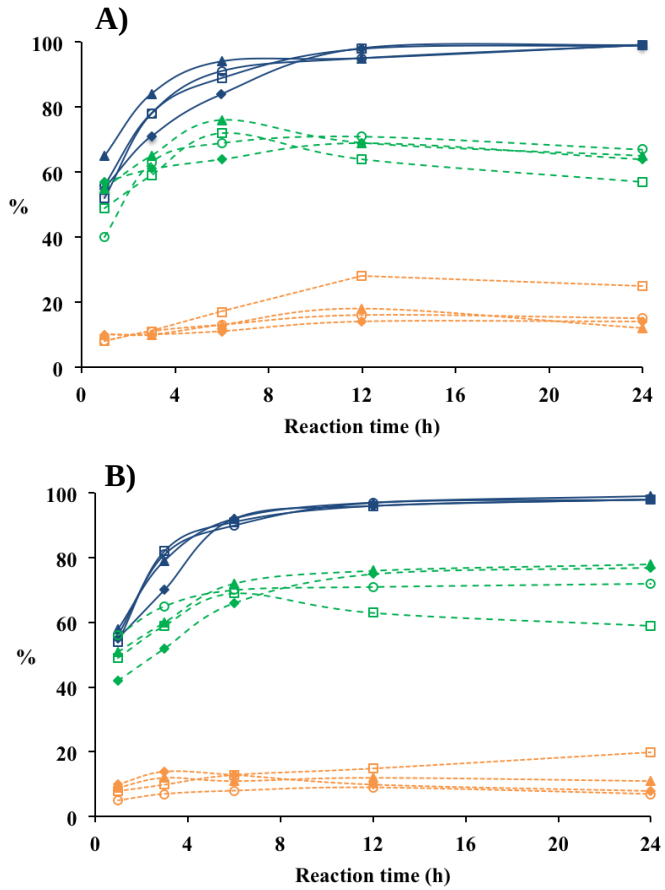

Figure 45. Catalytic activity vs reaction time. Blue lines: conversion; green lines: selectivity to glycerol carbonate; orange lines: selectivity to glycidol A) for several HC1 catalysts: ♦ $HC1R_{24}$, ○ $HC1RMw_6$, ▲ $HC1USR_{24}$, □ $HC1USRMw_6$ and B) for serveral HC2 catalysts: ♦ $HC2R_{24}$, ○ $HC2RMw_6$, ▲ $HC2USR_{24}$, □ $HC2USRMw_6$. Reaction conditions dimethyl carbonate/glycerol = 3.5:1 weight ratio; stirring 1000 rpm; N_2 atmosphere; 0.15 g of catalyst; temperature: 90 ºC; time: 1, 3, 6, 12 and 24 h.

A significant increase of conversion from 1 to 8 h of reaction was observed for all catalysts arriving to values around 90-95 %. Conversion values increased more slowly from 8 h of reaction yielding practically total conversion after 24 h of reaction. With respect to the selectivity to glycerol carbonate, we also observed an initial increase with the reaction time until 8 h achieving values in the range 65-75 %. After this reaction time, stable or slight lower selectivity to glycerol carbonate was detected for all catalysts at expenses of the formation of higher amounts of glycidol. The highest selectivity values to glycidol were yielded for the catalysts the precursors of which were mixed under ultrasounds and aged with microwaves ($HC1USMw_6$ and $HC2USMw_6$) after 24 h of reaction (20-25 %).

Finally, the catalytic life of one of the catalysts ($HC2USR_{24}$) was evaluated from four consecutive runs performed reusing the catalyst at the same reaction conditions used for the first catalytic test (Fig. 46).

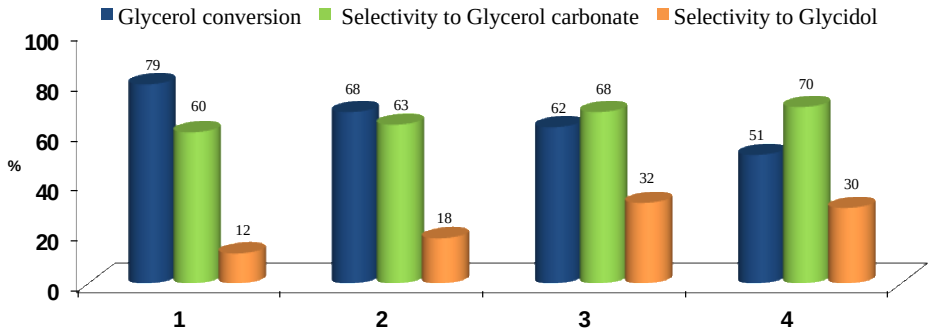

Figure 46. Reuse studies of catalyst $HC2USR_{24}$. Reaction conditions: dimethyl carbonate/glycerol = 3.5:1 weight ratio; stirring 1000 rpm; N_2 atmosphere; 0.15 g of catalyst; temperature: 90 ºC; time: 3 h.

After each catalytic run, recovering of the catalyst was performed by filtration, mild-washing in methanol at room temperature and dried before reaction. Several catalytic reuses favoured the decarboxylation of glycerol carbonate resulting in the formation of higher amounts of glycidol but still maintaining high selectivity values to glycerol carbonate with a progressive loss of conversion. By comparing the XRD pattern of the reused catalyst with that of its corresponding fresh catalyst (Fig. 47), we observed a decrease of the crystallinity of the CaAl-LDH phase for the

reused sample since there was a clear decrease in the intensity of the peaks, which were also wider, corresponding to this phase. It is interesting to note the layered disorder produced in the catalyst during reaction, as confirmed by the decrease of the (006) peak intensity related to the stacking of the layers. This could favour the accessibility of the reagents to the catalytic active sites. Additionally, an increase in the crystallinity of the katoite phase and the appearance of a new crystalline phase, identified as calcite ($CaCO_3$), were also detected (Fig. 47).

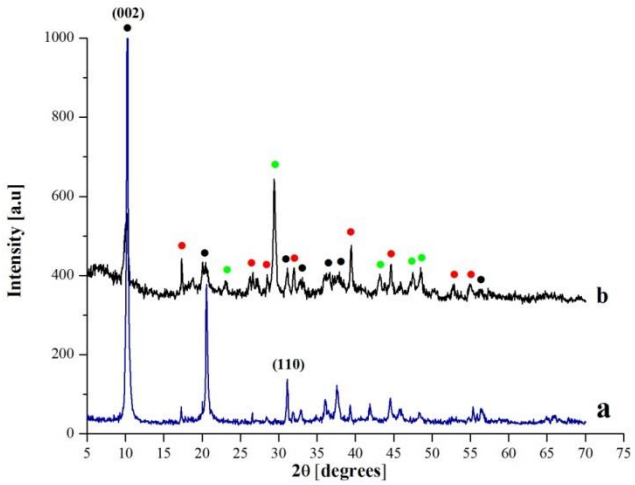

Figure 47. XRD patterns of catalyst HC2USR$_{24}$. a) Fresh catalyst and b) Reused catalyst. ● $Ca_2Al(OH)_6NO_3{\cdot}2H_2O$; ● katoite, and ● calcite phases.

The formation of calcite can be explained by the reaction of the CO_2, generated during decarboxylation of glycerol to glycidol, with the Ca of the catalyst. Thus, the progressive loss of conversion observed could be attributed to the loss of some basic centres during reaction.

Interestingly, for catalytic reuses 3 and 4 (see Figure 46), the sum of the selectivity values to glycerol carbonate and glycidol was 100 % in front of the 72 % and 81 % observed for reuses 1 and 2, respectively. This means that with the reuses there is a loss of the centres responsible for the condensation products formation.

Conclusions

Several CaAl-layered double hydroxides have been synthesized, by modifying the preparation conditions, and tested for the transesterification of glycerol to glycerol carbonate. Although these catalysts showed some differences in the crystalline phases obtained (in general, LDH structure with some amounts of katoite), they had similar surface and basic characteristics. This explains their similar catalytic behaviour observed after 3 h of reaction resulting in high glycerol conversion (70-84 %) and moderate selectivity values to glycerol carbonate (52-65 %). It is important to remark the interest of these results taking into account the low surface areas of these catalysts (7-25 m^2/g) compared to those of the catalysts previously tested by other authors for this reaction. After 24 h of reaction, practically all catalysts arrived to total glycerol conversion with selectivity values to glycerol carbonate between 65 and 75 %. Several catalytic reuses favoured the decarboxylation of glycerol carbonate resulting in the formation of higher amounts of glycidol (30 %) but still maintaining high selectivity values to glycerol carbonate (70 %). This decarboxylation was confirmed by the appearance of a new crystalline phase, $CaCO_3$, in the reused catalyst.

Acknowledgments

Authors acknowledge Ministerio de Economía y Competitividad of Spain and Feder Funds (CTQ2011-24610), and Catalan Government for FI grant (2012FI_B 00564).

4.2.2 Effect of the preparation conditions on the catalytic activity of calcined Ca/Al-layered double hydroxides for the obtention of glycerol carbonate

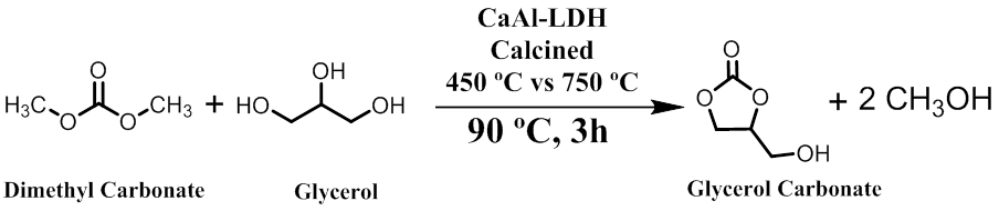

Abstract

The effect of the preparation conditions of several calcined Ca/Al layered double hydroxide compounds on the catalytic transesterification of glycerol with dimethyl carbonate to obtain glycerol carbonate has been studied. The CaAl-LDH precursors were prepared by aging under microwaves or conventional heating, and using chlorides or nitrates as interlayer anions. Calcination conditions, such as temperature, time and calcination system, were modified. After 3 h of reaction, the catalysts obtained by calcination at 450 ºC for 15 h in air exhibited moderate-high glycerol conversion (46-76 %) and moderate selectivity to glycerol carbonate (41-65 %). Calcination at 450 ºC at longer calcination time or the use of a dynamic inert-atmosphere system during calcination led to higher conversion (89-94 %) and higher selectivity to glycerol carbonate (72-73 %). This has been related to the higher basicity of these catalysts. Finally, calcination at 750 ºC resulted in high conversion (88-98 %) and high selectivity to glycerol carbonate (60-85 %) due to the presence in the catalysts of highly basic CaO. Several catalytic reuses favoured the decarboxylation of glycerol carbonate resulting in the formation of higher amounts of glycidol (42 %). The progressive loss of conversion and selectivity to glycerol carbonate observed has been attributed to the loss of some CaO basic centres during reaction by calcite formation.

Introduction

During biodiesel production, by transesterification of vegetable oils with methanol, glycerol (glycerine or 1,2,3-propanotriol) is formed as by-product in high amounts (10 wt % of the total product). The price of glycerol is falling as fast as biodiesel plants are being built. Research is currently starting to find new outlets to convert the surplus of glycerol into high-added value products that improve the economy of the whole process.[5,7,8,174–176]

Glycerol carbonate (4 -hydroxymethyl-1,3-dioxolan-2-one) is one of the most attractive glycerol derivatives due to its low toxicity, good biodegradability and high boiling point.[118] This compound has many applications in different industrial sectors, such as intermediate in polymer synthesis,[5,11] biolubricant owing to its adhesion to metallic surfaces and resistance to oxidation, hydrolysis, and pressure,[8] protector in the carbohydrates chemistry, component of gas separation membranes, in coatings, or in the production of polyurethane foams[179] and surfactants.[180] Glycerol carbonate could also serve as a source of glycidol, which is employed in textile, plastics, pharmaceutical and cosmetics industries.[181] Traditionally, glycerol carbonate has been industrially produced by reacting glycerol with phosgene but due to the high toxicity and corrosive nature of this reagent, new routes have been investigated.[118]

One alternative option consists of obtaining glycerol carbonate by the catalytic transesterification reaction of glycerol with organic cyclic carbonates (ethylene carbonate or propene carbonate) or with non-cyclic carbonates (diethyl carbonate or dimethyl carbonate).[12,118,156,158–161,184–186] Dimethyl carbonate is preferred since the reaction can be performed at milder conditions and the co-product methanol can be easily separated. A wide variety of solid base catalytic systems, such an alkaline earth metal oxides, basic zeolites, mixed metal oxides derived from hydrotalcites, have been tested for this reaction.[118] CaO catalyst led to 70 % of conversion and 70 % of yield to glycerol carbonate at 75 ºC after 15 min of reaction.[184] Calcined Mg/Al/Zr,[158] calcined Mg/Zr/Sr [159] and doping transition metals cations into Mg/Al hydrotalcites [161] reuslted in yields to glycerol carbonate

between 55-94 % at reaction temperatures in the range 75-100 ºC. More recently, Z. Liu *et al*. (2015) reported full conversion of glycerol and 96 % yield of glycerol carbonate at 80 ºC for 1.5 h in the presence of $Li/Mg_4AlO_{5.5}$ obtained by impregnating calcined Mg/Al hydrotalcite with $LiNO_3$.[186] Finally, Yadav *et al*. (2014) performed this reaction in autoclave at 170 ºC for 3 h obtaining conversion values around 85 % and selectivity to glycerol carbonate values between 84-88 % when using Mg/Al hydrotalcites supported on hexagonal mesoporous silica as catalysts.[156]

Hydrocalumite-type compounds belong to the layered double hydroxides family (LDHs) with formula $[M(II)_{1-x}M(III)_x(OH)_2][X^{q-}_{x/q}\cdot nH_2O]$ where $[Ca_2Al(OH)_6]^+$ represents the hydrocalumite layer composition, and $[X^{q-}_{x/q}\cdot nH_2O]$ the interlayer composition.[13] Especifically, the hydrocalumite name is used when the interlayer anion is chloride. The CaAl-LDH structure collapses at temperatures between 400 and 600 ºC resulting in the formation of amorphous mixed oxides, $Ca(Al)O_x$. At higher calcination temperatures crystalline CaO and mayenite ($Ca_{12}Al_{14}O_{33}$) phases are obtained. These basic mixed oxides have been scarcely used as catalysts for aldol condensation, Meerwein-Ponndorf-Verley or isomerization of 1-butene reactions.[25,49,103]

The aim of this work was to study the effect of the preparation conditions of several calcined Ca/Al hydrocalumite-type compounds on the catalytic transesterification of glycerol with dimethyl carbonate to obtain glycerol carbonate. The CaAl-LDH precursors have been prepared by aging under microwaves or conventional heating, and using chlorides or nitrates as interlayer anions. Calcination conditions, such as temperature, time and calcination system, have been modified.

Experimental

Samples preparation

Ten CaAl-LDH samples were synthesized by the co-precipitation method from different starting salts under vigorous magnetic stirring using deionized/decarbonated water, as well as nitrogen atmosphere. Two aqueous

solutions containing $CaCl_2 \cdot 2H_2O$ (sigma-Aldrich) and $AlCl_3 \cdot 6H_2O$ (Riedel-de Haën) (series HC1) or $Ca(NO_3)_2 \cdot 4H_2O$ (sigma-Aldrich) and $Al(NO_3)_3 \cdot 9H_2O$ (sigma-Aldrich) (series HC2), were prepared with a 2:1 Ca^{2+}/Al^{3+} molar ratio by adding an aqueous solution of 2 M NaOH (Panreac) at 60 ºC and constant pH of 11.5.[105] After complete addition of the metallic salts, the two mother solutions were aged by several treatments: by refluxing in conventional heating at 60 ºC for 24 h ($HC1R_{24}$ and $HC2R_{24}$), by refluxing under microwaves (Milestone ETHOS-TOUCH CONTROL) at 60 ºC for 6 h ($HC1RMw_6$ and $HC2RMw_6$), in autoclave by conventional heating at 180 ºC for 1 h ($HC1AC_1$ and $HC2AC_1$), and in autoclave under microwaves at 180 ºC for 1 h ($HC1AMw_1$ and $HC2AMw_1$) and for 3 h ($HC1AMw_3$ and $HC2AMw_3$). All samples were filtered at room temperature, washed with deionized and decarbonated water and then dried in an oven at 80 ºC overnight.

For the preparation of the catalysts, all the hydrocalumite-type compounds were calcined in a furnace Carbolite CWF11/5P8 at 450 ºC for 15 h ($cHC1R_{24}$, $cHC2R_{24}$, $cHC1RMw_6$, $cHC2RMw_6$, $cHC1AC_1$, $cHC2AC_1$, $cHC1AMw_1$, $cHC2AMw_1$, $cHC1AMw_3$, $cHC2AMw_3$). To determine the influence of the calcination time, and the effect of using a dynamic inert atmosphere system during calcination, one of the CaAl-LDH samples ($HC1AMw_3$) was calcined 450 °C for 24 h ($cHC1AMw_3$-24h), and other sample by flowing nitrogen gas (1 ml/s) at 450 °C for 10 h in a quartz reactor ($cHC1AMw_3$-N_2). Finally, in order to study the effect of the calcination temperature, several samples were calcined at 750 ºC for 4 h ($cHC1AC_1$-750, $cHC1AMw_1$-750, $cHC1AMw_3$-750, $cHC2AC_1$-750 and $cHC2AMw_1$-750). Table 11 summarizes the preparation conditions of all samples.

Table 11. Preparation conditions of calcined CaAl-LDHs.

Sample*	Aging conditions of the precursors				Calcination		
	Heating	Technique	T (ºC)	Time (h)	T (ºC)	Time (h)	System
cHC1R_{24}	conventional	refluxing	60	24	450	15	static/air
cHC1RMw_6	microwave	refluxing	60	6	450	15	static/air
cHC1AC_1	conventional	autoclave	180	1	450	15	static/air
cHC1AMw_1	microwave	autoclave	180	1	450	15	static/air
cHC1AMw_3	microwave	autoclave	180	3	450	15	static/air
cHC1AMw_3-24	microwave	autoclave	180	3	450	24	static/air
cHC1AMw_3-N_2	microwave	autoclave	180	3	450	10	dynamic/N_2
cHC2R_{24}	conventional	refluxing	60	24	450	15	static/air
cHC2RMw_6	microwave	refluxing	60	6	450	15	static/air
cHC2AC_1	conventional	autoclave	180	1	450	15	static/air
cHC2AMw_1	microwave	autoclave	180	1	450	15	static/air
cHC2AMw_3	microwave	autoclave	180	3	450	15	static/air
cHC1AC_1-750	conventional	autoclave	180	1	750	4	static/air
cHC1AMw_1-750	microwave	autoclave	180	1	750	4	static/air
cHC1AMw_3-750	microwave	autoclave	180	3	750	4	static/air
cHC2AC_1-750	conventional	autoclave	180	1	750	4	static/air
cHC2AMw_1-750	microwave	autoclave	180	1	750	4	static/air

*** HC1:** Chloride salts, **HC2:** Nitrate salts

HC2R_{24} sample was modified with a KNO_3 solution, with the purpose of modify the basicity of the sample. For this purpose, 1 g of sample was mixed (dropwise) with 0.043 g of KNO_3 contained in a 1.5 ml of aqueous solution. The resulting sample was calcined at 450 ºC for 15 h.

Elemental Analysis

Elemental analysis of the hydrocalumite-type compounds was obtained with an ICP-OES analyser (Induced Coupled Plasma – Optical Emission Spectroscopy) from Spectro Arcos. The digestion of all samples was carried out with concentrated HNO_3. Analyses were performed by triplicate.

X-ray diffraction (XRD)

Powder X-ray diffraction patterns of the calcined samples were obtained with a Siemens D5000 diffractometer using nickel-filtered CuKα radiation and

detecting between 2θ values of 5º-70º. Crystalline phases were identified using the Joint Committee on Powder Diffraction Standards (JCPDS) files (086-2340- calcite, 089-6723-mayenite, 037-1497- lime).

Nitrogen Physisorption

BET surface areas were calculated from the nitrogen adsorption isotherms at -196 ºC using a Quantachrome Quadrasorb SI surface analyzer and a value of 0.164 nm^2 for the cross-section of the nitrogen molecule. Samples were degassed at 90 ºC.

Scanning electron microscopy (SEM)

Scanning electron micrographs were obtained with a JEOL JSM-35 C scanning microscope operating at an accelerating voltage in the range 15-30 kV, work distance of 14 mm and magnification values between 5000 and 30000x.

Transmission electron microscopy (TEM)

Transmission electron microscopy of the samples was performed using a JEOL electron microscope Model 1011 with an operating voltage of 80 kV. Samples were dispersed in acetone and a drop of the suspension was poured on to a carbon coated cooper grip and dried at room temperature before measurements. The magnification values used were between 20 and 100 k.

Hammett's indicators

Basicity of the catalysts was evaluated using Hammett indicators: phenolphthalein (pKa = 8.2), nile blue A (pKa = 10.1), tropaeolin O (pKa = 11), thyazole yellow G (pKa = 13.4) and 2,4-dinitroaniline (pKa = 15). 25 mg of catalyst was taken along with 2.5 ml dry methanol and 1 ml of indicator, and kept in a shaker for 2 h.

Catalytic Tests

For the catalytic tests, dimethyl carbonate and glycerol were mixed in a 3.5:1 weight ratio in a 50 ml round bottom 3-neck jacketed glass reactor fitted with a magnetic stirrer, a reflux condenser and a thermometer. The mixture was heated at 90 ºC with constant stirring at 1000 rpm under N_2. Then, 0.15 g of catalyst was

added to start the reaction. After 3 h of reaction, the mixture was filtered and evaporated in a rotatory evaporator. 1 μl of the concentrated residue was analysed by gas chromatography.

Gas chromatography analyses were performed in a Shimadzu GC-2010 apparatus, equipped with a split injection mode and a flame ionization detector. The column was a 60 m length SUPRAWAX-280 with a film thickness of 50 μm and an internal diameter of 0.25 mm. Glycerol conversion and selectivity to glycerol carbonate and glycidol were determined from calibration lines obtained from commercial products.

Results and discussion

X-ray diffraction (XRD)

XRD patterns of the cHC1 samples, prepared from chloride salts and calcined at 450 ºC for 15 h, mainly showed the presence of an amorphous phase due to the expected mixture of calcium and aluminium oxides, $Ca(Al)O_x$ (Figure 48a-e). Additionally, several crystalline peaks were observed for most of the samples ($cHC1AC_1$, $cHC1RMw_6$, $cHC1AMw_1$ and $cHC1AMw_3$) that were identified as calcite ($CaCO_3$). The presence of the calcite phase can be related to the air atmosphere used during calcination. By increasing the calcination time in air, from 15 to 24 h, the calcite content increased and new crystalline peaks, corresponding to the mayenite phase, $Ca_{12}Al_{14}O_{33}$ appeared (Figure 48f). The use of nitrogen flowing through the sample during calcination for 10 h favoured the crystallization of mayenite and a small amount of CaO was observed (Figure 48g). This could be associated with the easier elimination of the gases generated during calcination in this dynamic system. Additionally, calcite was also observed in low amounts. Some CO_2 formed during calcination could react with some Ca^{2+} to form calcite in this sample. This CO_2 comes from carbonates located as interlayer anions in the starting hydrocalumite, as observed by FT-IR and Raman spectroscopy (Figure 24 and Figure 25).

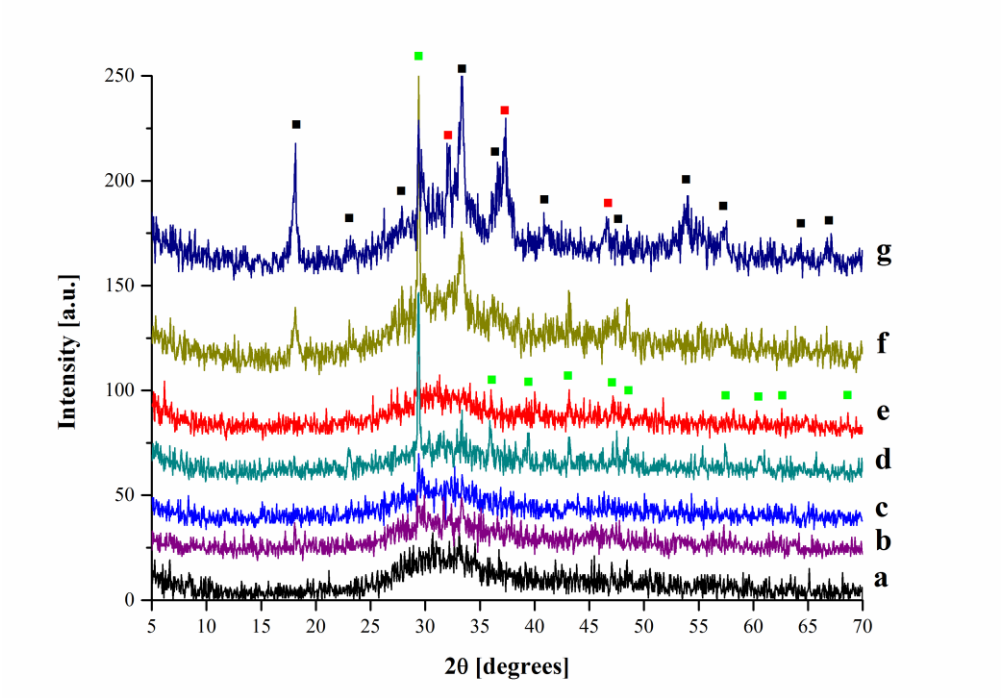

Figure 48. XRD patterns of the samples obtained from chlorides salts a) cHC1R_{24}, b) cHC1RMw_6, c) cHC1AC_1, d) cHC1AMW_1, e) cHC1AMw_3, f) cHC1AMW_3-24, g) cHC1AMw_3-N_2. ■ Calcite phase; ■ Mayenite phase ■ CaO phase.

XRD patterns of the cHC2 samples, prepared from nitrate salts and calcined at 450 ºC for 15 h, are shown in Figure 49. cHC2 samples were more crystalline than cHC1 samples (Figure 48). The cHC2 samples aged under reflux only exhibited crystalline peaks corresponding to the calcite phase (Figure 49a and 49b) whereas the cHC2 samples aged in autoclave showed, in addition to lower amounts of calcite, the presence of the mayenite phase, which was more crystalline for the sample aged under microwaves at longer time (Figure 49e). Therefore, the use of nitrate anions for the preparation of hydrocalumite-type compounds favoured the formation, after calcination, of the mayenite phase when using autoclave-aging conditions, especially under microwaves.

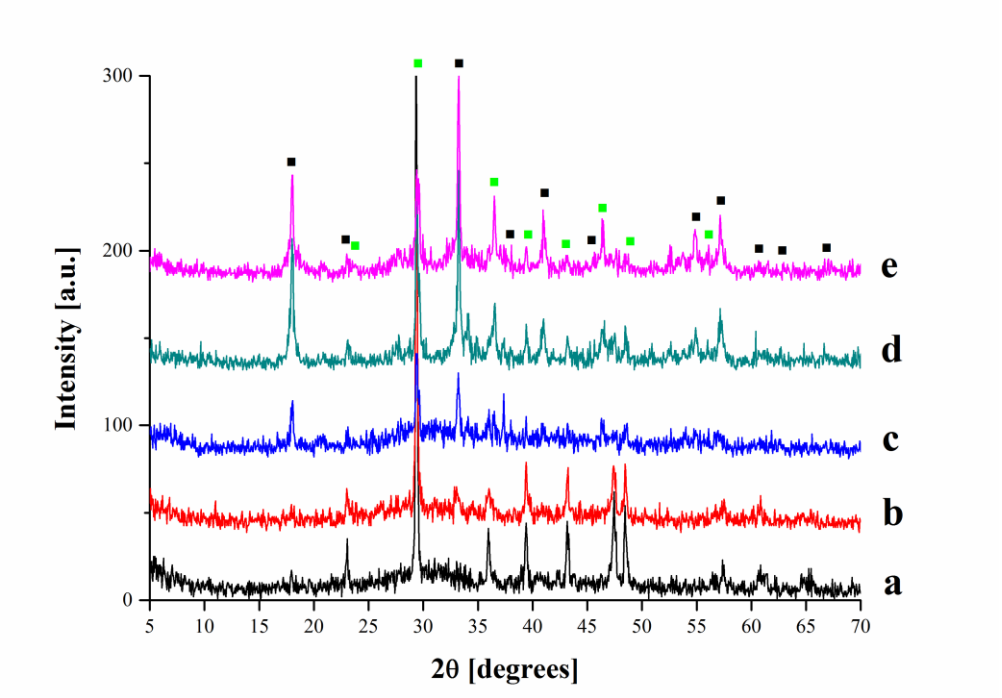

Figure 49. XRD patterns of the samples prepared from nitrate salts a) $cHC2R_{24}$, b) $cHC2RMW_6$, c), $cHC2AC_1$ d) $cHC2AMW_1$, e) $cHC2AMW_3$. ■ Calcite phase; ■ Mayenite phase.

Several Ca/Al LDHs were calcined at higher temperature (750 ºC for 4 h). A mixture of CaO and mayenite phase was obtained in all cases (Figure 50). These samples did not show the calcite phase since this compound decomposes at lower temperature than the calcination temperature used. The samples obtained from chloride salts and aged under microwaves exhibited, after calcination at these conditions, higher amounts of the CaO phase.

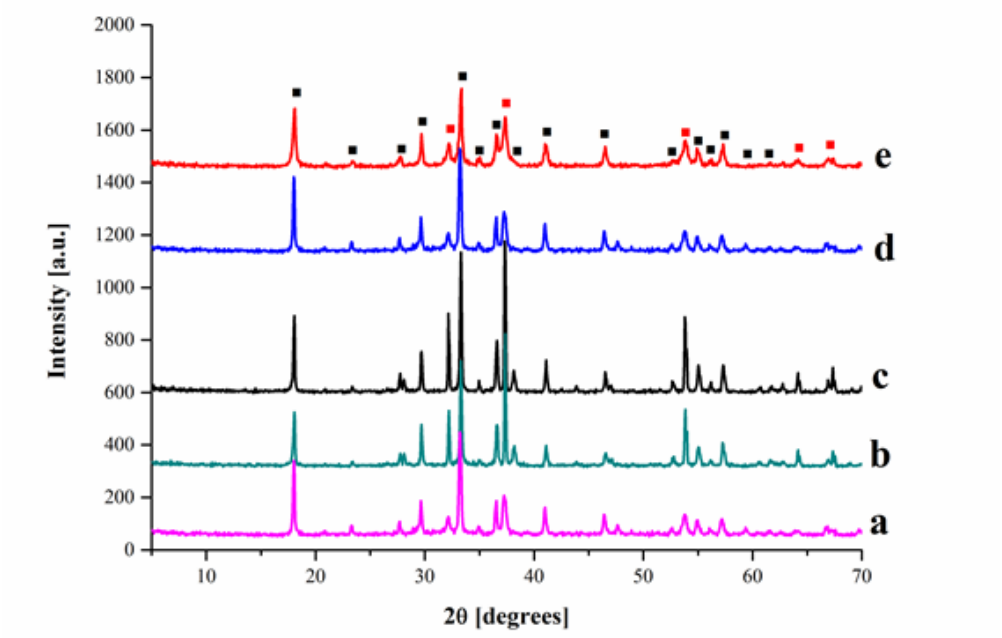

Figure 50. XRD patterns of the samples a) cHC1AC$_1$-750, b) cHC1AM$_{W1}$-750, c) cHC1AM$_{W3}$-750, d) cHC2AC$_1$-750, e) cHC2AM$_{W1}$-750. ■ Mayenite phase; ■ CaO phase.

Elemental analysis

Ca/Al molar ratio of cHC1 samples were around 2, in agreement with the Ca/Al molar ratio of the starting solutions used for the coprecipitation of their precursors, except for the sample aged at longer time in autoclave with microwaves (cHC1AMw$_3$), which had slight higher Ca/Al molar ratio (Table 12). Longer aging times in autoclave with microwaves could involve some dealumination of the hydrocalumite layers, explaining the higher Ca/Al molar ratio of cHC1AMw$_3$. This effect was previously observed in the preparation of hydrotalcites with microwaves.[18] Ca/Al molar ratio values of the samples whose precursors were prepared from nitrates (cHC2) were lower than those obtained from the samples synthesized with chloride salts (cHC1) (Table 12). This has been related to the presence in their precursors of different amounts of katoite phase ($Ca_3Al_2(OH)_{12}$),[105] which has a Ca/Al ratio of 1.5. Thus, cHC2AMw$_3$, whose precursor had the highest amount of katoite, showed the lowest Ca/Al ratio (Table 12).

Table 12. Characterization results of the samples.

Samples	Ca/Al	Surface Area (m^2g^{-1})	Average Pore Size (Å)	Pore Volume (cm^3g^{-1})	Hammett Indicators
$cHC1R_{24}$	1.98	11	147	0.08	6.8<H_>8.2
$cHC1RMw_6$	1.87	12	129	0.07	6.8<H_>8.2
$cHC1AC_1$	1.96	11	100	0.05	6.8<H_>8.2
$cHC1AMw_1$	1.93	13	160	0.10	6.8<H_>8.2
$cHC1AMw_3$	2.12	7	79	0.03	6.8<H_>8.2
$cHC1AMw_3$-24	2.12	9	88	0.04	8.2<H_>10.1
$cHC1AMw_3$-N_2	2.12	9	104	0.04	10.1<H_>13.4
$cHC2R_{24}$	1.79	9	124	0.05	6.8<H_>8.2
$cHC2RMw_6$	1.63	10	86	0.04	6.8<H_>8.2
$cHC2AC_1$	1.76	9	96	0.04	6.8<H_>8.2
$cHC2AMw_1$	1.42	8	98	0.07	6.8<H_>8.2
$cHC2AMw_3$	1.38	4	144	0.03	6.8<H_>8.2
$cHC1AC_1$-750	1.96	5	95	0.02	13.4<H_>15
$cHC1AMw_1$-750	1.93	4	100	0.02	13.4<H_>15
$cHC1AMw_3$-750	2.12	5	128	0.03	13.4<H_>15
$cHC2AC_1$-750	1.76	7	103	0.06	13.4<H_>15
$cHC2AMw_1$-750	1.42	7	129	0.05	13.4<H_>15

Nitrogen physisorption

All calcined samples presented nitrogen adsorption-desorption isotherms of type IV, which according to the IUPAC classification corresponded to mesoporous solids with pore size distribution in the mesoporous range (20-500 Å).

Table 12 shows the surface area, average pore size and pore volume values obtained for all samples. Calcined Ca/Al LDHs had low surface areas in the range 4-13 m^2/g (Table 12). This agrees with the results reported by other authors for calcined hydrocalumite-type compounds.[30,49] Regarding the surface areas of the

samples calcined at 450 ºC, we observe that cHC1 samples exhibited slight higher surface areas than cHC2 samples. This can be related to the lower crystallinity observed by XRD for cHC1 samples (Figure 48). After calcination at higher temperature (750 ºC), a decrease of surface area was observed, as expected, due to the presence of CaO and mayenite phases with higher crystallinity (Figure 50).

Scanning electron microscopy (SEM) and Transmission electron microscopy (TEM)

Figure 51 shows some representative SEM and TEM images of the samples. SEM allowed us to observe that calcined samples retained the original hexagonal morphology of their precursors, the hydrocalumite-type compounds.[105] This means that despite the thermal decomposition and the consequent changes suffered by the structure due to the loss of water, anions and dehydroxilation processes, there were not significant changes in the crystal morphology of the particles. Samples calcined at 750 °C showed a greater deformation of the edges, more compact and more agglomerated particles than those calcined at 450 °C, explaining their lower surface areas.

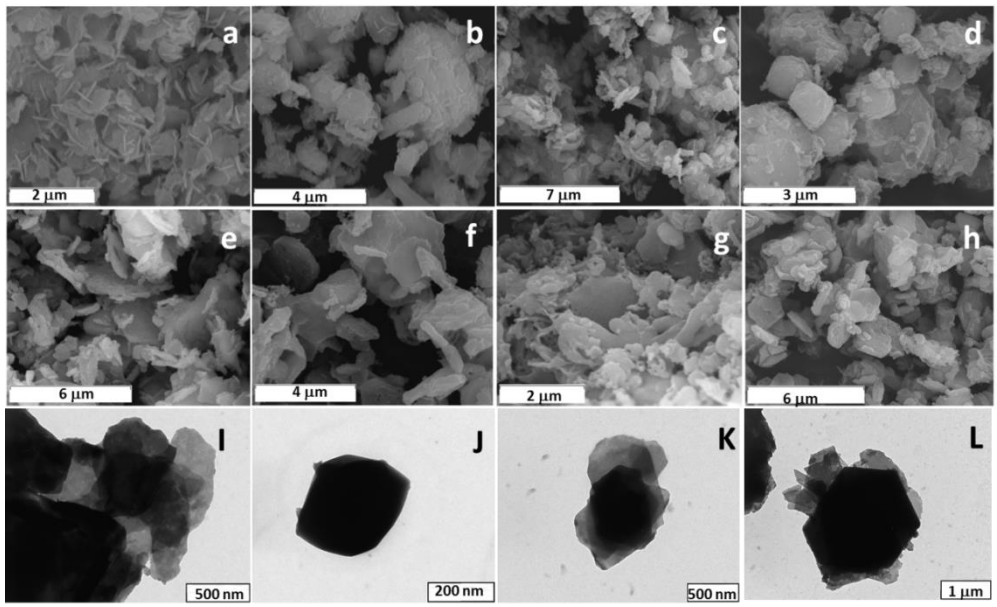

Figure 51. SEM images of a) cHC1AC$_1$ (x20000), b) cHC1AMw$_1$ (x13000), c) cHC2AC$_1$ (x8000), d) cHC2AM$_{W1}$ (x17000), e) cHC1AC$_1$-750 (x9500), f) cHC1AM$_{W1}$-750 (x12000), g) cHC2AC$_1$-750 (x20000), h) cHC2AM$_{W1}$-750 (x9000), and TEM images of i) cHC1R$_{24}$ (x60000), j) cHC1RM$_{W6}$ (x80000), k) cHC2R$_{24}$ (x50000), l) cHC2RM$_{W6}$ (x25000).

TEM images also confirmed the presence of hexagonal sheets, but not so well differentiated as in their precursors [105] and more compacted, probably because of the water release and crystallographic phase transformation. This would also account for the low specific surface areas measured for the calcined solids (Table 12).

Hammett's indicators

Hammett indicators results showed that all the samples calcined at 450 ºC for 15 h in air had the same basicity (6.8<H_<8.2) (Table 12). However, the sample calcined at higher calcination time, cHC1AMw$_3$-24, showed higher basicity strenght (8.2<H_<10.1), probably due to the presence of mayenite phase in this sample, and the sample calcined in an inert atmosphere in a dynamic system, cHC1AMw$_3$-N$_2$, exhibited the highest basicity strength (10.1<H_<13.4) regarding the samples calcined at 450 ºC. This could be attributed to the presence of a low amounts of CaO (known for its basicity), and lower amounts of calcite phase. The presence of higher amounts of more crystalline calcite in the samples calcined at 450 ºC for 15 h in air could justify the lower basicity of these samples. The use of higher calcination time or an inert atmosphere could reduce the formation of this calcite phase, and therefore higher basicity was obtained. Finally, the stronger basicity observed for the samples calcined at 750 ºC (13.4<H_<15) can be related to the presence of CaO, highly basic, together with the absence of calcite, which decomposed at these higher calcination temperatures.

Catalytic Activity

Figure 52 and 53 show the catalytic results obtained by using the cHC1 and cHC2 catalysts prepared by calcination at 450 ºC for the transesterification of glycerol with dimethyl carbonate after 3 h of reaction. All the catalysts calcined at the same conditions (cHC1R$_{24}$, cHC2R$_{24}$, cHC1RMw$_6$, cHC2RMw$_6$, cHC1AC$_1$, cHC2AC$_1$, cHC1AMw$_1$, cHC2AMw$_1$, cHC1AMw$_3$, cHC2AMw$_3$) exhibited moderate-high glycerol conversion (46-76 %) and moderate selectivity to glycerol carbonate (41-65 %). On the whole, these values were slight lower with respect to glycerol conversion and similar with respect to glycerol carbonate selectivity than

those obtained when using their corresponding hydrocalumite-type precursors as catalysts for this reaction at the same reaction conditions (chapter 4.2.1).[105] This can be explained by the lower basicity strength of the catalysts calcined at 450 ºC, as deduced from Hammett indicators (Table 12).

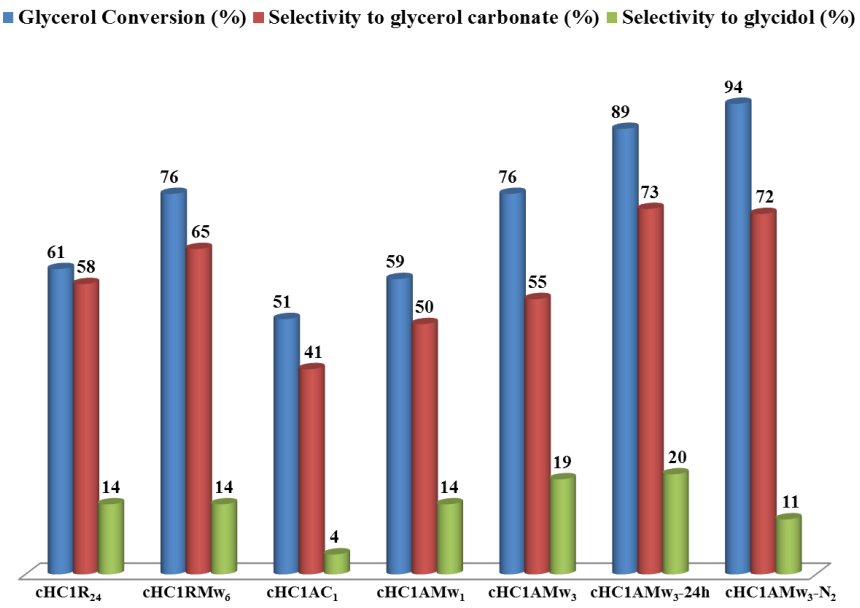

Figure 52. Catalytic activity results of the cHC1 catalysts obtained by calcination at 450 ºC. Reaction conditions: dimethyl carbonate/glycerol = 3.5:1 weight ratio; stirring 1000 rpm; N_2 atmosphere; 0.15 g of catalyst; temperature: 90 ºC; time: 3 h.

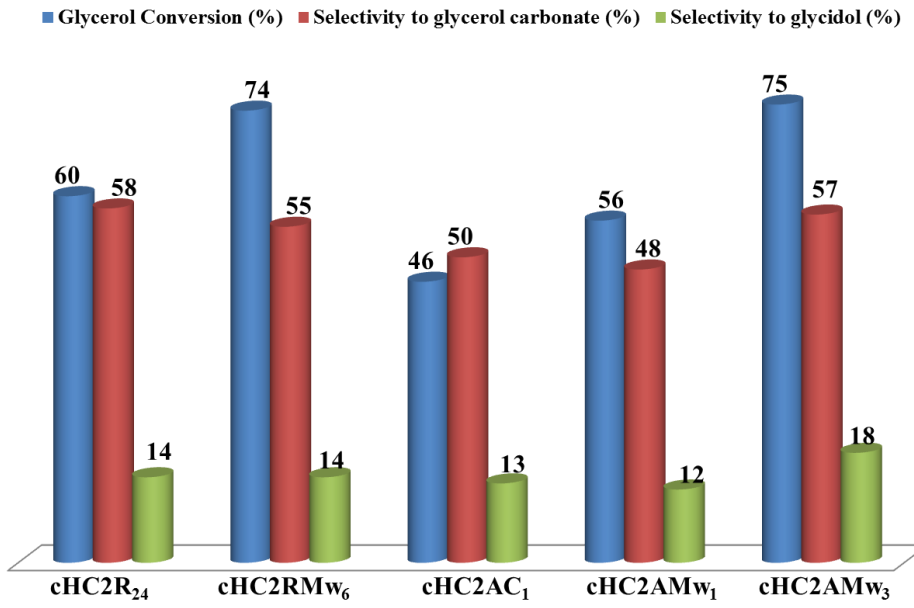

Figure 53. Catalytic activity results of the cHC2 catalysts obtained by calcination at 450 ºC. Reaction conditions: dimethyl carbonate/glycerol = 3.5:1 weight ratio; stirring 1000 rpm; N_2 atmosphere; 0.15 g of catalyst; temperature: 90 ºC; time: 3 h.

Conversion and selectivity values to glycerol carbonate were slightly higher for the catalysts whose precursors were aged under microwaves by refluxing as well as autoclave. This could be correlated with the higher amounts of calcite observed for these catalysts, which neutralizes the strongest basic centers responsible for the deactivation. Interestingly, the two catalysts calcined at 450 ºC but at longer calcination time (cHC1AMw$_3$-24h) or using a dynamic inert-atmosphere system during calcination (cHC1AMw$_3$-N_2) led to higher conversion (89-94 %) and higher selectivity to glycerol carbonate (72-73 %) values than cHC1AMw$_3$. The presence of mayenite and calcite with low crystallinity together with the mixed oxide Ca(Al)O_x (Figure 48), only observed in these two catalysts, could justify these results together with the higher basicity observed in these two catalysts. These results are very interesting taking into account the low surface area of these catalysts, and the lower reaction time used. Additionally, glycidol was detected for all catalysts in different amounts (4-20 %). The formation of glycidol during this reaction, by decarboxylation of glycerol carbonate, has been previously reported by

other authors over catalysts with high basicity strength.[186] No other reaction products were detected by gas chromatography.

The results for the modified catalyst confirm an increase in the conversion of glycerol and in the selectivity to glycerol carbonate of the catalyst (76 % and 66 %, respectively) compared with the catalytic results of the non modified catalyst (61 % and 58 %, respectively). The selectivity of glycidol was very similar for both catalysts (14 % in fron of 13 %).

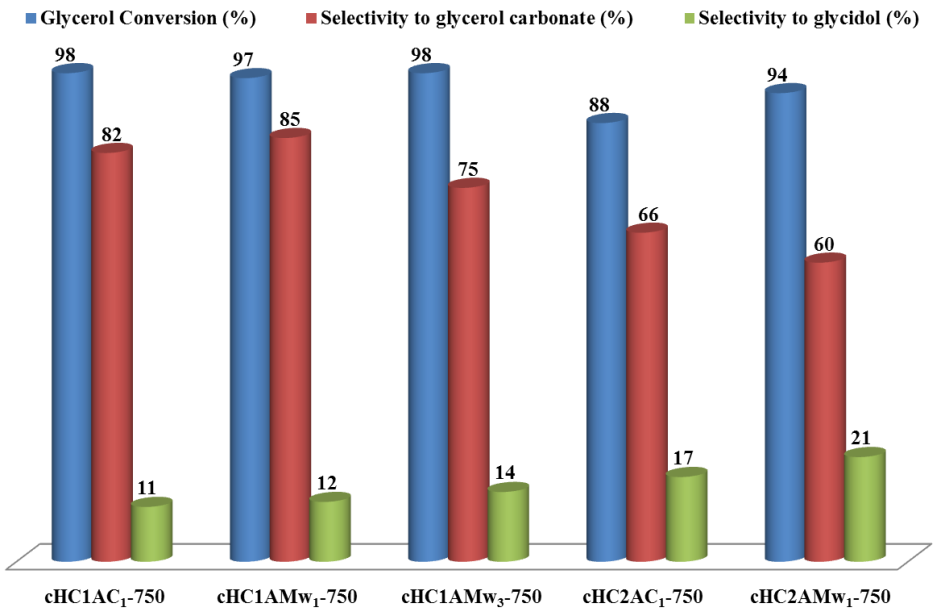

Figure 54. Catalytic activity results of several catalysts calcined at 750 ºC. Reaction conditions: dimethyl carbonate/glycerol = 3.5:1 weight ratio; stirring 1000 rpm; N_2 atmosphere; 0.15 g of catalyst; temperature: 90 ºC; time: 3 h.

Figure 54 shows the catalytic activity results of the catalysts calcined at 750 ºC. These samples had much higher conversion (88-98 %) and much higher selectivity to glycerol carbonate (60-85 %) than their corrresponding catalysts calcined at 450 ºC, especially catalysts cHC1. This can be related to the higher basicity of the catalysts calcined at 750 ºC with respect to those calcined at 450 ºC, as confirmed by the results obtained by using Hammett indicators (Table 12). The higher amounts of CaO, highly basic, detected in cHC1 catalysts (Figure 50) could explain the differences observed between cHC1 and cHC2 catalysts (Figure 54).

Finally, the catalytic life of one of the catalysts (cHC1AM$_{W1}$-750) was evaluated from four consecutive runs performed reusing the catalyst at the same reaction conditions used for the first catalytic test. After each catalytic run, recovering of the catalyst was performed by filtration, mild-washing in methanol at room temperature and dried before reaction. Several catalytic reuses favoured the decarboxylation of glycerol carbonate resulting in the formation of higher amounts of glycidol with a progressive loss of conversion and glycerol carbonate selectivity. This behaviour was previously observed for their hydrotaculamite-type precursors[18] but with these calcined hydrocalumites the formation of glycidol was more marked arriving to 42 % after 4 reuses (Figure 55).

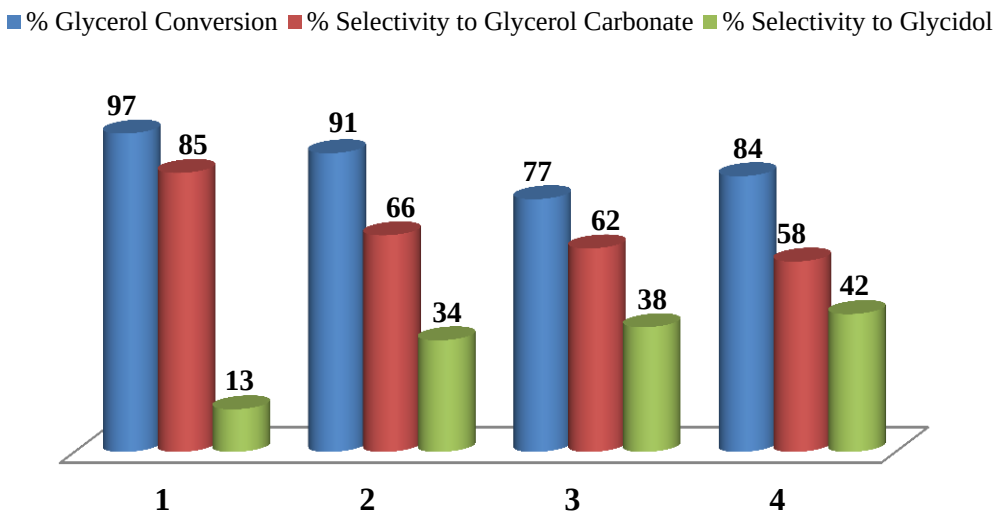

Figure 55. Reuse studies of catalyst cHC1AMW$_1$-750. Reaction conditions: dimethyl carbonate/glycerol = 3.5:1 weight ratio; stirring 1000 rpm; N_2 atmosphere; 0.15 g of catalyst; temperature: 90 ºC; time: 3 h

By comparing the XRD pattern of the reused catalyst with that of its corresponding fresh catalyst (Figure 56), we observed a decrease in the crystallinity of the mayenite phase and the desappearance of CaO accompanied by the formation of calcite for the reused sample. The formation of calcite can be explained by the reaction of the CO_2, generated during decarboxylation of glycerol to glycidol, with the Ca of the catalyst. Thus, the progressive loss of conversion and selectivity to

glycerol carbonate observed could be attributed to the loss of some CaO basic centres during reaction.

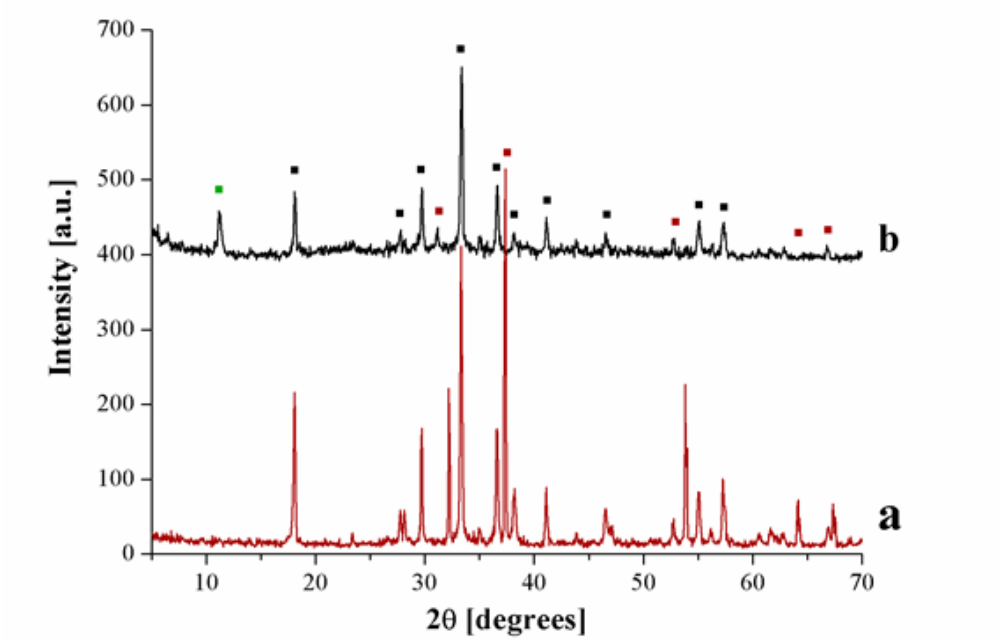

Figure 56. XRD patterns of the catalyst cHC1AMw$_1$-750: a) fresh catalyst and b) after reaction. Reaction conditions: dimethyl carbonate/glycerol = 3.5:1 weight ratio; stirring 1000 rpm; N_2 atmosphere; 0.15 g of catalyst; temperature: 90 ºC; time: 3 h. ■ Mayenite phase; ■ CaO phase.

Conclusions

Calcined samples, prepared from chloride salts and calcined at 450 ºC for 15 h, mainly showed the presence of an amorphous Ca(Al)O_x phase together with some amounts of calcite ($CaCO_3$) in most of them. By increasing the calcination time, the calcite content increased and new crystalline peaks, corresponding to the mayenite phase, $Ca_{12}Al_{14}O_{33}$ appeared. The use of nitrogen flowing through the sample during calcination favoured the crystallization of mayenite. The use of nitrate anions for the preparation of hydrocalumite-type compounds favoured the formation, after calcination, of the mayenite phase when using autoclave-aging conditions, especially under microwaves. When calcined at 750 ºC for 4 h, a mixture of CaO and mayenite phase was obtained in all cases. All catalysts showed low surface areas (4-13 m^2/g)

and retained the original hexagonal morphology of their precursors, the hydrocalumite-type compounds, as observed by SEM and TEM. The basicity strenght was higher for the samples calcined at higher temperature, as determined by using Hammett indicators.

The catalysts obtained by calcination at 450 ºC for 15 h in air showed moderate-high glycerol conversion (46-76 %) and moderate selectivity to glycerol carbonate (41-65 %) after 3 h of reaction. The use of longer calcination time at 450 ºC or a dynamic inert-atmosphere system during calcination led to higher conversion (89-94 %) and higher selectivity to glycerol carbonate (72-73 %) values. This has been related to the presence of mayenite and calcite with low crystallinity together with the mixed oxide $Ca(Al)O_x$ in these two catalysts, which had higher basicity strength than the catalysts calcined at 450 ºC for 15 h. Calcination at 750 ºC resulted in high conversion (88-98 %) and high selectivity to glycerol carbonate (60-85 %) due to the presence in the catalysts of CaO, highly basic. The progressive loss of conversion and selectivity to glycerol carbonate observed after several reuses has been attributed to the loss of some CaO basic centres during reaction, resulting in the formation of higher amounts of glycidol (42 %).

Acknowledgments

Authors acknowledge Ministerio de Economía y Competitividad of Spain and Feder Funds (CTQ2011-24610), and Catalan Government for FI grant (2012FI_B00564).

4.2.3 Boosted selectivity towards glycerol carbonate using microwaves for the transesterification of glycerol

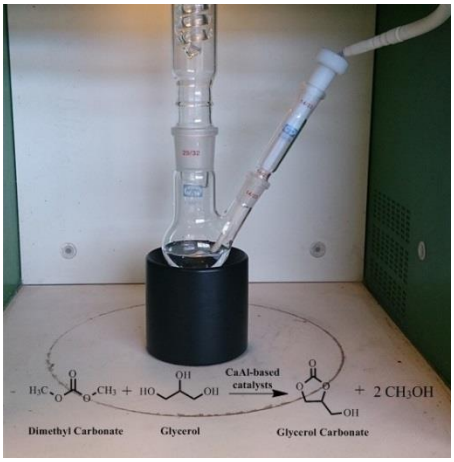

Abstract

Several hydrocalumite-type materials (CaAl-LDHs) and some of their calcined forms, obtained at different calcination temperature, have been tested as catalysts for the transesterification of glycerol towards glycerol carbonate under microwaves. The results have been compared with those obtained using conventional heating during reaction. Interestingly, the use of microwaves increased conversion and especially selectivity to glycerol carbonate for all catalysts while the selectivity to glycidol was similar. Glycerol conversion values were between 63-95 % in microwaves and 61-91 % by conventional heating, and selectivity to glycerol carbonate between 53-92 % in microwaves and 30-80 % by conventional heating depending on the catalyst used. This can be related to the best homogeneity in heating provided by microwaves compared to conventional heating.

Introduction

The interest in new industrial applications of glycerol is increasing parallel to the growth of biodiesel production[5,7,8,174,177] since glycerol is formed as by-product in high amounts (10 wt % of the total product) during biodiesel manufacture. The inherent non-toxic and edible nature of glycerol further encourages its industrial utilization.

One interesting option is the catalytic conversion of glycerol to glycerol carbonate, (4-hydroxymethyl-1,3-dioxolan-2-one), which has many applications in different industrial sectors, such as intermediate in organic synthesis (e.g. monomer in the synthesis of polycarbonates, polyurethanes and polyglycerols),[5,11] biolubricant owing to its adhesion to metallic surfaces and resistance to oxidation, hydrolysis, and pressure,[8] protector in the carbohydrates chemistry, component of gas separation membranes, in coatings, or in the production of polyurethane foams [179] and surfactants.[180]

Traditionally, glycerol carbonate has been produced by reacting glycerol with phosgene but due to the high toxicity and corrosive nature of this reagent, new alternative routes have been investigated.[118] An alternative catalytic route to obtain glycerol carbonate is the transesterification reaction of glycerol with organic cyclic carbonates (ethylene carbonate or propene carbonate) or with non-cyclic carbonates (diethyl carbonate or dimethyl carbonate). Dimethyl carbonate is preferred since the reaction can be performed at milder conditions and the co-product methanol can be easily separated. Ochoa-Gomez *et al*. (2009) studied the influence of different basic and acid homogeneous and heterogeneous catalysts at different reaction conditions. The best results were obtained using basic heterogeneous catalysts.[12] CaO catalyst led to 70 % of conversion and 70 % of yield to glycerol carbonate at 75 ºC after 15 min of reaction. [184] Hydrotalcite-based catalysts have been widely employed for this reaction.[156,158–161,185,186] Calcined Mg/Al/Zr,[158] calcined Mg/Zr/Sr[159] and doping transition metals cations into Mg/Al hydrotalcites resulting in yields to glycerol carbonate between 55-94 % at reaction temperatures in the range 75-100 ºC for this transesterification reaction.[161] Z. Liu *et al*. (2015) reported full conversion

of glycerol and 96 % yield of glycerol carbonate at 80 ºC for 1.5 h in the presence of $Li/Mg_4AlO_{5.5}$ obtained by impregnating calcined Mg/Al hydrotalcite with $LiNO_3$.[186] In previous works, we studied the catalytic behaviour of several Ca/Al hydrocalumite-type compounds, synthesized using microwaves and ultrasounds, and their calcined forms for the for the transesterification of glycerol with dimethyl carbonate to obtain glycerol carbonate (see chapters 4.2.1 and 4.2.2).

Microwave radiation is known to offer additional advantages over traditional thermal heat sources since it provides a rapid, energy-efficient way of heating materials and promotes or accelerates chemical reactions by selectively heating the reactants in a way that it is not possible in conventional heating.[163] While the conventional reflux set up is relatively slow and inefficient to transfer the energy into a reaction mixture as it relies on convection currents and on the thermal conductivity of medium (reaction vessel, reactants and solvent phase etc.); microwave irradiation works through 'in-core' volumetric heating (direct coupling of microwave energy with reaction mixture) which results in rapid and uniform temperature attainment.[187–195] As compared with conventional methods, focused microwave heating is known to reduce side reactions and sharply decrease the creaction time thus improving the selectivity of the reaction, increasing yields and purity of the products, and decreasing the amounts of the solvents used as well.[194,195] Microwaves irradiation haven used for glycerol valorisation to perform the acetalization of several aldehydes and ketones with glycerol in catalyst and solvent free conditions,[169] for the synthesis of acrylonitrile under mild conditions,[196] and for the obtention of glycidol from glycerol carbonate.[197] To the best of our knowledge there are no reports on heterogeneous-catalyzed transesterification of glycerol to glycerol carbonate under microwaves.

The aim of this work was to study the effect of using microwaves during the transesterification of glycerol with dimethyl carbonate, in the presence of several Ca/Al hydrocalumite-type compounds and their calcined forms, on the conversion and selectivity to glycerol carbonate values.

Experimental

Preparation of catalysts

Hydrocalumite-type compounds were synthesized by the co-precipitation method from different starting salts: chlorides (serie HC1) or nitrates (serie HC2). Two different aqueous solutions containing $CaCl_2 \cdot 2H_2O$ (Sigma-Aldrich) and $AlCl_3 \cdot 6H_2O$ (Riedel-de Haën) or $Ca(NO_3)_2 \cdot 4H_2O$ (Sigma-Aldrich) and $Al(NO_3)_3 \cdot 9H_2O$ (Sigma-Aldrich) were prepared with a 2:1 Ca^{2+}/Al^{3+} molar ratio. These solutions were added dropwise to a 500 ml four neck round-botton flack in an oil bath at 60 ºC previously filled with 250 ml of a mixture of water/ethanol in a 2:3 volumetric ratio. The pH was kept constant at 11.5 ± 0.1, by the simultaneous addition of an aqueous solution of 2 M NaOH (Panreac). Magnetic stirring or ultrasounds were used for mixing during precipitation (US is added to notation for the samples prepared with ultrasounds). After complete addition of the metallic salts, the mother solutions were aged by refluxing under conventional heating at 60 ºC for 24 h ($HC1R_{24}$, $HC2R_{24}$, $HC1USR_{24}$, $HC2USR_{24}$) or under microwaves (Milestone ETHOS-TOUCH CONTROL) at 60 ºC for 6 h ($HC1RMw_6$, $HC2RMw_6$, $HC1USRMw_6$, $HC2USRMw_6$). Finally, all samples were filtered at room temperature, washed with deionized and decarbonated water and then dried in an oven at 80 ºC overnight. Several of these hydrocalumite-type compounds were calcined in a furnace Carbolite CWF11/5P8 at 450 ºC for 15 h ($cHC1R_{24}$, $cHC2R_{24}$, $cHC1RMw_6$, $cHC2RMw_6$), and at 750 ºC for 4 h ($cHC1R_{24}$-750, $cHC1RMw_6$-750).

Characterization methods

Powder X-ray diffraction patterns of the samples were obtained with a Siemens D5000 diffractometer using nickel-filtered CuKα radiation and detecting between 2θ values of 5º-70º. Crystalline phases were identified using the Joint Committee on Powder Diffraction Standards (JCPDS) files (035-0105- Calcium Aluminium Hydroxide Chloride Hydrate-$Ca_2Al(OH)_6Cl \cdot 2H_2O$, 089-6723- Calcium Aluminun Nitrate Hydroxide Hydrate- $Ca_2Al(OH)_6NO_3 \cdot 2H_2O$, 089-0217- Katoite-$Ca_3Al_2(OH)_{12}$, 086-2341- calcite -$CaCO_3$ and 089-6723-mayenite, 0.7-1497-Lime-CaO).

Elemental analysis of the samples was obtained with an ICP-OES analyser (Induced Coupled Plasma – Optical Emission Spectroscopy) from Spectro Arcos. The digestion of all hydrocalumites was carried out with concentrated HNO_3. Analyses were performed by triplicate.

BET surface areas were calculated from the nitrogen adsorption isotherms at -196 ºC using a Quantachrome Quadrasorb SI surface analyzer and a value of 0.164nm^2 for the cross-section of the nitrogen molecule. Samples were degassed at 90 ºC.

Basicity of the catalysts was evaluated using Hammett indicators: phenolphthalein (pKa = 8.2), nile blue A (pKa = 10.1), tropaeolin O (pKa = 11), thyazole yellow G (pKa = 13.4) and 2,4-dinitroaniline (pKa = 15). 25 mg of catalyst was taken along with 2.5 ml dry methanol and 1 ml of indicator, and kept in a shaker for 2 h.

Catalytic Tests

For the catalytic tests, 0.15 g of catalysts was used. Dimethyl carbonate and glycerol were mixed in a 3.5:1 weight ratio in a 50 ml round bottom glass reactor fitted with a reflux condenser and a thermocouple. The mixture was heated at 90 ºC under N_2 under microwaves (Milestone ETHOS-TOUCH CONTROL). After 3 h of reaction, the mixture was filtered and evaporated in a rotatory evaporator. 1 µl of the concentrated residue was analysed by gas chromatography. Catalytic tests were compared with those performed at the same reaction conditions but using conventional heating instead microwaves.

Gas chromatography analysis were performed in a ZHIMADSU GC-2010 apparatus, equipped with a split injection mode and a flame ionization detector. The column was a SUPRAWAX-280 with 60 m length, a film thickness of 50 µm and an internal diameter of 0.25 mm. Glycerol conversion and selectivity to glycerol carbonate and glycidol were determined from calibration lines obtained from commercial products.

Results and Discussion

Catalysts characterization

Table 13 summarizes the main characterization results of the catalysts. More detailed characterization of the samples can be found in previous works ([105], chapters 4.1.1).

Table 13. Characterization of the catalysts

Catalysts	Crystalline phases (XRD)	Ca/Al (ICP)	BET Area (m^2/g)	Basicity (Hammet Indicators)
$HC1R_{24}$	$Ca_2Al(OH)_6Cl{\cdot}2H_2O$	1.98	13	10.1<H_>13.4
$HC1RMw_6$	$Ca_2Al(OH)_6Cl{\cdot}2H_2O$	1.87	10	10.1<H_>13.4
$HC1USR_{24}$	$Ca_2Al(OH)_6Cl{\cdot}2H_2O$[a]	1.97	6	10.1<H_>13.4
$HC1USRMw_6$	$Ca_2Al(OH)_6Cl{\cdot}2H_2O$[a]	1.88	7	10.1<H_>13.4
$HC2R_{24}$	$Ca_2Al(OH)_6NO_3{\cdot}2H_2O$[a]	1.79	9	10.1<H->13.4
$HC2RMw_6$	$Ca_2Al(OH)_6NO_3{\cdot}2H_2O$[a]	1.63	9	10.1<H->13.4
$HC2USR_{24}$	$Ca_2Al(OH)_6NO_3{\cdot}2H_2O$[a]	1.78	16	10.1<H->13.4
$HC2USRMw_6$	$Ca_2Al(OH)_6NO_3{\cdot}2H_2O$[a]	1.85	25	10.1<H->13.4
$cHC1R_{24}$-450	Amorphous Ca(Al)Ox	1.98	11	6.8<H_>8.2
$cHC1RMw_6$-450	Amorphous Ca(Al)Ox + $CaCO_3$[b]	1.87	12	6.8<H_>8.2
$cHC2R_{24}$-450	Amorphous Ca(Al)Ox + $CaCO_3$[c]	1.79	9	6.8<H_>8.2
$cHC2RMw_6$-450	Amorphous Ca(Al)Ox + $CaCO_3$[c]	1.63	10	6.8<H_>8.2
$cHC1R_{24}$-750	Mayenite+CaO	1.98	4	13.4<H_>15
$cHC1RMw_6$-750	Mayenite+CaO	1.87	5	10.1<H_>13.4

[a] Katoite phase was detected in low amounts (5-23 %) [105]
[b] Calcite was detected in very low amounts (see Figure 48).
[c] Calcite was more crystalline and was detected in higher amounts than in $cHC1RMw_6$ (see Figure 49).

XRD patterns of the hydrocalumite-type compounds showed the crystalline phase corresponding to the CaAl-LDH structure. Crystalline katoite was also observed in different amounts for the samples HC1 coprecipitated under ultrasounds and for all HC2 samples.[105] XRD patterns of the samples calcined at 450 ºC exhibited the presence of an amorphous phase due to the expected mixture of calcium and aluminium oxides, $Ca(Al)O_x$. Additionally, several crystalline peaks

were detected for most of the samples (cHC1RMw$_6$, cHC2R$_{24}$ and cHC2RMw$_6$), which were identified as calcite ($CaCO_3$). Calcite was more crystalline and was observed in higher amounts for the samples the precursors of which were prepared with nitrates (cHC2R$_{24}$ and cHC2RMw$_6$). Ca/Al molar ratio of HC1 samples were around 2, in agreement with the Ca/Al molar ratio of the starting solutions used for coprecipitation. Ca/Al molar ratio values of the samples prepared from nitrates (HC2) were lower than those obtained for the samples synthesized from chloride salts (Table 13). There is a clear correlation between the amount of katoite phase and the decrease in the Ca/Al molar ratio observed for the HC2 samples. All the HC1 and HC2 samples exhibited nitrogen adsorption-desorption isotherms type IV according to IUPAC classification, corresponding to solids with mesoporous contribution. All samples showed low surface areas (Table 13).

Hydrocalumite-type compounds had higher basicity strength (10.1< H_ <13.4) than the samples calcined at 450 ºC (6.8<H_>8.2) but lower than the samples calcined at 750 ºC (13.4<H_>15). This can be explained by the presence of calcite in the samples calcined at 450 ºC. XRD results of samples calcined at 750 °C showed the mayenite and CaO phases; justifying the higher basicity strenght in the samples calcined at 750 ºC. However, cHC1R$_{24}$-750 sample presented a greater amount of CaO than the cHC1RMw$_6$-750 sample, which is reflected in increased basicity strength in the cHC1R$_{24}$-750 sample (13.4<H_>15).in comparison with the cHC1RMw$_6$-750 sample (10.1<H_>13.4).

Catalytic Tests

Figures 57 and 58 show the catalytic results obtained by HC1 and HC2 catalysts for the transesterification of glycerol with methyl carbonate after 3 h of reaction using microwaves and conventional heating during reaction. All these catalysts exhibited high conversion and the formation of two reaction products: glycerol carbonate, as main product, and glycidol, in lower amounts. Interestingly, the use of microwaves instead of conventional heating clearly increased the conversion but especially the selectivity to glycerol carbonate for all catalysts while the selectivity to glycidol was similar. No other reaction products were detected. There are no great differences between HC1 and HC2 catalysts. This can be explained by the similar surface and basic characteristics observed for these catalysts (Table 13).

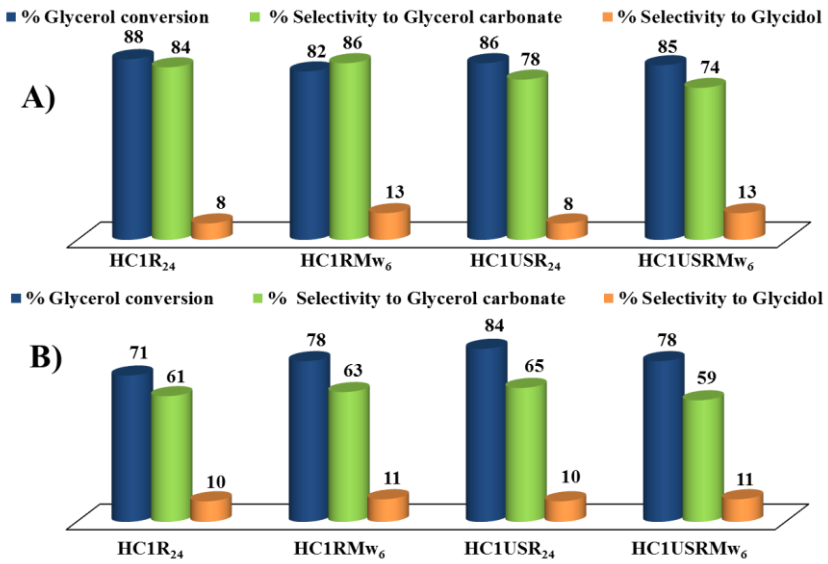

Figure 57. Catalytic activity of the catalysts HC1 A) under microwaves and B) by conventional heating. Reaction conditions: dimethyl carbonate/glycerol = 3.5:1 weight ratio; N_2 atmosphere; 0.15 g of catalyst; temperature: 90 ºC; time: 3 h.

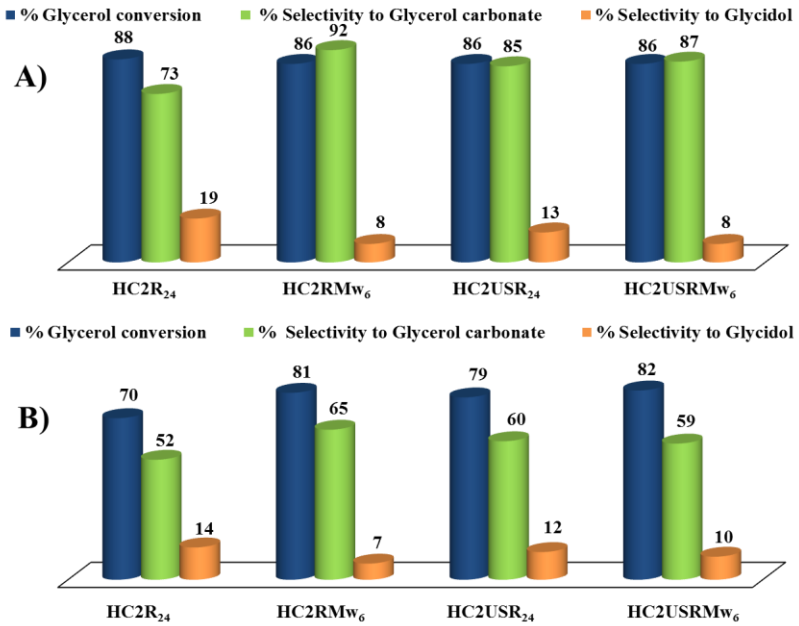

Figure 58. Catalytic activity of the catalysts HC2 A) under microwaves and B) by conventional heating. Reaction conditions: dimethyl carbonate/glycerol = 3.5:1 weight ratio; N_2 atmosphere; 0.15 g of catalyst; temperature: 90 ºC; time: 3 h.

Figures 59 and 60 show the catalytic results obtained by the catalysts calcined at different temperatures for the transesterification of glycerol with dimethyl carbonate after 3 h of reaction using microwaves and conventional heating during reaction. For all these catalysts we observed that again the use of microwaves increased conversion and especially selectivity to glycerol carbonate. Focused microwave heating is known to reduce side reactions thus improving the selectivity of the reaction, increasing yields and purity of the products.[194,195] It is also well known that microwaves can accelerate organic reactions (oxidation, polymerization, reduction).[101] This has been attributed to the higher homogenity of heating when using microwaves with respect to conventional heating. Interestingly, the sum of the selectivity values to glycerol carbonate and glycidol was higher when using microwaves than when using conventional heating during reaction. Therefore, the use of microwaves favors the transesterification reaction.

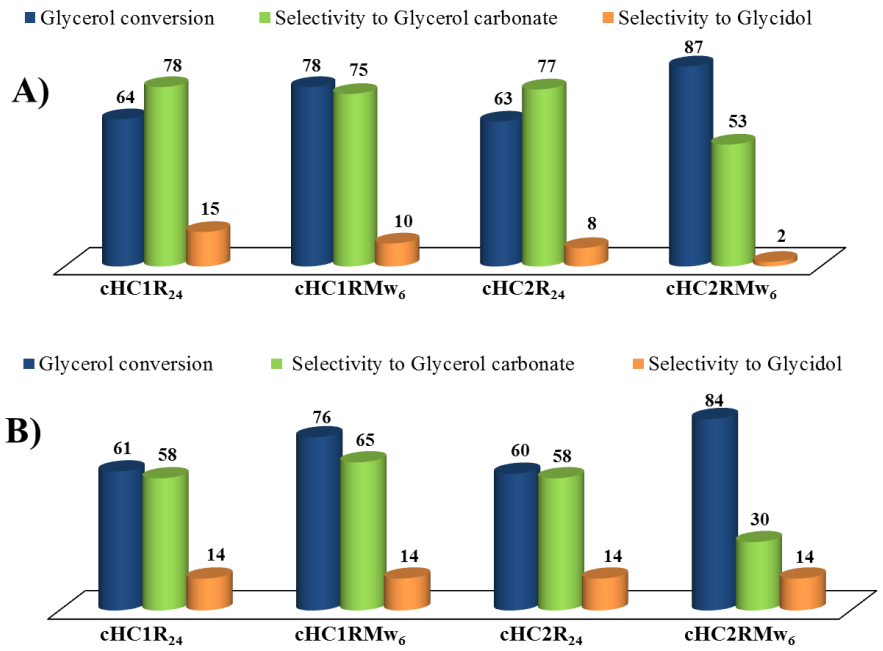

Figure 59. Catalytic activity of the samples calcined at 450 ºC A) under microwaves and B) by conventional heating. Reaction conditions: dimethyl carbonate/glycerol = 3.5:1 weight ratio; N_2 atmosphere; 0.15 g of catalyst; temperature: 90 ºC; time: 3 h.

On the whole, the catalytic results of the samples calcined at 450 ºC were worse than those of the hydrocalumite-type compounds while the best catalytic results were achieved with the samples calcined at 750 ºC. This can be correlated with the different basicity strenght of the catalysts, which varies in this order: samples calcined at 750 ºC > hydrocalumite-type compounds > samples calcined at 450 ºC (Table 13) as a consequence of the different composition of the samples.

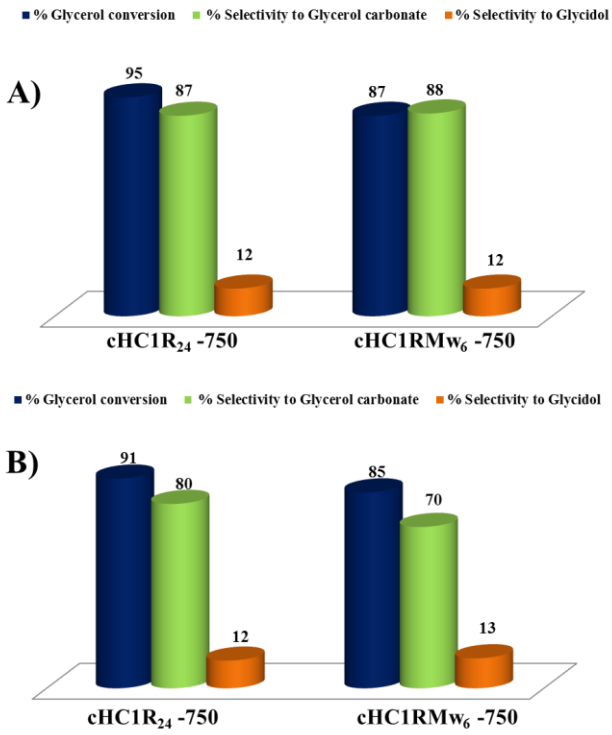

Figure 60. Catalytic activity of the samples calcined at 750 ºC A) under microwaves and B) by conventional heating. Reaction conditions: dimethyl carbonate/glycerol = 3.5:1 weight ratio; N_2 atmosphere; 0.15 g of catalyst; temperature: 90 ºC; time: 3 h.

The catalytic life of one of the catalysts ($HC2USRMw_6$) was evaluated from four consecutive runs performed reusing the catalyst at the same reaction conditions used for the first catalytic test (Fig. 61). After each catalytic run, recovering of the catalyst was performed by filtration, mild-washing in methanol at room temperature and dried before reaction. Several catalytic reuses resulted in a progressive loss of conversion and selectivity to glycerol carbonate, and glycidol. This progressive loss of activity could be attributed to the loss of some basic centres during reaction. It is important to note that this behavior is different to that observed when reusing one hydrocalumite-type compound by conventional heating (Figure 46, Chapter 4.2.1), the results of which exhibited similar selectivity to glycerol carbonate values and a significant increase of selectivity to glycidol after reusing. The homogeneity of the

heating under microwaves could explain the similar activity values obtained under reusing.

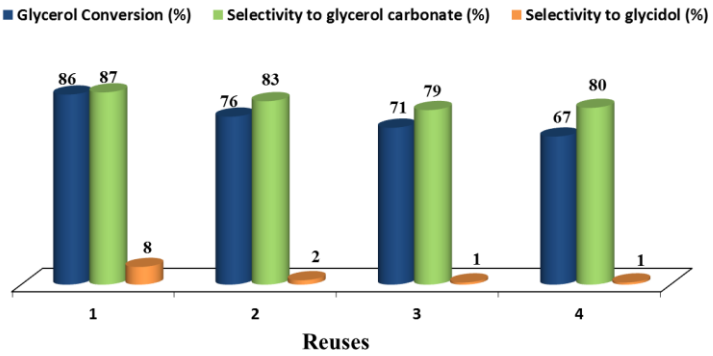

Figure 61. Reuse studies of catalyst HC2USRMw$_6$ under microwaves. Reaction conditions: dimethyl carbonate/glycerol = 3.5:1 weight ratio; N_2 atmosphere; 0.15 g of catalyst; temperature: 90 ºC; time: 3 h.

Conclusions

Several CaAl-layered double hydroxides and several calcined CaAl-layered double hydroxides have been tested as catalysts for the transesterification of glycerol to glycerol carbonate using microwaves or conventional heating during reaction. The catalytic results of the samples calcined at 450 ºC were worse than those of the hydrocalumite-type compounds (with glycerol conversion values between 87-63 % in the case of the samples calcined at 450 ºC and 88-82 % in the hydrocalumite-type compounds, and selectivity of glycerol carbonate values between 78-53 % and 92-73 %, respectively) while the best catalytic results were achieved with the samples calcined at 750 ºC (glycerol conversion between 95-87 % and selectivity to glycerol carbonate between 88 and 87 %). This can be correlated with the different basicity strength of the catalysts. The use of microwaves during reaction resulted in higher conversion and, especially, higher selectivity to glycerol carbonte for all catalysts.

Acknowledgments

Authors acknowledge Ministerio de Economía y Competitividad of Spain and Feder Funds (CTQ2011-24610), and Catalan Government for FI grant (2012FI_B 00564).

UNIVERSITAT ROVIRA I VIRGILI
HYDROCALUMITE-BASED CATALYSTS FOR GLYCEROL REVALORIZATION.
Judith Cecilia Granados Reyes
Dipòsit Legal: T 1362-2015

UNIVERSITAT ROVIRA I VIRGILI
HYDROCALUMITE-BASED CATALYSTS FOR GLYCEROL REVALORIZATION.
Judith Cecilia Granados Reyes
Dipòsit Legal: T 1362-2015

CHAPTER 4

Results and discussion

Catalytic decarboxylation of glycerol carbonate to glycidol

UNIVERSITAT ROVIRA I VIRGILI
HYDROCALUMITE-BASED CATALYSTS FOR GLYCEROL REVALORIZATION.
Judith Cecilia Granados Reyes
Dipòsit Legal: T 1362-2015

4.3 Catalytic decarboxylation of glycerol carbonate to glycidol

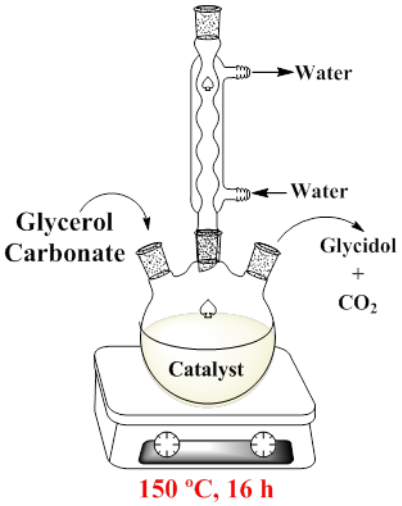

Abstract

In this work, several layered double hydroxides of Ca/Al, Mg/Al and Ni/Al and various aluminium (oxi)hydroxides, prepared with microwaves, have been tested as catalysts for the decarboxylation of glycerol carbonate to glycidol in a preliminary study. Catalysts were characterized by XRD, elemental analysis nitrogen physisorption and TEM. The best catalytic result was achieved using a catalyst prepared by coprecipitation of Ca and Al salts at pH 8 and later modification with H_3PO_4, obtaining 72 % of selectivity to glycidol for a carbonate glycerol conversion of 36 % at 150 ºC after 16 h of reaction. These values are comparable to those described in the literature using conventional heating at 150 ºC after 23 h of reaction.

Introduction

Nowadays, the biofuels, which are derived from renewable raw materials, have emerged as an alternative to reduce carbon dioxide emissions from fossil fuels, and mitigate air pollution and global warming. Biodiesel is produced from vegetable oils and methanol by a transesterification reaction which generates glycerol as a byproduct in large amounts.[5,7,8]

Although glycerol has many industrial applications, its large surplus has led to a decrease on its price in recent years. In order to revalorise this material, it is necessary to transform it into products with high-added value such as glycerol carbonate, among others. Glycerol carbonate is a relatively new material in the chemical industry. It can be used for gas separation membranes, as solvent, biolubricant or as a source of new polymers.[12,116] Additionally, glycerol carbonate is the most valuable intermediate for the production of glycidol, which is a precursor for the synthesis of polymers (e.g. polycarbonates or polyurethanes). Glycidol is also used as a stabilizer for natural oils and vinyl polymers, as demulsifier, in surface coatings, in the chemical synthesis of several intermediates, pharmaceuticals and as a gelation agent in solid propellants [9,12,197].

Traditionally, the industrial production of glycidol is performed by the epoxidation of allyl alcohol and hydrogen peroxide in the presence of a homogeneous catalyst. However, it requires a large number of steps to obtain the desired product. Moreover, some of the homogeneous catalysts tested for this reaction were decomposed during reaction, increasing the final cost of the process.

This reaction has been also studied by using heterogeneous catalysts. Wróblewska *et al*. (2002) has studied this reaction using different heterogeneous titanium catalysts, they was getting this reaction efficiently.[198–203] Other authors have also used titanium catalyst in this reaction obtaining acceptable results.[204,205]

Another route to obtain glycidol is through the decarboxylation reaction of glycerol carbonate. Malkemus and Currier (1958) patented the synthesis of glycidol from glycerol carbonate using a metal salt as catalyst, obtaining glycidol yields of 80–90 % at high temperature and low pressure.[206] Gaset *et al*. (2001) patented the

production of glycidol from glycerol carbonate and glycerol as co-reagent in 1 h of reaction, at 3.5 kPa and 183 ºC, using zeolite-A as catalyst, obtaining 72 % yield of glycidol.[181] Mouloungui (2004) studied the formation of glycidol from glycerol carbonate and using glycerol as co-reactant. In this reaction a glycerol/glycerol carbonate ratio of 0.1/0.15 was added to a thin film reactor. Zeolite was used as catalyst (10 % of weight with respect to the total glycerol carbonate). The temperature was adjusted to 175 °C for 2 h at 35 mbar of pressure. The results show that this new process produced glycidol anhydride with 87 % of selectivity, 86 % of yield and 99 % of purity. Mouloungui (2004) also reported the mechanism for this reaction (Figure 62), where the heterocyclization of two hydroxyl groups of glycerol are inserted into a cyclocarbonate group, followed by oligomerization of glycerol carbonate, and finally followed by controlled depolymerization by the action of bifunctional zeolites.[207]

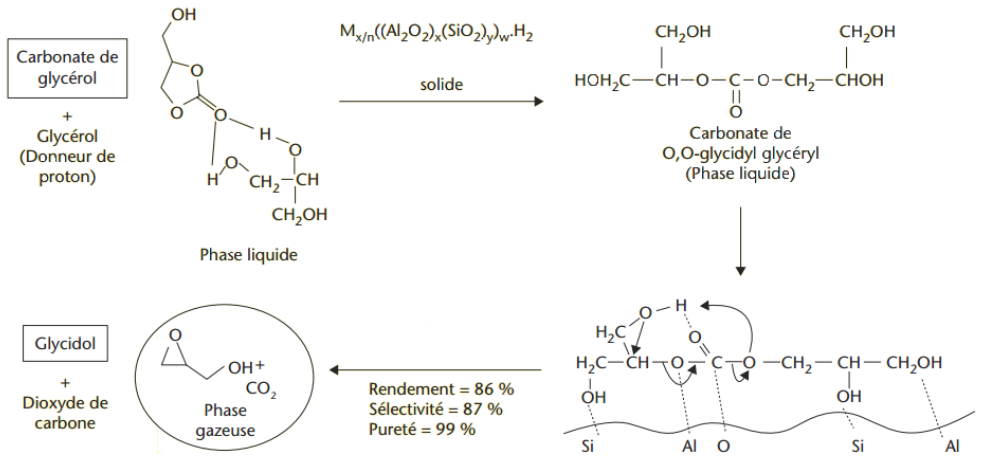

Figure 62. Reaction mechanism of the catalytic synthesis of glycidol by oligomerization of glycerol carbonate.[207]

Recently, Yuichiro *et al.* (2011) patented the process for glycidol synthesis by using sodium sulfate anhydrous as catalyst, at 200 ºC for 6 h at low pressure in the presence of a solvent containing no active hydrogen, obtaining yields of 80 %.[208]

Choi *et al*. (2013) studied the decarboxylation of glycerol carbonate to produce glycidol using various ionic liquids as catalysts and solvent at a specified temperature under a reduced pressure of 2.67 kPa. In their work, the ionic liquids bearing an anion with medium hydrogen-bond basicity exhibited the higher glycidol yields. Moreover, the yield of glycidol increased to 98 % when adding a high-boiling aprotic solvent to the reaction.[209] The aforementioned studies are restricted to very specific reactions conditions (low pressure and with significant constraints in the nature of the solvent). However, the new methodology used by Bolívar-Diaz *et al*. (2013) presents an effective transformation of glycerol carbonate to glycidol in dry media, in atmospheric pressure and using a heterogeneous catalyst. In their work, Bolivar-Diaz *et al*. studied the transformation of glycerol carbonate into glycidol using a ZSM-5 zeolite catalyst and Co_3O_4/ZnO catalyst, in the absence of solvent. They used conventional thermal activation, ultrasound-activation and microwave-activation in the liquid; reporting the highest selectivity to glycidol greater than 99 % and a high glycerol carbonate conversion of 71 %.[197]

In this work we present the preliminary results of using various layered double hydroxides materials and several aluminium (oxi)hydroxides as catalysts for the decarboxylation of glycerol carbonate to obtain glycidol.

Experimental

Catalysts preparation

One CaAl-hydrocalumite, with a 2:1 molar ratio of Ca^{2+}/Al^{3+}, was synthesized by the co-precipitation method from nitrate salts following the synthesis methodology detailed in section 4.1. The solutions were added to a mixture of 250 ml water/ethanol (2:3) under ultrasounds at 60 ºC and pH 11.5, and later aged by conventional heating by refluxing at 60 ºC for 24 h. This sample was named as $HC2USR_{24}$. Another sample was synthesized following the method used for the synthesis of the hydrocalumite but coprecipitating the mixture of Ca and Al nitrate salts at pH 8 (sample $HC2USR_{24}$-pH8). In order to increase the acidity of this later sample, one fraction was impregnated with 0.7 M H_3PO_4 solution, and dried at 80 ºC overnight (sample $HC2USR_{24}$-pH8-I).

Two hydrotalcites (i.e. NiAl-hydrotalcite and MgAl-hydrotalcite) were also synthesized by the coprecipitation method. The NiAl-hydrotalcite (takovite) was synthesized from nitrates salts with a Ni/Al molar ratio of 4:1, The solutions of $Ni(NO_3)_2 \cdot 6H_2O$ and $Al(NO_3)_3 \cdot 9H_2O$ were added dropwise to a solution of 40 ml of NaOH 0.01 M, at room temperature, under vigorous magnetic stirring. The pH was kept constant at 8, by the simultaneous addition of an aqueous solution of 1 M NaOH. After complete addition of the metallic salts, the resulting solution was aged at room temperature for 18 h (sample NiAl-HT). MgAl-hydrotalcite was synthetised by the co-precipitation of $Mg(NO_3)_2 \cdot 6H_2O$ and $Al(NO_3)_3 \cdot 9H_2O$, with a 3:1 molar ratio of Mg/Al. The solution of salts were added dropwise to a solution of 200 ml of $(NH_4)_2CO_3$ 0.05 M. under vigorous magnetic stirring at 70 ºC. The pH was kept constant at 8, by the simultaneous addition of an aqueous solution of 1 M NH_3. After complete addition of the metallic salts, the resulting solution was aged at 70 ºC for 18 h (MgAl-HT).

Finally, three aluminium (oxi)hydroxide samples were prepared by precipitating 100 ml of 0.1 M aqueous solution of Al $(NO_3)_3 \cdot 9H_2O$ with a 0.25 % aqueous ammonia solution until pH 8 at 75 °C. The mother solution was aged under reflux in a microwave (ETHOS TOUCH CONTROL) at 75 °C for 1, 2 and 3 h (H1, H2 and H3).

All samples were filtered at room temperature, washed with deionized water and then dried in an oven at 80 ºC overnight. Table 14 summarizes the preparation conditions used and the nomenclature assigned to each sample.

Table 14. Aging treatments of the samples.

Sample	Precipitation		Aging		
	Ultrasound	T (ºC)	Heating	T (ºC)	Time (h)
$HC2USR_{24}$	Si	60	conventional	60	24
$HC2USR_{24}$-pH8	Si	60	conventional	60	24
$HC2USR_{24}$-pH8-I [a]	Si	60	conventional	60	24
NiAl-HT	No	R.T	conventional	R.T	18
MgAl-HT	No	70	conventional	70	18
H1	No	75	microwave	75	1
H2	No	75	microwave	75	2
H3	No	75	microwave	75	3

[a] Sample impregnated with a solution of 0.7 M H_3PO_4
R.T: Room temperature

Catalysts characterization

Samples were characterized with X-ray diffraction with a Siemens D5000 diffractometer, using nickel-filtered CuKα radiation. The patterns were recorded over a range of 2θ angles from 5º to 70º. Crystalline phases were identified using the Joint Committee on Powder Diffraction Standards (JCPDS) files, 89-6723-Calcium Aluminun Nitrate Hydroxide Hydrate, 89-0217- Katoite, 15-0087-Takovite, 89-0460-Hydrotalcite, 73-6509-Boehmite, 74-1775-Gibbsite and 74-0087-Bayerite.

The elemental analysis of $HC2USR_{24}$-pH8 and $HC2USR_{24}$-pH8-I samples was performed using an ICP-OES analyser (Induced Coupled Plasma – Optical Emission Spectroscopy) from Spectro Arcos. The digestion of the samples was carried out with concentrated HNO_3.

The Brunauer, Emmett and Teller (BET) theory was used to calculate the total surface area of the samples through that the nitrogen adsorption isotherms at -196 ºC using a Quadrasorb *SI* Surface analyzer.

Transmission electron microscopy (TEM) of the samples was performed using a JEOL electron microscope Model 1011 with an operating voltage of 80 kV. The magnification values used were between 20 and 100 k.

Catalytic Activity

The catalytic activitiy of the catalysts was studied in the decarboxylation reaction of glycerol carbonate (GC) to obtain glycidol. For this purpose, 1.77 g of glycerol carbonate into a round bottom flask 3-necked coupled to a reflux, which was heated at 150 °C for 16 h under inert atmosphere. After the reaction was completed, the reaction products were analysed by gas chromatography in a ZHIMADSU GC-2010 apparatus, equipped with a split injection mode and a flame ionization detector. The column was a SUPRAWAX-280 (60 m, 50 μm and 0.25 mm). Glycerol carbonate conversion and selectivity to glycidol were determined from calibration lines obtained from commercial products.

Results and discussion

Catalysts characterization

Figure 63 shows the XRD patterns obtained for the CaAl samples. Sample $HC2USR_{24}$ was identified as an hydrocalumite-type compound, especifically Calcium Aluminun Nitrate Hydroxide Hydrate phase (with formula $Ca_2Al(OH)_6NO_3{\cdot}2H_2O$) (Figure 63a). This phase belongs to the group *P-3c1* (Nº 165, indexed in the hexagonal group) with theroretical *a* and *c* parameter values of 5.74 Å and 17.23 Å, respectively. Additionally, katoite ($Ca_3Al_2(OH)_{12}$), was observed in low amounts.

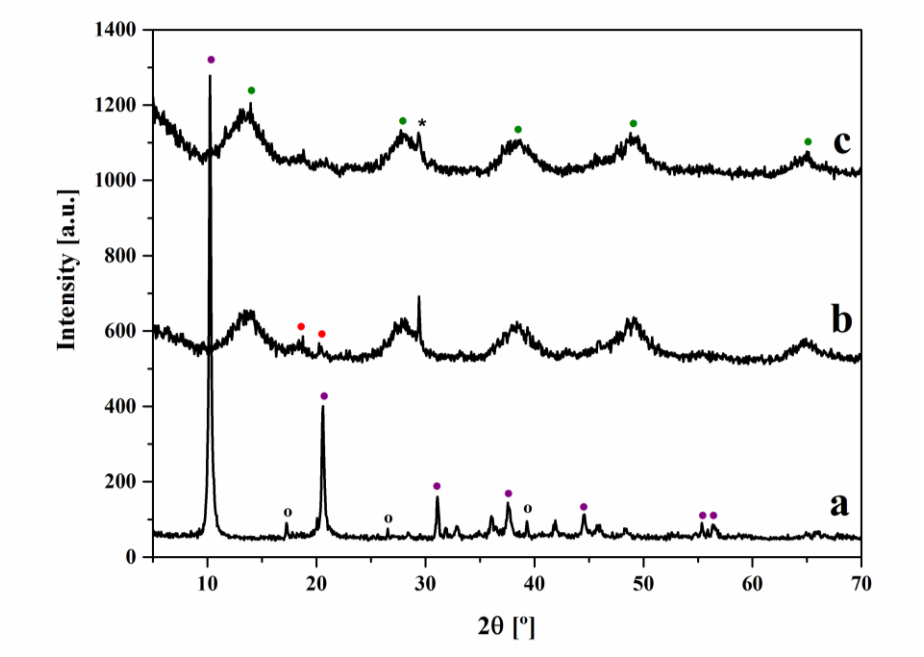

Figure 63. XRD patterns of the CaAl samples a) HC2USR$_{24}$, b) HC2USR$_{24}$-pH8, c) HC2USR$_{24}$-pH8-I. (●) hydrocalumite phase, (o) katoite phase. (●) Bayerite Phase, (●) Boehmite phase (*) Calcite phase.

XRD pattern of sample HC2USR$_{24}$-pH8 revealed the formation of an amorphous boehmite phase (γ-AlO(OH)), accompanied by the presence of the calcite phase and a bayerite phase (α-Al(OH)$_3$) in very low amounts. The boehmite phase belongs to the orthorhombic lattice system (Cmc2$_1$ space group and the *a,b,c* cell parameters values are 2.87, 12.24, 3.70, respectively). The hydrocalumite phase was not observed. Therefore, a decrease in the pH of precipitation from 11.5 to 8 avoided the formation of the hydrocalumite phase. This can be related to the high pH of precipitation required to obtain Ca(OH)$_2$. In fact, the pH of a saturated Ca(OH)$_2$ solution is about 12.4. When this sample was modified with a phosphoric acid solution (HC2USR$_{24}$-pH8-I), the corresponding XRD pattern (Figure 63c) was very similar to that of the HC2USR$_{24}$-pH8 sample, with a slight decrease in the calcite amount.

Figure 64 presents the XRD results for the hydrotalcite samples. For the NiAl-HT sample (Figure 64b), a single crystalline phase identified as takovite, with formula Ni$_6$Al$_2$(OH)$_{16}$(CO$_3$,OH)·4H$_2$O, was observed. XRD pattern of MgAl-HT

(Figure 64a) exhibited the formation of the hydrotalcite phase with formula $(Mg_{0.667}Al_{0.333})(OH)_2(CO_3)_{0.167}(H_2O)_{0.5}$. This sample was less crystalline than NiAl-HT and also had bayerite phase in low amounts.

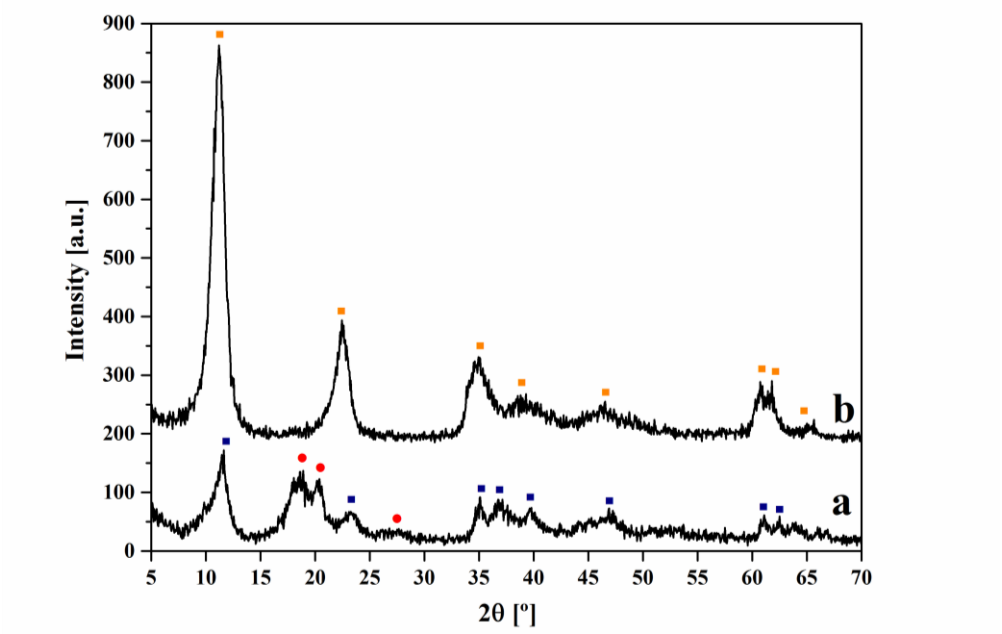

Figure 64. XRD patterns of the hydrotalcite samples a) MgAl-HT, b) NiAl-HT. (▪) hydrotalcite phase, (●) Bayerite phase, (▪) Takovite phase.

Finally, Figure 65 shows the results obtained for the aluminium (oxi)hydroxides samples. The sample aged at 1 h with microwaves (H1, Figure 65a), presented an amorphous phase, which did not correspond to any crystalline aluminium (oxi)hydroxide phase. By increasing the aging time to 2 h, the formation of two crystalline phases was observed: the bayerite phase (α-$Al(OH)_3$) in higher amounts and the gibbsite phase (γ-$Al(OH)_3$). The bayerite phase belongs to the space group $P2_1/a$ (Nº 14) and had cell parameters (*a*,*b*,*c*) with values 5.06, 8.67 and 4.71, respectively. The gibbsite phase belongs to the same space group ($P2_1/n$ (Nº 14)) and the monoclinic lattice system, with cell parameters 8.67, 5.07 and 9.72, which that corresponds to *a*, *b* and *c*, respectively.

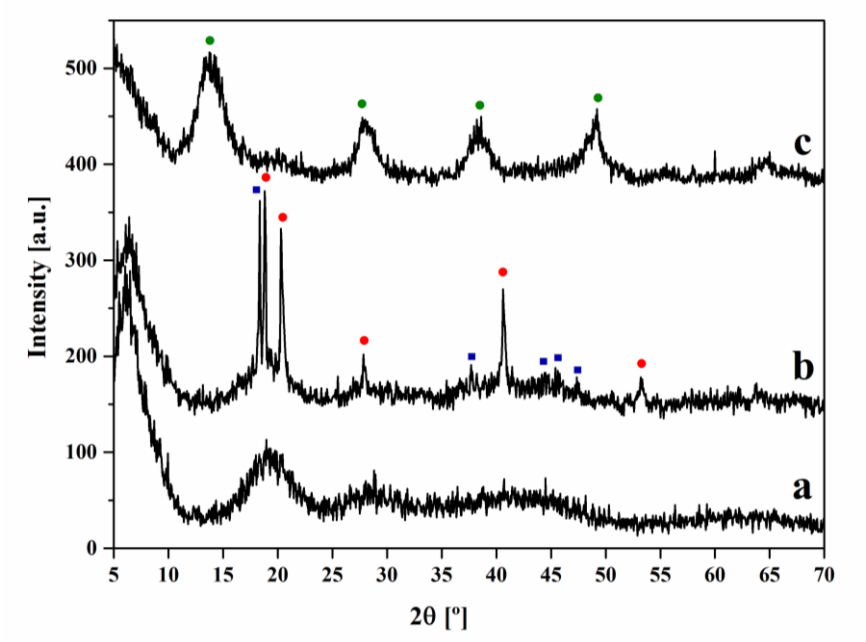

Figure 65. XRD patterns of the aluminium (oxi)hydroxides samples a) H1, b) H2, c) H3. (■) Gibbsite phase, (●) Bayerite phase, (●) Boehmite phase.

For the sample aged with microwaves at 3 h (H3, Figure 65c) only the boehmite phase (γ-AlO(OH)) was observed.

The M^{2+}/Al^{3+} ratio of the Ni/Al and Mg/Al hydrotalcites practically matched the theoretical values while for the hydrocalumite HC2USR$_{24}$ the Ca^{2+}/Al^{3+} molar ratio was lower than 2 because of the presence in low amounts of the katoite phase, as commented in previous chapters. Finally, the Ca^{2+}/Al^{3+} molar ratio of HC2USR$_{24}$-pH8 and HC$_2$USR$_{24}$-pH8-I were much higher than the theoretical value used for their synthesis. This can be related to the low incorporation of Ca^{2+} due to the low pH used for precipitation.

Table 15. Sample characterization

Sample	M^{2+}/Al^{3+}	Surface Area (m^2g^{-1})	Average Pore radius (Å)	Pore Volume (cm^3g^{-1})
$HC2USR_{24}$	1.78	16	238	0.110
$HC2USR_{24}$-pH8	0.97	28	143	0.199
$HC2USR_{24}$-pH8-I	0.97	39	138	0.219
NiAl-HT	3.92	3	24	0.003
MgAl-HT	3.01	83	44	0.183
H1	---	1	133	0.010
H2	---	7	28	0.010
H3	---	97	22	0.108

From nitrogen physisorption results, we observe that the samples $HC2USR_{24}$-pH8 and $HC2USR_{24}$-pH8-I had higher surface area than the hydrocalumite sample ($HC2USR_{24}$) (Table 15). This can be explained by the lower cristallinity of the amorphous oxihydroxides identified in the samples $HC2USR_{24}$-pH8 and $HC2USR_{24}$-pH8-I in comparison with the higher crystallinity of the hydrocalumite $HC2USR_{24}$ (Figure 63). Regarding hydrotalcites, MgAl-HT showed higher surface area than NiAl-HT. This can be related to the lower crystallinity observed for the MgAl hydrotalcite (Figure 64). Finally, the aluminium oxihydroxide obtained after 3 h of aging with microwaves (H3) had much higher surface area than those obtained at less aging time (Table 15). The results for the H1 sample can be related to the shape of its nitrogen adsorption isotherm, which corresponded to macroporous or nonporous materials (type II). However, H2 and H3 samples showed type IV isotherm, corresponding to mesoporous solids. The higher surface area of H3 with respect to H2 can be attributed to the lower crystallinity observed for this sample.

TEM images of the hydrocalumite and hydrotalcites samples exhibited the typical lamellar structure of this type of compounds with different particle sizes (Figure 66). Thus, sample $HC2USR_{24}$ had hexagonal lamellar particles with sizes around 50 nm whereas NiAl-HT showed particle sizes between 20 and 30 nm and

MgAl-HT had particles of 30 and 100 nm. The rest of samples showed particles more or less agglomerated.

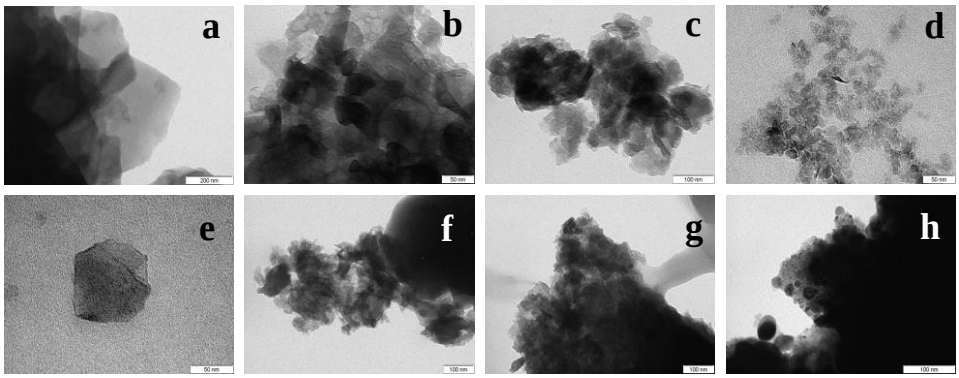

Figure 66. TEM images of a) HC2USR$_{24}$ (x120000), b) HC2USR$_{24}$-pH8 (x200000), c) HC2USR$_{24}$-pH8-I (x300000), d) NiAl-HT (x300000), e) MgAl-HT (x400000), f) H1(x150000), g) H2 (x150000), h) H3 (x250000).

Catalytic Activity

Table 16 shows the catalytic results of the catalysts prepared for the decarboxylation of glycerol carbonate at 150 ºC after 16 h of reaction. All catalysts were very active but different selectivity values to glycidol were obtained. In addition to the glycidol formation, another compound, which presented a longer retention time by gas chromatography, was observed. This product could be a polymerization product of glycerol carbonate to poly-(glyceril-1,2-dicarbonate), which would then release a carbon dioxide forming glycidol.[210] Hydrocalumite was wery active (total conversion) but glycidol was not formed. MgAl hydrotalcite also showed moderate conversion but nul selectivity to glycidol. However, NiAl-HT resulted in 26 % of selectivity to glycidol for a 35 % of conversion. The different acid-base properties due to the presence of different cations in the hydrotalcite layers can justify these results.

Regarding the catalytic results of the aluminium (oxi)hydroxides, we observed a similar selectivity to glycidol (12-20 %) for HC2USR$_{24}$-pH8, H1 and H3, which are composed by amorphous boehmite or amorphous aluminium hydroxide. The impregnation of HC2USR$_{24}$-pH8 with H_3PO_4 considerably improved the

selectivity up to 70 % to glycidol although conversion decreased. The presence of crystalline aluminium hydroxides (bayerite and gibbsite) in catalyst H2 also favoured the formation of glycidol (64 %)

Table 16. Catalitic activity results

Catalyst	% Conversion GC	% Selectivity to Glycidol
$HC2USR_{24}$	100	0
$HC2USR_{24}$-pH8	86	12
$HC2USR_{24}$-pH8-I	35	72
NiAl-HT	30	26
MgAl-HT	55	0
H1	12	20
H2	16	64
H3	20	13

These results can be compared with those obtained by Bolivar-Diaz *et al* (2013) who reported a glycerol carbonate conversion of 35 % with two catalysts (ZSM-5 and RT-10CoZn). These catalysts presented selectivity values to glycidol of 100 % for the ZSM-5 zeolite and 60 % for RT-10CoZn catalyst. The reaction was achieved by refluxing under conventional heating at 150 ºC for 23 h of reaction.[197] In this preliminary work, we obtained, with the catalyst $HC2USR_{24}$-pH8-I, conversion of glycerol carbonate of 35 % and selectivity to glycidol of 72 % at 150 ºC at shorter time (16 h). More studies with different reaction techniques (microwaves, low pressure) should be performed to improve these catalytic results.

Conclusions

Several layered double hydroxides of Ca/Al, Mg/Al and Ni/Al and various aluminium (oxi)hydroxides have been prepared and characterized by XRD, elemental analysis nitrogen physisorption and TEM techniques. These catalysts have been tested for the decarboxylation of glycerol carbonate to glycidol at 150 ºC for 16 h in a preliminary study. The best catalytic result was achieved using a catalyst prepared by coprecipitation of Ca and Al salts at pH 8 and later modification with H_3PO_4, obtaining 72 % of selectivity to glycidol for a carbonate glycerol conversion

of 36 % at 150 ºC after 16 h of reaction. The presence of crystalline aluminium hydroxides (bayerite and gibbsite) in the aluminium hydroxide prepared by aging 2 h under microwaves also favoured the formation of glycidol (64 %) for a conversion of 16 %. These values are comparable to those described in the literature using conventional heating during reaction.

Acknowledgments

Authors acknowledge Ministerio de Economía y Competitividad of Spain and Feder Funds (CTQ2011-24610), and Catalan Government for FI grant (2012FI_B00564).

UNIVERSITAT ROVIRA I VIRGILI
HYDROCALUMITE-BASED CATALYSTS FOR GLYCEROL REVALORIZATION.
Judith Cecilia Granados Reyes
Dipòsit Legal: T 1362-2015

UNIVERSITAT ROVIRA I VIRGILI
HYDROCALUMITE-BASED CATALYSTS FOR GLYCEROL REVALORIZATION.
Judith Cecilia Granados Reyes
Dipòsit Legal: T 1362-2015

CHAPTER 5

General Conclusions

UNIVERSITAT ROVIRA I VIRGILI
HYDROCALUMITE-BASED CATALYSTS FOR GLYCEROL REVALORIZATION.
Judith Cecilia Granados Reyes
Dipòsit Legal: T 1362-2015

Synthesis and characterization of hydrocalumite-type materials

- Several hydrocalumites were synthesized by coprecipitation of nitrate or chloride salts with and without ultrasounds, and aged hydrothermally in autoclave or by refluxing with and without microwaves.
- The presence of nitrates as interlayer anions resulted in hydrocalumites slight less crystalline than those prepared with chlorides, and favour the formation of katoite.
- The use of ultrasounds during coprecipitation led to more crystalline hydrocalumites.
- The use of autoclave and microwaves during aging, especially at longer times, also favoured the formation of katoite, in addition to hydrocalumite.
- All samples showed low surface areas and low pore volumes. Interestingly, the hydrocalumite prepared from nitrates by coprecipitation in ultrasounds and aged under microwaves resulted in the highest surface area measured. This sample also showed an additional mesoporosity consequence of the different particle size distribution observed by SEM and TEM with respect to the rest of samples.
- Hydrocalumite-type materials were studied by Raman, near infrared, mid-infrared and far infrared spectroscopies.
- The mid-infrared results showed the characteristic bands of the hidrocalumites, as well as the formation of the calcite phase at low amounts. Moreover, the samples stirred by ultrasounds ($HCUSR_{24}$ and $HCUSRMw_6$) exhibited a band at 1508 cm^{-1} due to a higher adsorption of the carbonate, and Raman results confirmed the presence of carbonate in these samples because the samples stirred by ultrasounds presented a band at 1076 cm^{-1} attributed to interlayer carbonate bonded to the water.
- The Far-IR spectra provided information about the cations located in the interlayer space, and confirm the presence of the Cl^- anion in the interlayer space.

- Near infrared spectra showed the characteristic overtones bands of the hydrocalumites. However, it was not possible to observe significant differences between the samples due to the all hydrocalumites have the same composition.
- TF-IR spectroscopy indicated that the thermal decomposition of these samples occurs through successive steps of dehydration, dehydroxylation and layered structure decomposition.
- PN adsorption over the samples outgassed as such at room temperature mainly evidenced very weak Brønsted acidity, possibly increased by the magnetic stirring. Ultrasound technique during precipitation appears to increase the amount of weak Lewis sites, likely Ca ions, characterized by bands at 2253-2255 cm^{-1}. The amount of Lewis sites indeed increased after activation of the samples at 100 °C (i.e. over dehydrated surface) and after outgassing at 400 °C, stronger Lewis sites are detected (CN stretching bad at 2258-2259 cm^{-1}). However, at this temperature the laminar structure was likely lost.
- All these samples were characterized by strong basicity of the O^{2-} anions, evidenced by the formation of CH_2CN^- anions after AN adsorption at high temperature. Moreover, $HCUSR_{24}$ sample showed the higher basicity than the other samples tested.

Catalytic transesterification of glycerol with dimethyl carbonate to obtain glycerol carbonate

- Several hydrocalumite-based catalysts were tested for the transesterification reaction of glycerol with dimethyl carbonate to obtain glycerol carbonate.
- The Hydrocalumites-type catalysts showed some differences in the crystalline phases obtained, LDH structure with some amounts of katoite, they had similar surface and basic characteristics. This explains their similar catalytic behaviour observed after 3 h of reaction resulting in high glycerol conversion (70-84 %) and moderate selectivity values to glycerol carbonate (52-65 %). It is important to remark the interest of these results taking into

account the low surface areas of these catalysts (7-25 m^2/g) compared to those of the catalysts previously tested by other authors for this reaction.

- After 24 h of reaction, practically all catalysts arrived to total glycerol conversion with selectivity values to glycerol carbonate between 65 and 75 %.
- Several catalytic reuses favoured the decarboxylation of glycerol carbonate resulting in the formation of higher amounts of glycidol (30 %) but still maintaining high selectivity values to glycerol carbonate (70 %). This decarboxylation was confirmed by the appearance of a new crystalline phase, $CaCO_3$, in the reused catalyst.
- Calcined samples, prepared from chloride salts and calcined at 450 ºC for 15 h, mainly showed the presence of an amorphous $Ca(Al)O_x$ phase together with some amounts of calcite ($CaCO_3$) in most of them. By increasing the calcination time, the calcite content increased and new crystalline peaks, corresponding to the mayenite phase, $Ca_{12}Al_{14}O_{33}$ appeared.
- The use of nitrogen flowing through the sample during calcination favoured the crystallization of mayenite and the formation of CaO in low amount.
- The use of nitrate anions for the preparation of hydrocalumite-type compounds favoured the formation, after calcination, of the mayenite phase when using autoclave-aging conditions, especially under microwaves.
- When calcined at 750 ºC for 4 h, a mixture of CaO and mayenite phase was obtained in all cases. All catalysts showed low surface areas (4-13 m^2/g) and retained the original hexagonal morphology of their precursors, the hydrocalumite-type compounds, as observed by SEM and TEM. The basicity strenght was higher for the samples calcined at higher temperature, as determined by using Hammett indicators.
- The catalysts obtained by calcination at 450 ºC for 15 h in air showed moderate-high glycerol conversion (46-76 %) and moderate selectivity to glycerol carbonate (41-65 %) after 3 h of reaction.

- The use of longer calcination time at 450 ºC or a dynamic inert-atmosphere system during calcination led to higher conversion (89-94 %) and higher selectivity to glycerol carbonate (72-73 %) values. This has been related to the higher basicity observed for these two catalysts compared with those calcinaded at 450 ºC in air for 15 h.
- Calcination at 750 ºC resulted in high conversion (88-98 %) and high selectivity to glycerol carbonate (60-85 %) due to the presence in the catalysts of CaO, highly basic.
- The progressive loss of conversion and selectivity to glycerol carbonate observed after several reuses has been attributed to the loss of some CaO basic centres during reaction, resulting in the formation of higher amounts of glycidol (42 %).
- Several CaAl-layered double hydroxides and several calcined CaAl-layered double hydroxides have been tested as catalysts for the transesterification of glycerol to glycerol carbonate using microwaves or conventional heating during reaction.The catalytic results of the samples calcined at 450 ºC were worse than those of the hydrocalumite-type compounds (glycerol conversion between 87-63 % in the case of the samples calcined at 450 ºC and 88-82 % in the hydrocalumite-type compounds, and selectivity of glycerol carbonate between 78-53 % and 92-73 %, respectively). This can be correlated with the different basicity strenght of the catalysts.

Catalytic decarboxylation of glycerol carbonate to glycidol

- By comparing several crystalline layered double hydroxides of Ca/Al, Mg/Al and Ni/Al tested for this reaction, the selectivity to glycidol was nul except for the Ni/Al hydrotalcite, which led to 26 %. The different acid-base properties due to the presence of different cations in the hydrotalcite layers can justify these results.
- The best catalytic result was achieved using a catalyst prepared by coprecipitation of Ca and Al salts at pH 8 and later modification with

H_3PO_4, obtaining 72 % of selectivity to glycidol for a carbonate glycerol conversion of 36 % at 150 ºC after 16 h of reaction.

- The presence of a mixture of bayerite and gibbsite in the aluminium hydroxide prepared by precipitating until pH 8 and later aging 2 h under microwaves also favoured the formation of glycidol (64 %) for a conversion of 16 %.

UNIVERSITAT ROVIRA I VIRGILI
HYDROCALUMITE-BASED CATALYSTS FOR GLYCEROL REVALORIZATION.
Judith Cecilia Granados Reyes
Dipòsit Legal: T 1362-2015

CHAPTER 6

References

UNIVERSITAT ROVIRA I VIRGILI
HYDROCALUMITE-BASED CATALYSTS FOR GLYCEROL REVALORIZATION.
Judith Cecilia Granados Reyes
Dipòsit Legal: T 1362-2015

(1) Bournay, L.; Casanave, D.; Delfort, B.; Hillion, G.; Chodorge, J. A. *Catal. Today* **2005**, *106* (1-4), 190.

(2) Quispe, C. A. G.; Coronado, C. J. R.; Carvalho Jr., J. A. *Renew. Sustain. Energy Rev.* **2013**, *27*, 475.

(3) Tan, H. W.; Abdul Aziz, A. R.; Aroua, M. K. *Renew. Sustain. Energy Rev.* **2013**, *27*, 118.

(4) Gholami, Z.; Abdullah, A. Z.; Lee, K.-T. *Renew. Sustain. Energy Rev.* **2014**, *39*, 327.

(5) Behr, A.; Eilting, J.; Irawadi, K.; Leschinski, J.; Lindner, F. *Green Chemistry* **2008**, *10*, 13.

(6) Ardi, M. S.; Aroua, M. K.; Hashim, N. A. *Renew. Sustain. Energy Rev.* **2015**, *42*, 1164.

(7) Rahmat, N.; Abdullah, A. Z.; Mohamed, A. R. *Renew. Sustain. Energy Rev.* **2010**, *14* (3), 987.

(8) Pagliaro, M.; Ciriminna, R.; Kimura, H.; Rossi, M.; Della Pina, C. From glycerol to value-added products. *Angewandte Chemie - International Edition* **2007**, *46*, 4434–4440.

(9) Pagliaro, M.; Rossi, M. *The future of glicerol*, 2nd ed.; RSC *Green Chemestry* **2010**.

(10) Pachauri, N.; He, B. *ASABE meeting presentation* **2006**; Paper No: 066223.

(11) Zhou, C.-H. C.; Beltramini, J. N.; Fan, Y.-X.; Lu, G. Q. M. *Chem. Soc. Rev.* **2008**, *37* (3), 527.

(12) Ochoa-Gómez, J. R.; Gómez-Jiménez-Aberasturi, O.; Maestro-Madurga, B.; Pesquera-Rodríguez, A.; Ramírez-López, C.; Lorenzo-Ibarreta, L.; Torrecilla-Soria, J.; Villarán-Velasco, M. C. *Appl. Catal. A Gen.* **2009**, *366* (2), 315.

(13) Segni, R.; Vieille, L.; Leroux, F.; Taviot-Guého, C. *J. Phys. Chem. Solids* **2006**, *67* (5-6), 1037.

(14) Vieille, L.; Rousselot, I.; Leroux, F.; Besse, J.; Taviot-gue, C.; Mate, L.; Pascal, B. *Chem. Mater.* **2003**, *15* (12), 4361.

(15) Taylor, H. F. *Mineralogical magazine*. **1973**, *39*, 377.

(16) Cavani, F.; Trifirò, F.; Vaccari, A. *Catal. Today* **1991**, *11*, 173.

(17) Suslick, K. S. *Science* **1990**, *247* (4949), 1439.

(18) Bergadà, O.; Vicente, I.; Salagre, P.; Cesteros, Y.; Medina, F.; Sueiras, J. E. *Microporous Mesoporous Mater.* **2007**, *101* (3), 363.

(19) Bish, D. L.; Howard, S. a. *J. Appl. Crystallogr.* **1988**, *21* (2), 86.

(20) Brunauer, S.; Deming, L. S.; Deming, W. E.; Teller, E. *J. Am. Chem. Soc.* **1940**, *62* (7), 1723.

(21) De Boer, J. H. *Adv. Catal.* **1956**, *8*, 17.

(22) Forano, C.; Hibino, T.; Leroux, F.; Taviot-Guého, C. *Handbook of Clay Science*; Developments in Clay Science **2006**, *1*.

(23) Vieille, L.; Rousselot, I.; Leroux, F.; Besse, J.-P.; Taviot-Guého, C. *Chem. Mater.* **2003**, *15* (23), 4361.

(24) Cota, I.; Ramírez, E.; Medina, F.; Sueiras, J. E.; Layrac, G.; Tichit, D. *Appl. Clay Sci.* **2010**, *50* (4), 498.

(25) Mora, M.; López, M. I.; Jiménez-Sanchidrián, C.; Ruiz, J. R. *Catal. Letters* **2010**, *136* (3-4), 192.

(26) Sánchez-Cantú, M.; Pérez-Díaz, L. M.; Tepale-Ochoa, N.; González-Coronel, V. J.; Ramos-Cassellis, M. E.; Machorro-Aguirre, D.; Valente, J. S. *Fuel* **2013**, *110*, 23.

(27) Campos-Molina, M. J.; Santamaría-González, J.; Mérida-Robles, J.; Moreno-Tost, R.; Albuquerque, M. C. G.; Bruque-Gámez, S.; Rodríguez-Castellón, E.; Jiménez-López, A.; Maireles-Torres, P. *Energy & Fuels* **2010**, *24* (2), 979.

(28) Kuwahara, Y.; Tsuji, K.; Ohmichi, T.; Kamegawa, T.; Mori, K.; Yamashita, H. *Catal. Sci. Technol.* **2012**, *2* (9), 1842.

(29) Choy, J.; Choi, S.; Oh, J.; Park, T. *Appl. Clay Sci.* **2007**, *36* (1-3), 122.

(30) Linares, C. F.; Ocanto, F.; Bretto, P.; Monsalve, M. *Bull. Mater. Sci.* **2014**, *37* (4), 941.

(31) Zhang, M.; Reardon, E. J. *Sci. China, Ser. C Life Sci.* **2005**, *48*, 165.

(32) Zhang, P.; Qian, G.; Xu, Z. P.; Shi, H.; Ruan, X.; Yang, J.; Frost, R. L. *J. Colloid Interface Sci.* **2012**, *367* (1), 264.

(33) Zhang, P.; Qian, G.; Shi, H.; Ruan, X.; Yang, J.; Frost, R. L. *J. Colloid Interface Sci.* **2012**, *365* (1), 110.

(34) Liu, Q.; Li, Y.; Zhang, J.; Chi, Y.; Ruan, X.; Liu, J.; Qian, G. *Chem. Eng. J.* **2011**, *175*, 33.

(35) Zhang, M.; Reardon, E. J. *Environ. Sci. Technol.* **2003**, *37* (13), 2947.

(36) Zhou, J. Z.; Xu, Z. P.; Qiao, S.; Liu, J.; Liu, Q.; Xu, Y.; Zhang, J.; Qian, G. *Appl. Clay Sci.* **2011**, *54* (3-4), 196.

(37) Qian, G.; Feng, L.; Zhou, J. Z.; Xu, Y.; Liu, J.; Zhang, J.; Xu, Z. P. *Chem. Eng. J.* **2012**, *181-182*, 251.

(38) Zhang, P.; Qian, G.; Cheng, H.; Yang, J.; Shi, H.; Frost, R. L. *Spectrochim. Acta. A. Mol. Biomol. Spectrosc.* **2011**, *79* (3), 548.

(39) Dai, Y.; Qian, G.; Cao, Y.; Chi, Y.; Xu, Y.; Zhou, J.; Liu, Q.; Xu, Z. P.; Qiao, S. *J. Hazard. Mater.* **2009**, *170* (2-3), 1086.

(40) Wajima, T.; Oya, K.; Shibayama, A.; Sugawara, K.; Munakata, K. *ISIJ Int.* **2011**, *51* (7), 1179.

(41) Grover, K.; Komarneni, S.; Katsuki, H. *Water Res.* **2009**, *43* (15), 3884.

(42) De Sá, F. P.; Cunha, B. N.; Nunes, L. M. *Chem. Eng. J.* **2013**, *215-216*, 122.

(43) Wu, Y.; Chi, Y.; Bai, H.; Qian, G.; Cao, Y.; Zhou, J.; Xu, Y.; Liu, Q.; Xu, Z. P.; Qiao, S. *J. Hazard. Mater.* **2010**, *176* (1-3), 193.

(44) Phillips, J. D.; Vandeperre, L. J. *J. Nucl. Mater.* **2011**, *416* (1-2), 225.

(45) Raki, L.; Beaudoin, J.; Alizadeh, R.; Makar, J.; Sato, T. *Materials (Basel).* **2010**, *3* (2), 918.

(46) Raki, L.; Beaudoin, J. J.; Mitchell, L. *Cem. Concr. Res.* **2004**, *34* (9), 1717.

(47) Matschei, T.; Lothenbach, B.; Glasser, F. P. *Cem. Concr. Res.* **2007**, *37* (2), 118.

(48) Mora, M.; López, M. I.; Jiménez-Sanchidrián, C.; Ruiz, J. R. *Solid State Sci.* **2011**, *13* (1), 101.

(49) Lopez-Salinas, E.; Serrano, M. E. L.; Jacome, M. A. C.; Secora, I. S. *J. Porous Mater.* **1996**, *2* (4), 291.

(50) Birnin-Yauri, U.; Glasser, F. *Cem. Concr. Res.* **1998**, *28* (12), 1713.

(51) Miyata, S. *Clays and Clay Minerals* **1983**, *31* (4), 305.

(52) Sankaranarayanan, S.; Antonyraj, C. A.; Kannan, S. *Bioresour. Technol.* **2012**, *109*, 57.

(53) Guo, Q.; Tian, J. *Chem. Eng. J.* **2013**, *231*, 121.

(54) González, M. D.; Cesteros, Y.; Salagre, P. *Microporous Mesoporous Mater.* **2011**, *144* (1-3), 162.

(55) González, M. D.; Cesteros, Y.; Salagre, P.; Medina, F.; Sueiras, J. E. *Microporous Mesoporous Mater.* **2009**, *118* (1-3), 341.

(56) Vicente, I.; Salagre, P.; Cesteros, Y.; Medina, F.; Sueiras, J. E. *Appl. Clay Sci.* **2010**, *48* (1-2), 26.

(57) Sánchez, T.; Salagre, P.; Cesteros, Y. *Microporous Mesoporous Mater.* **2013**, *171*, 24.

(58) Benito, P.; Labajos, F. M.; Rives, V. *Pure Appl. Chem.* **2009**, *81* (8), 1459.

(59) Fetter, G.; Hernández, F.; Maubert, A. M.; Lara, V. H.; Bosch, P. *J. Porous Mater.* **1997**, *4* (1), 27.

(60) Fetter, G.; Botello, a.; Lara, V. H.; Bosch, P. *J. Porous Mater.* **2001**, *8* (3), 227.

(61) Fetter, G.; Olguín, M. T.; Bosch, P.; Bulbulian, S. *J. Porous Mater.* **2000**, *7* (4), 469.

(62) Rivera, J. a.; Fetter, G.; Bosch, P. *Microporous Mesoporous Mater.* **2006**, *89* (1-3), 306.

(63) Paredes, S. P.; Fetter, G.; Bosch, P.; Bulbulian, S. *J. Nucl. Mater.* **2006**, *359* (3), 155.

(64) Paredes, S. P.; Fetter, G.; Bosch, P.; Bulbulian, S. *J. Mater. Sci.* **2006**, *41* (11), 3377.

(65) Jobbágy, M.; Blesa, M. a.; Regazzoni, A. E. *J. Colloid Interface Sci.* **2007**, *309* (1), 72.

(66) Kannan, S.; Vir Jasra, R. *J. Mater. Chem.* **2000**, *10* (10), 2311.

(67) Sampieri, A.; Fetter, G.; Pfeiffer, H.; Bosch, P. *Solid State Sci.* **2007**, *9* (5), 394.

(68) S. Mohmel, I. Kuirzawski, D. Uecker, D. Muller, W. G. *Cryst. Res. Technol.* **2002**, *37* (4), 359.

(69) Tichit, D.; Rolland, A.; Prinetto, F.; Fetter, G.; de Jesus Martinez-Ortiz, M.; Valenzuela, M. a.; Bosch, P. *J. Mater. Chem.* **2002**, *12* (12), 3832.

(70) Pérez-Barrado, E.; Pujol, M. C.; Aguiló, M.; Cesteros, Y.; Díaz, F.; Pallarès, J.; Marsal, L. F.; Salagre, P. *Appl. Clay Sci.* **2013**, *80-81*, 313.

(71) Lee, J. H.; Lee, Y. S.; Kim, H.; Jung, D.-Y. *Eur. J. Inorg. Chem.* **2011**, *2011* (22), 3334.

(72) Álvarez, M. G.; Chimentão, R. J.; Barrabés, N.; Föttinger, K.; Gispert-Guirado, F.; Kleymenov, E.; Tichit, D.; Medina, F. *Appl. Clay Sci.* **2013**, *83-84*, 1.

(73) Mallakpour, S.; Dinari, M. *Polym. Plast. Technol. Eng.* **2014**, *53* (10), 1047.

(74) Mallakpour, S.; Dinari, M. *J. Therm. Anal. Calorim.* **2014**, *119* (3), 1905.

(75) Mallakpour, S.; Dinari, M.; Hatami, M. *J. Therm. Anal. Calorim.* **2015**, *120* (2), 1293.

(76) Li, Y.; Wang, J.; Li, Z.; Liu, Q.; Liu, J.; Liu, L.; Zhang, X.; Yu, J. *Chem. Eng. J.* **2013**, *218*, 295.

(77) Resini, C.; Montanari, T.; Barattini, L.; Ramis, G.; Busca, G.; Presto, S.; Riani, P.; Marazza, R.; Sisani, M.; Marmottini, F.; Costantino, U. *Appl. Catal. A Gen.* **2009**, *355* (1-2), 83.

(78) Montanari, T.; Sisani, M.; Nocchetti, M.; Vivani, R.; Delgado, M. C. H.; Ramis, G.; Busca, G.; Costantino, U. *Catal. Today* **2010**, *152* (1-4), 104.

(79) Wang, J.; Kalinichev, A. G.; Amonette, J. E.; Kirkpatrick, R. J. *Am. Mineral.* **2003**, *88*, 398.

(80) Kloprogge, J. T.; Wharton, D.; Hickey, L.; Frost, R. L. *Am. Mineral.* **2002**, *87* (5-6), 623.

(81) Roelofs, J. C. A. A.; van Bokhoven, J. A.; van Dillen, A. J.; Geus, J. W.; de Jong, K. P. *Chemistry* **2002**, *8* (24), 5571.

(82) Frost, R. L.; Musumeci, A. W. *J. Colloid Interface Sci.* **2006**, *302* (1), 203.

(83) Burrueco, M. I.; Mora, M.; Jiménez-Sanchidrián, C.; Ruiz, J. R. *J. Mol. Struct.* **2013**, *1034*, 38.

(84) Frost, R. L.; Scholz, R.; López, A.; Theiss, F. L. *Spectrochim. Acta. A. Mol. Biomol. Spectrosc.* **2014**, *118*, 187.

(85) Frost, R. L.; Reddy, B. J. *Spectrochim. Acta. A. Mol. Biomol. Spectrosc.* **2006**, *65* (3-4), 553.

(86) Kloprogge, J. *Appl. Clay Sci.* **2001**, *18* (1-2), 37.

(87) Lercher, J. A.; Gründling, C.; Eder-Mirth, G. *Catal. Today* **1996**, *27* (3-4), 353.

(88) Lavalley, J. C. *Catal. Today* **1996**, *27* (3-4), 377.

(89) Salla, I.; Montanari, T.; Salagre, P.; Cesteros, Y.; Busca, G. *J. Phys. Chem. B* **2005**, *109*, 915.

(90) Bevilacqua, M.; Alejandre, A. G.; Resini, C.; Casagrande, M.; Ramirez, J.; Busca, G. *Phys. Chem. Chem. Phys.* **2002**, *4* (18), 4575.

(91) Thibault-Starzyk, F.; Travert, A.; Saussey, J.; Lavalley, J. *Top. Catal.* **1998**, *6*, 111.

(92) Busca, G.; Montanari, T.; Bevilacqua, M.; Finocchio, E. *Colloids Surfaces A Physicochem. Eng. Asp.* **2008**, *320* (1-3), 205.

(93) Aboulayt, A.; Binet, C.; Lavalley, J.-C. *J. Chem. Soc. Faraday Trans.* **1995**, *91* (17), 2913.

(94) Morterra, C.; Peñarroya Mentruit, M.; Cerrato, G. *Phys. Chem. Chem. Phys.* **2002**, *4* (4), 676.

(95) Koubowetz, F.; Latzel, J.; Noller, H. *J. Colloid Interface Sci.* **1980**, *74* (2), 322.

(96) Prinetto, F.; Manzoli, M.; Ghiotti, G.; Martinez Ortiz, M. D. J.; Tichit, D.; Coq, B. *J. Catal.* **2004**, *222* (1), 238.

(97) Grover, K.; Komarneni, S.; Katsuki, H. *Appl. Clay Sci.* **2010**, *48* (4), 631.

(98) Domínguez, M.; Pérez-Bernal, M. E.; Ruano-Casero, R. J.; Barriga, C.; Rives, V.; Ferreira, R. A. S.; Carlos, L. D.; Rocha, J. *Chem. Mater.* **2011**, *23* (7), 1993.

(99) Vicente, I.; Salagre, P.; Cesteros, Y.; Medina, F.; Sueiras, J. E. *Appl. Clay Sci.* **2010**, *48* (1-2), 26.

(100) Pertlik, F. *GeoLines* **2003**, *15*, 113.

(101) Kingston, H. M.; Haswell, S. J. *Microwave-enhanced Chemistry Funfamentals, Sample Preparation and Applications.*, First Edit.; ACS Professional Reference Book, **1997**.

(102) Constantino, V. R. L.; Pinnavaia, T. J. *Inorg. Chem.* **1995**, *34* (4), 883.

(103) Cota, I.; Ramírez, E.; Medina, F.; Sueiras, J. E.; Layrac, G.; Tichit, D. *Appl. Clay Sci.* **2010**, *50* (4), 498.

(104) Frost, R. L.; Palmer, S. J.; Theiss, F. *J. Raman Spectrosc.* **2011**, *42* (5), 1163.

(105) Granados-Reyes, J.; Salagre, P.; Cesteros, Y. *Microporous Mesoporous Mater.* **2014**, *199*, 117.

(106) Mora, M.; López, M. I.; Jiménez-Sanchidrián, C.; Ruiz, J. R. *Solid State Sci.* **2011**, *13* (1), 101.

(107) Ryczkowski, J. *Catal. Today* **2001**, *68* (4), 263.

(108) Busca, G. *Catal. Today* **1998**, *41* (1-3), 191.

(109) Hadjiivanov, K. *Adv. Catal.* **2014**, *57*, 99.

(110) Ingemar Odenbrand, C. U.; Brandin, J. G. M.; Busca, G. *J. Catal.* **1992**, *135* (2), 505.

(111) Busca, G. *Chem. Rev.* **2010**, *110* (4), 2217.

(112) Morandi, S.; Manzoli, M.; Prinetto, F.; Ghiotti, G.; Gérardin, C.; Kostadinova, D.; Tichit, D. *Microporous Mesoporous Mater.* **2012**, *147* (1), 178.

(113) Kloprogge, J. T.; Frost, R. L. *J. Solid State Chem.* **1999**, *146* (2), 506.

(114) Vieira, A. C.; Moreira, R. L.; Dias, A. *J. Phys. Chem. C* **2009**, *113* (30), 13358.

(115) Trombetta, M.; Busca, G.; Lenarda, M.; Storaro, L.; Ganzerla, R.; Piovesan, L.; Jimenez, A.; Alcantara-rodr, M.; Rodr, E. *Appl. Catal. A Gen.* **2000**, *193*, 55.

(116) Li, J.; Wang, T. *Chem. Eng. Process. Process Intensif.* **2010**, *49* (5), 530.

(117) Teng, W. K.; Ngoh, G. C.; Yusoff, R.; Aroua, M. K. *Energy Convers. Manag.* **2014**, *88*, 484.

(118) Teng, W. K.; Ngoh, G. C.; Yusoff, R.; Aroua, M. K. *Energy Convers. Manag.* **2014**, *88*, 484.

(119) Teles, J. H.; Rieber, N.; Harder, W. US 5359094, **1994**.

(120) Mouloungui, Z.; Yoo, J.-W.; Gachen, C.-A.; Gaset, A.; Vermeersch, G. EP0739888 A1, **1996**.

(121) Claude, S.; Mouloungui, Z.; Yoo, J.-W.; Gaset, A. US006025504A, **2000**.

(122) Claude, S.; Mouloungui, Z.; Yoo, J.-W.; Gaset, A. EP 0 955 298 B1, **2001**.

(123) Yoo, J.-W.; Mouloungui, Z. *Nanotechnology in Mesostructured Materials, Proceedings of the 3rd International Materials Symposium*; Studies in Surface Science and Catalysis; Elsevier, **2003**, *146*.

(124) Okutsu, M.; Kitsuki, T. EP1156042 A1, **2001**.

(125) Li, Q.; Zhang, W.; Zhao, N.; Wei, W.; Sun, Y. *Catal. Today* **2006**, *115* (1-4), 111.

(126) Okutsu, M.; Kitsuki, T. JP 2007039347, **2007**.

(127) Sasa, T.; Okutsu, M.; Uno, M. P 2008285457 A, **2008**.

(128) Aresta, M.; Dibenedetto, A.; Nocito, F.; Ferragina, C. *J. Catal.* **2009**, *268* (1), 106.

(129) Aresta, M.; Dubois, J. L.; Dibenedetto, A.; Nocito, F.; Ferragina, C. Arkema. EP 08305653.1, **2008**.

(130) Dibenedetto, A.; Angelini, A.; Aresta, M.; Ethiraj, J.; Fragale, C.; Nocito, F. *Tetrahedron* **2011**, *67* (6), 1308.

(131) Climent, M. J.; Corma, A.; De Frutos, P.; Iborra, S.; Noy, M.; Velty, A.; Concepción, P. *J. Catal.* **2010**, *269* (1), 140.

(132) Fujita, S.; Yamanishi, Y.; Arai, M. *J. Catal.* **2013**, *297*, 137.

(133) Ryu, Y. B.; Baek, J. H.; Kim, Y.; Lee, M. S. *J. Nanosci. Nanotechnol.* **2015**, *15* (1), 321.

(134) Chen, J.; Wang, C.; Dong, B.; Leng, W.; Huang, J.; Ge, R.; Gao, Y. *Chinese J. Catal.* **2015**, *36* (3), 336.

(135) Kondawar, S. E.; Potdar, A. S.; Rode, C. V. *RSC Adv.* **2015**, *5* (21), 16452.

(136) Hasbi Ab Rahim, M.; He, Q.; Lopez-Sanchez, J. A.; Hammond, C.; Dimitratos, N.; Sankar, M.; Carley, A. F.; Kiely, C. J.; Knight, D. W.; Hutchings, G. J. *Catal. Sci. Technol.* **2012**, *2* (9), 1914.

(137) Jagadeeswaraiah, K.; Kumar, C. R.; Prasad, P. S. S.; Loridant, S.; Lingaiah, N. *Appl. Catal. A Gen.* **2014**, *469*, 165.

(138) Zhang, J.; He, D. *React. Kinet. Mech. Catal.* **2014**, *113* (2), 375.

(139) Wang, L.; Ma, Y.; Wang, Y.; Liu, S.; Deng, Y. *Catal. Commun.* **2011**, *12* (15), 1458.

(140) George, J.; Patel, Y.; Pillai, S. M.; Munshi, P. *J. Mol. Catal. A Chem.* **2009**, *304* (1-2), 1.

(141) Li, H.; Gao, D.; Gao, P.; Wang, F.; Zhao, N.; Xiao, F.; Wei, W.; Sun, Y. *Catal. Sci. Technol.* **2013**, *3* (10), 2801.

(142) Zhang, J.; He, D. *J. Colloid Interface Sci.* **2014**, *419*, 31.

(143) Liu, Y. *Spec. Petrochemicals* **2014**, *31* (1), 25.

(144) Li, H.; Xin, C.; Jiao, X.; Zhao, N.; Xiao, F.; Li, L.; Wei, W.; Sun, Y. *J. Mol. Catal. A Chem.* **2015**, *402*, 71.

(145) Ma, J.; Song, J.; Liu, H.; Liu, J.; Zhang, Z.; Jiang, T.; Fan, H.; Han, B. *Green Chem.* **2012**, *14* (6), 1743.

(146) Yu, Q. Y.; Huang, S. Y.; Huang, Q. Z.; Wang, Q. P.; Sun, G. S.; Huang, Z. Q.; Huang, M. *Xiandai Huagong/Modern Chem. Ind.* **2014**, *34* (4), 112.

(147) Jo, Y. J.; Lee, O. K.; Lee, E. Y. *Bioresour. Technol.* **2014**, *158*, 105.

(148) Waghmare, G. V; Vetal, M. D.; Rathod, V. K. *Ultrason. Sonochem.* **2015**, *22*, 311.

(149) Algoufi, Y. T.; Hameed, B. H. *Fuel Process. Technol.* **2014**, *126*, 5.

(150) Pan, S.; Zheng, L.; Nie, R.; Xia, S.; Chen, P.; Hou, Z. *Chinese J. Catal.* **2012**, *33* (11-12), 1772.

(151) Hu, J.; Gu, Y.; Guan, Z.; Li, J.; Mo, W.; Li, T.; Li, G. *ChemSusChem* **2011**, *4* (12), 1767.

(152) Álvarez, M. G.; Plíšková, M.; Segarra, A. M.; Medina, F.; Figueras, F. *Appl. Catal. B Environ.* **2012**, *113-114*, 212.

(153) Alvarez, M. G.; Segarra, A. M.; Contreras, S.; Sueiras, J. E.; Medina, F.; Figueras, F. *Chem. Eng. J.* **2010**, *161* (3), 340.

(154) Álvarez, M. G.; Chimentão, R. J.; Figueras, F.; Medina, F. *Appl. Clay Sci.* **2012**, *58*, 16.

(155) Zheng, L.; Xia, S.; Hou, Z.; Zhang, M.; Hou, Z. *Chinese J. Catal.* **2014**, *35* (3), 310.

(156) Yadav, G. D.; Chandan, P. A. *Catal. Today* **2014**, *237*, 47.

(157) Hong, M.; Gao, L.; Xiao, G. *J. Chem. Res.* **2014**, *38* (11), 679.

(158) Malyaadri, M.; Jagadeeswaraiah, K.; Sai Prasad, P. S.; Lingaiah, N. *Appl. Catal. A Gen.* **2011**, *401* (1-2), 153.

(159) Parameswaram, G.; Srinivas, M.; Babu, B. H.; Prasad, P. S. S.; Lingaiah, N. *Catal. Sci. Technol.* **2013**, *3*, 3242.

(160) Takagaki, A.; Iwatani, K.; Nishimura, S.; Ebitani, K. *Green Chem.* **2010**, *12* (4), 578.

(161) Liu, P.; Derchi, M.; Hensen, E. J. M. *Appl. Catal. B Environ.* **2014**, *144* (1), 135.

(162) Liu, Z.; Wang, J.; Kang, M.; Yin, N.; Wang, X.; Tan, Y.; Zhu, Y. *J. Ind. Eng. Chem.* **2015**, *21*, 394.

(163) Fernández, Y.; Arenillas, A.; Bermúdez, J. M.; Menéndez, J. A. *J. Anal. Appl. Pyrolysis* **2010**, *88* (2), 155.

(164) Escribà, M.; Eras, J.; Duran, M.; Simon, S.; Butchosa, C.; Villorbina, G.; Balcells, M.; Canela, R. *Tetrahedron* **2009**, *65* (50), 10370.

(165) Cabrera, D. M. L.; Líbero, F. M.; Alves, D.; Perin, G.; Lenardão, E. J.; Jacob, R. G. *Green Chem. Lett. Rev.* **2012**, *5* (3), 329.

(166) Xie, J.; Hse, C.-Y.; Shupe, T. F.; Qi, J.; Pan, H. *J. Appl. Polym. Sci.* **2014**, *131* (9), n/a.

(167) Iaych, K.; Dumarçay, S.; Fredon, E.; Gérardin, C.; Lemor, A.; Gérardin, P. *J. Appl. Polym. Sci.* **2011**, *120* (4), 2354.

(168) Zhanga, X.-Z.; Zhoua, W.-J.; Yanga, M.; Wangb, J.-X.; Baic, L. *J. Chem. Res.* **2012**, *36* (8), 489.

(169) Pawar, R. R.; Jadhav, S. V.; Bajaj, H. C. *Chem. Eng. J.* **2014**, *235*, 61.

(170) Zhou, W.-J.; Zhang, X.-Z.; Sun, X.-B.; Wang, B.; Wang, J.-X.; Bai, L. *Russ. Chem. Bull.* **2014**, *62* (5), 1244.

(171) Drago, C.; Liotta, L. F.; La Parola, V.; Testa, M. L.; Nicolosi, G. *Fuel* **2013**, *113*, 707.

(172) Bakhrou, N.; Lamaty, F.; Martinez, J.; Colacino, E. *Tetrahedron Lett.* **2010**, *51* (30), 3935.

(173) Bayramoğlu, D.; Gürel, G.; Sinağ, A.; Güllü, M. *Turkish J. Chem.* **2014**, *38* (4), 661.

(174) D'Aquino, R.; Ondrey, G. *Chem. Eng.* **2007**, *114* (9), 31.

(175) Barrault, J.; Jerome, F. *Eur. J. Lipid Sci. Technol.* **2008**, *110* (9), 825.

(176) Pagliaro, M.; Ciriminna, R.; Kimura, H.; Rossi, M.; Della Pina, C. *Eur. J. Lipid Sci. Technol.* **2009**, *111* (8), 788.

(177) Sonnati, M. O.; Amigoni, S.; Taffin de Givenchy, E. P.; Darmanin, T.; Choulet, O.; Guittard, F. *Green Chem.* **2013**, *15* (2), 283.

(178) Shieh, W.-C.; Dell, S.; Repič, O. *J. Org. Chem.* **2002**, *67* (7), 2188.

(179) Randall, D.; De vos, R. randall. EP 419114, **1991**.

(180) Weuthen, M.; Hees, U. weuthe. DE 4335947, **1995**.

(181) Yoo, J. W.; Mouloungui, Z.; Gaset, A. US Patent 6316641, **2001**.

(182) Hammond, C.; Lopez-Sanchez, J. A.; Ab Rahim, M. H.; Dimitratos, N.; Jenkins, R. L.; Carley, A. F.; He, Q.; Kiely, C. J.; Knight, D. W.; Hutchings, G. J. *Dalton Trans.* **2011**, *40* (15), 3927.

(183) Kim, D.-W.; Park, K.-A.; Kim, M.-J.; Kang, D.-H.; Yang, J.-G.; Park, D.-W. *Appl. Catal. A Gen.* **2014**, *473*, 31.

(184) Simanjuntak, F. S. H.; Kim, T. K.; Lee, S. D.; Ahn, B. S.; Kim, H. S.; Lee, H. *Appl. Catal. A Gen.* **2011**, *401* (1-2), 220.

(185) Kumar, A.; Iwatani, K.; Nishimura, S.; Takagaki, A.; Ebitani, K. *Catal. Today* **2012**, *185* (1), 241.

(186) Liu, Z.; Wang, J.; Kang, M.; Yin, N.; Wang, X.; Tan, Y.; Zhu, Y. *J. Ind. Eng. Chem.* **2015**, *21*, 394.

(187) Larhed, M.; Hallberg, A. *J. Org. Chem.* **1996**, *61* (26), 9582.

(188) Caddick, S.; Fitzmaurice, R. *Tetrahedron* **2009**, *65* (17), 3325.

(189) Appukkuttan, P.; Mehta, V. P.; Van der Eycken, E. V. *Chem. Soc. Rev.* **2010**, *39* (5), 1467.

(190) Polshettiwar, V.; Varma, R. S. *Green Chem.* **2010**, *12* (5), 743.

(191) Hemasri, Y. *Heterocycl. Commun.* **2009**, *15* (6), 423.

(192) Kappe, C. O. *Angew. Chemie-International Ed.* **2004**, *43*, 6250.

(193) Kappe, C. O.; Van der Eycken, E. *Chem. Soc. Rev.* **2010**, *39* (4), 1280.

(194) Kremsner, J. M.; Kappe, C. O. *J. Org. Chem.* **2006**, *71* (12), 4651.

(195) Henry, C.; Haupt, A.; Turner, S. C. *J. Org. Chem.* **2009**, *74* (5), 1932.

(196) Calvino-Casilda, V.; Guerrero-Pérez, M. O.; Bañares, M. A. *Appl. Catal. B Environ.* **2010**, *95* (3-4), 192.

(197) Bolívar-Diaz, C. L.; Calvino-Casilda, V.; Rubio-Marcos, F.; Fernández, J. F.; Bañares, M. a. *Appl. Catal. B Environ.* **2013**, *129*, 575.

(198) Wróblewska, A.; Milchert, E. *Chem. Pap.* **2002**, *56* (3), 150.

(199) Wróblewska, A. *Appl. Catal. A Gen.* **2006**, *309* (2), 192.

(200) Wroblewska, A.; Fajdek, A.; Wajzberg, J.; Milchert, E. *J. Adv. Oxid. Technol.* **2008**, *11* (3), 468.

(201) Wróblewska, A.; Fajdek, A.; Milchert, E.; Grzmil, B. *Polish J. Chem. Technol.* **2010**, *12* (1), 29.

(202) Wróblewska, A.; Fajdek, A. *J. Hazard. Mater.* **2010**, *179* (1-3), 258.

(203) Wróblewska, A.; Makuch, E. *J. Adv. Oxid. Technol.* **2014**, *17* (1), 44.

(204) Hutchings, G. J.; Lee, D. F.; Minihan, A. R. *Catal. Letters* **1996**, *39* (1-2), 83.

(205) Wu, P. *J. Catal.* **2003**, *214* (2), 317.

(206) Malkemus, J. D.; Currier, V. A. US2856413, 1958.

(207) Mouloungui, Z. *Oilseeds fats, Crop. Lipids* **2004**, *11*, 425.

(208) Yuichiro, S.; Tomoaki, S.; Hiroki, T.; Mitsuru, U. US007868192 B1, **2011**.

(209) Choi, J. S.; Simanjuntaka, F. S. H.; Oh, J. Y.; Lee, K. I.; Lee, S. D.; Cheong, M.; Kim, H. S.; Lee, H. *J. Catal.* **2013**, *297*, 248.